University of Nevada, Reno

Controls on Groundwater Chemistry in Rural Southwest Niger, West Africa

A thesis submitted in partial fulfillment of the requirements for the degree of Master of Science in Hydrogeology

by

Daniel M. Saftner

Dr. Alexandra Lutz/Thesis Advisor

December 2017

THE GRADUATE SCHOOL

We recommend that the thesis

prepared under our supervision by

DANIEL M. SAFTNER

entitled

Controls on Groundwater Chemistry in Rural Southwest Niger, West Africa

be accepted in partial fulfillment of the

requirements for the degree of

MASTER OF SCIENCE

Alexandra Lutz, Ph.D., Advisor

Ronald Hershey, Ph.D., Committee Member

Braimah Apambire, Ph.D., Graduate School Representative

David W. Zeh, Ph.D., Dean, Graduate School

December, 2017

Abstract

In a region characterized by frequent drought and rapid population growth, an understanding of the processes causing spatial and temporal variations in groundwater chemistry is crucial to sustain potable groundwater supplies in rural southwest Niger, West Africa. Seventy-one groundwater samples were collected at 14 locations during a 6-month dry period in three rural communities and were analyzed for major ion and trace element concentrations and physical parameter values. The objectives were to 1) identify and characterize the natural and anthropogenic factors controlling spatial and temporal variations in groundwater chemistry and 2) determine whether the extent to which these factors affect groundwater chemistry increases or decreases over time. Graphical analyses, such as Piper, Durov, and Stiff diagrams categorized the water chemistry of the study area as Ca-Mg-HCO_3 and a Gibbs plot indicated that the main source of dissolved solids is weathering of silicate minerals in both fresh and weathered granitoids. A principal component analysis (PCA) was used to determine that the degree of aquifer weathering and fracturing and the presence or absence of a laterite layer explain 52 % of the data variances. A hierarchical cluster analysis (HCA) demonstrated that samples with similar groundwater chemistry cluster by spatial proximity, degree of aquifer weathering and fracturing, presence or absence of laterite, or land cover. A Regional Kendall Test (RKT) indicated that the impact of the dissolution of Ca and Mg-rich silicate minerals on groundwater chemistry increased significantly ($p < 0.05$) throughout the study area. In areas with laterite, the influence of laterite weathering on groundwater chemistry reduced significantly. Nitrate and Cl concentrations were partitioned by land cover and subjected to an analysis of variance (ANOVA), revealing that concentrations of both variables are greatest in areas of high-population densities. These analyses have led to a better understanding of the mechanisms controlling groundwater chemistry in a weathered-granitoid aquifer in rural southwest Niger.

Dedication

This thesis is dedicated to those in Niger that struggle to obtain safe drinking water.

Acknowledgements

I would like to thank my advisor, Dr. Alexandra Lutz, for advisement in topics related to hydrogeology, statistics, and GIS and for encouraging me to pursue hydrologic research in West Africa. I would also like to thank my committee members: Dr. Braimah Apambire for providing me with knowledge about water and sanitation in Africa and Dr. Ronald Hershey for his input on groundwater geochemistry. I would like to acknowledge World Vision Niger for acting as my in-country affiliation and providing me with office space and logistical support. Additional thanks is merited to the World Vision Niger Integrated WASH team for helping me with site selection, fieldwork, and for teaching me the local hydrogeology. Financial support for this project was provided by the Desert Research Institute's Division of Hydrologic Sciences, Vice President for Research's Office, and Center for International Water and Sustainability. The Fulbright U.S. Student Program provided additional support for research and living expenses.

Contents

List of Tables

List of Figures

1.0 Introduction

The objective of this study is to contribute to sustainable drinking water supplies by describing processes causing spatial and temporal variations in groundwater chemistry during a six-month dry period in a rural region of southwest Niger. Accessing sustainable groundwater reserves is crucial in Niger, but is a challenge given the geographic vastness/diversity of the nation, frequent drought periods, rapid population growth, and limited resources. Multivariate statistical analyses were used to better understand the natural and anthropogenic factors that control groundwater chemistry in Niger. A trend analysis was applied to determine if uniform variations exist in these factors over time and space.

Access to safe and sustainable groundwater sources is vital to human health; yet approximately 663 million people lack access (WHO/UNICEF, 2015). In the context of this study, a sustainable groundwater source is one that, if used appropriately, can be maintained for an indefinite time without having adverse environmental, economic, or social consequences (Taylor et al., 2013). Globally, preventable water and sanitation-related illnesses cause an estimated 1.8 million deaths every year, with approximately 1,000 children dying every day (United Nations, 2016). In addition to health issues, more children fail to complete their schooling, and families lose money and time when a potable water source is not readily available (United Nations, 2016).

More than two-thirds of the population in Sub-Saharan Africa depart from their homes to collect water, while adult females are the primary collectors (Graham et al., 2016). Reducing this time demand has the potential to free up time to perform other tasks, including improving both domestic and personal hygiene, while preventing health-related challenges associated with water collection. Water collection is physically demanding and has led to musculoskeletal damage, soft tissue damage, and arthritis (Fry et al., 2010). Many students are forced to leave school early to

watch over their younger siblings while their mothers retrieve water or to fetch water themselves (Hemson, 2007). When there is no potable water supply, students have difficulty concentrating on their work because of fatigue and thirst.

The United Nations' Millennium Development Goals (MDGs) included a water-specific target to reduce the proportion of people without access to improved water sources by 50 % by the year 2015. Globally, this goal was met in 2010 – five years ahead of schedule, but there were a number of countries in Africa that did not meet this target, including Niger (United Nations, 2015). From 1990 to 2015, 1.9 billion people gained access to improved water sources (United Nations, 2015), including boreholes, protected springs, and piped water (Graham et al., 2016). The UN continues to prioritize access to water and sanitation. Specifically, the sixth Sustainable Development Goal (i.e., the successor to the MDGs) is to achieve universal access to safe and affordable drinking water and adequate sanitation and hygiene by 2030 (United Nations, 2016).

Despite recent progress, over 50 % of the rural Nigerien population lack access to safe drinking water, and less than 6 % have access to basic sanitation facilities (WHO/UNICEF, 2017). With a short life expectancy, low literacy rate, and poor standard of living, Niger has consistently ranked in the bottom two of the United Nations Human Development Index since 1995 (United Nations Development Programme, 2016). With an expected population growth from 20 to 70 million by 2050 (The World Bank, 2017), Niger's limited access to safe water translates to vulnerabilities in health, sanitation, and exacerbating socioeconomic issues.

Traditionally, drinking water in the study area has been collected from unimproved sources (i.e., sources that are unprotected from outside contamination), including surface-water bodies and poorly constructed wells. Over recent years, non-governmental organizations have improved residents' access to groundwater sources through improved technologies allowing deep borehole drilling though granitoid bedrock.

In general, groundwater provides a viable replacement to unimproved sources because its quality is superior. However, it may require treatment to make this source potable. Groundwater in Niger contains naturally occurring chemicals in excess of World Health Organization (WHO) drinking water guidelines, including Al, As, Pb, U, and F (Lutz et al., 2013), and anthropogenic contaminants such as NO_3 (World Vision Niger water-quality database), posing serious health risks if consumed.

Specifically, in the communities of Torodi, Koubo, and Sirimbana, groundwater-quality data are limited and groundwater studies non-existent, challenging use of these waters. As groundwater becomes more prominent in these rural regions, water quality and the sustainability of this resource will require closer monitoring. In pursuit of such understanding, the following research questions are proposed:

1) Are any chemical concentrations in excess of the WHO drinking water guidelines?
2) What are the chemical characteristics of groundwater in the study area?
3) What are the natural and anthropogenic factors controlling spatial and temporal variations in groundwater chemistry?
4) How does the groundwater chemistry vary over time and are there trends throughout the study area?

2.0 Background and Literature Review

2.1 Hydrogeography and Climate

Niger is a land-locked nation located in West Africa (Figure 1) that covers an area of approximately 1.3 million square kilometers. The study area (referred to herein as the "Torodi region" or the "region") includes the communities of Torodi, Koubo, and Sirimbana, located within the Torodi Department of the Tillabery Region. The capital city, Niamey, is 55 kilometers (km) to the northeast and the border with Burkina Faso lies 45 km to the southwest.

The region's climate is typical of the semiarid Sahel, where air temperatures range from 8 °C in January to 45 °C in May (Girard et al., 1997). Average total annual rainfall over a 35-year period (1981-2016) was approximately 540 millimeters (mm) (Figure 2). The rainy season occurs from May to September and the dry season from October to April (Table 1). Annual potential evapotranspiration can reach up to 2,500 mm and dominates precipitation throughout the year, especially during dry months (Bromley et al., 1997).

Rainfall in the Torodi region has strong inter-annual and spatial variability. In 2016, the measured total annual rainfall was 757 mm, with 75 % falling between July and August as high intensity storms (Table 1). Bromley (1997) observed rainfall amounts that varied by up to 30 mm over just a few kilometers for a single storm near the community of N'douroua in southwest Niger. Taupin et al. (1993) observed a 50 % variation (i.e., from 389 to 782 mm) in total rainfall from April-October 1992 over distances of less than 60 km within the HAPEX-Sahel study area in southwest Niger.

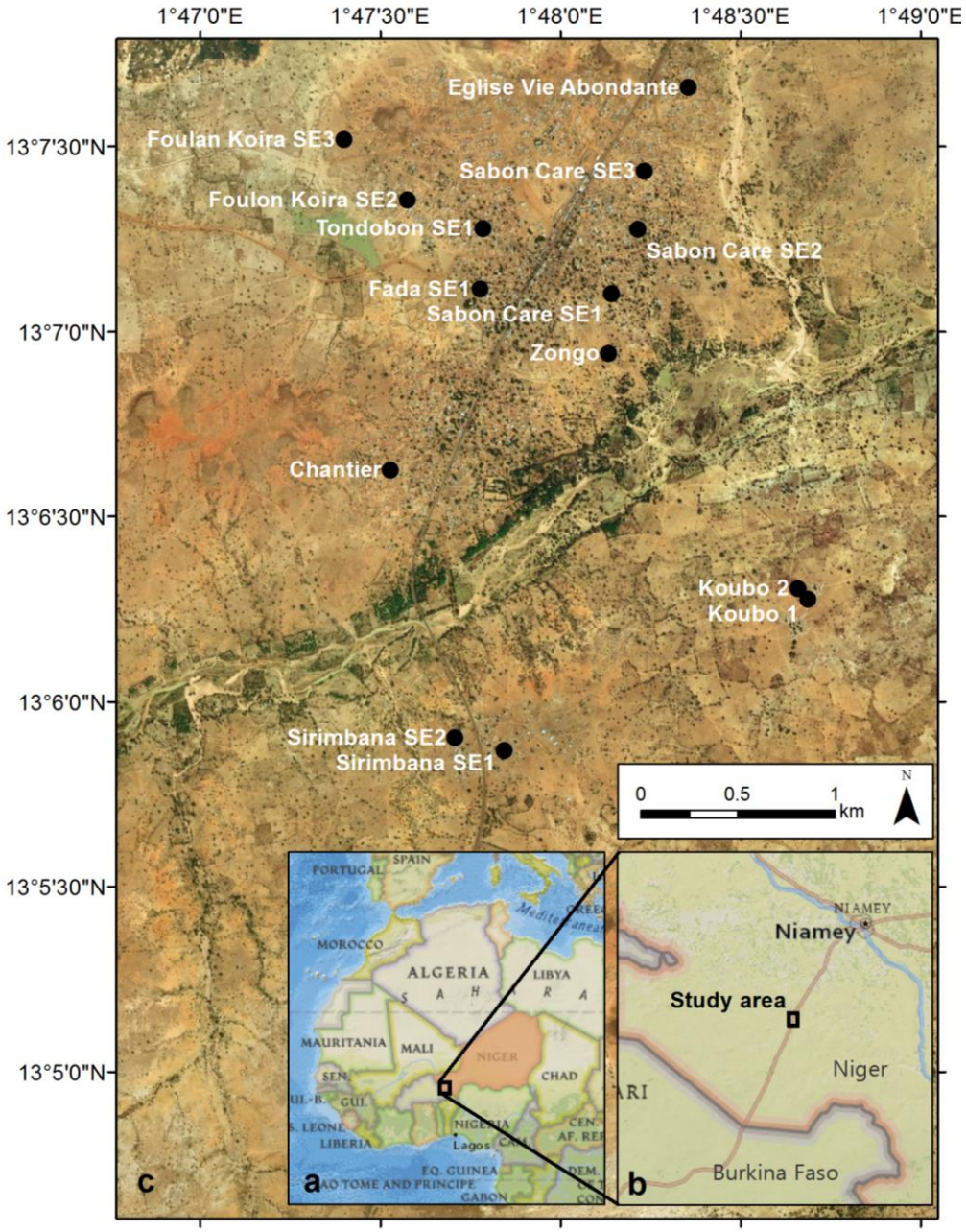

Figure 1. Maps of a) West Africa with Niger highlighted in orange, b) southwest Niger, and c) the study area and labeled sampling locations (black circles). All sampling locations north of the river bed are in the community of Torodi, while the two most southwesterly locations are in Sirimbana, and the two most southeasterly are in Koubo.

Table 1. Measured 2016 monthly rainfall in Torodi. Data received from Niger's Ministry of Meteorology.

Month	Rainfall (mm)	Percent (%) of annual rainfall
January	0	0
February	0	0
March	0.1	0
April	20.5	3
May	35	5
June	76.1	10
July	301	40
August	263.1	35
September	61	8
October	0	0
November	0	0
December	0	0

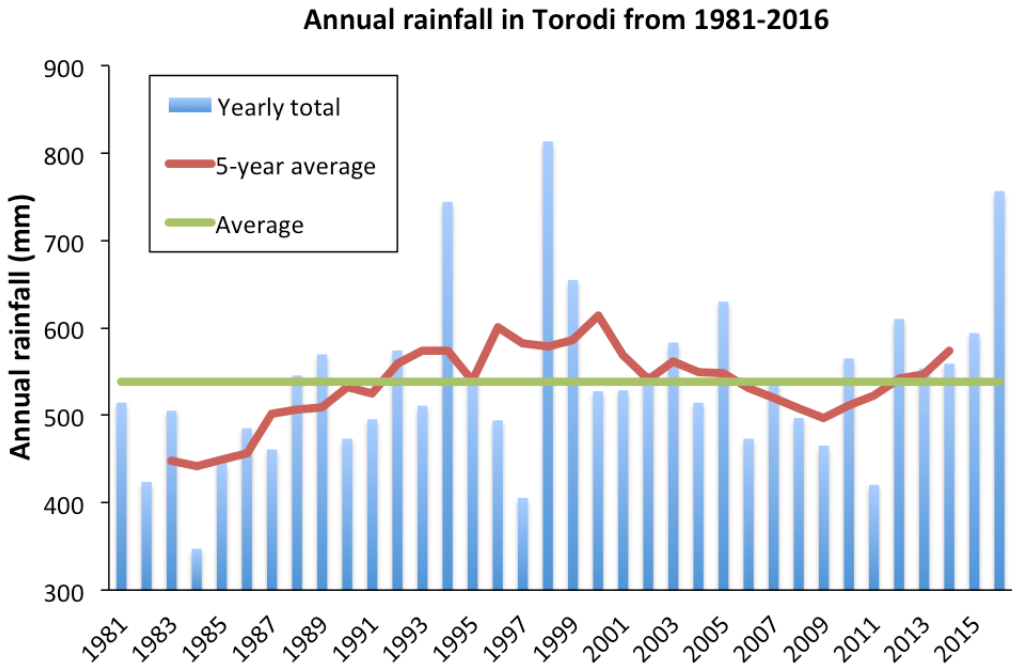

Figure 2. Total annual rainfall, average rainfall, and 5-year running average in Torodi from 1981 to 2016 (CHIRPS data archive and Ministry of Meteorology of Niger).

The Torodi region's drainage basin is part of the greater Niger River basin. The Torodi basin is defined by hills to the north and south, the Kobio basin to the west, and another basin to the east. The Goroubi River, a major tributary of the Niger River, flows through the region from the southwest to the northeast (Figure 3). Locally, the Goroubi is fed by three tributary-like streams, known as "koris" (Girard et al., 1997).

Flow is seasonal in all local tributaries of the Niger River, including the Goroubi River where flow duration depends on storm frequencies and intensities (Girard et al., 1997). Once the flow ceases in the early dry-season, ponds form in low-lying areas of the riverbed, where some remain until the following rainy season. Based on the 2016 Landsat 8 image collection, the Goroubi River flowed for at least six months. Landsat 8 images reveal that the koris rarely flow for longer than one month.

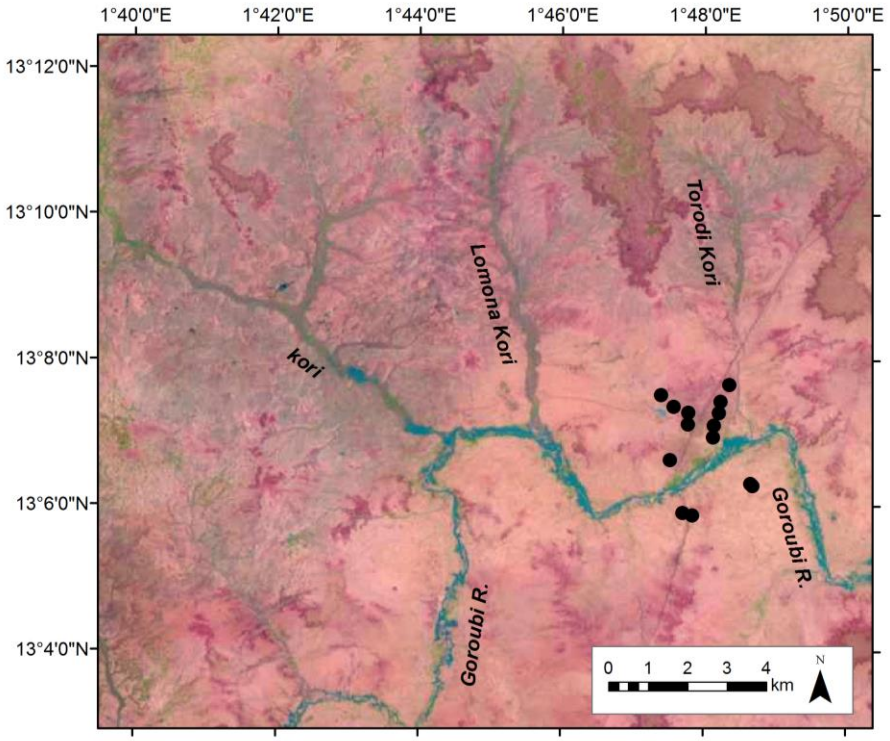

Figure 3. The hydrographic network of the study area and sampling locations shown as black dots (Landsat 8 image archive).

A lake in the northwest of the study area, approximately 150 m southwest of site Foulon Koira SE2 (Figure 1c, light green area), typically reaches peak volume in September. The lakebed is approximately 750 m long and 250 meters wide and can retain water until the following rainy season (Landsat 8 image collection). During intense rain events, sheet flow is generated over the bare, crusted soil and moves downslope until it reaches a water body, forms a temporary pool, or ponds beneath strips of vegetation (Bromley et al., 1997).

Land cover in the region is summarized in Table 2 and illustrated in Figure 4 and mostly consists of bare soil, agricultural fields, and rural residential areas, though there are also expansive areas of sand, steppe vegetation, riparian zones, and ephemeral lakes and rivers that are sandy or clayey surfaces when out of season. Residential areas have relatively high population densities and the land is covered predominantly by houses and dirt roads. The agricultural fields did not contain crops during the study period because it was not the growing season. The land is flat, with an elevation range of 14.5 meters; a low of 210 meters above sea level (masl) at Zongo and a high of 224.5 masl at Sirimbana SE1 (sites are labeled in Figure 1c).

Table 2. Percentage of each land-cover category in the study area, number of sampling locations in each category, and number of samples collected in each category.

Land cover	Percent (%) of study area	Number of sites	Number of samples
Bare soil	28	4	22
Agriculture	26	3	14
Residential	21	7	35
Sand	17	0	0
Steppe	5	0	0
Riparian	3	0	0

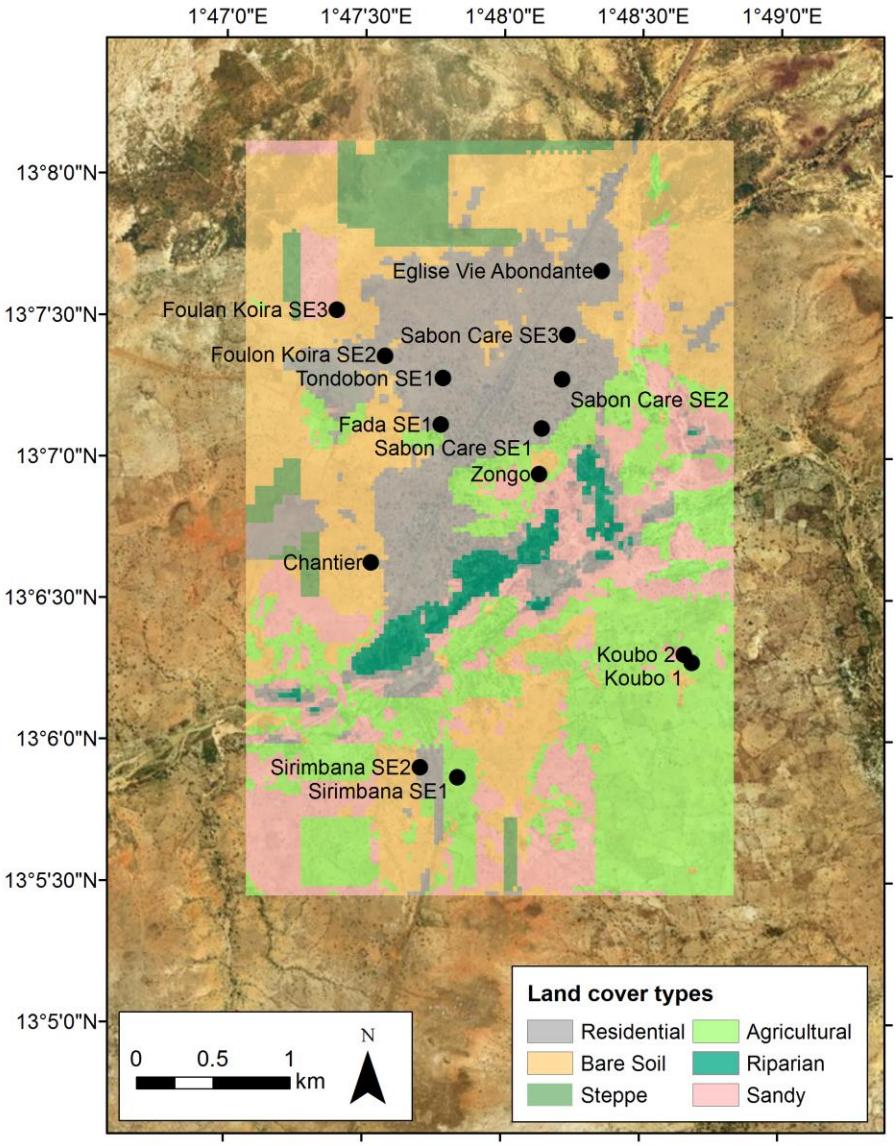

Figure 4. Land-cover map of the Torodi study area. Sampling locations shown as black dots.

Two factors largely distinguish southern from northern sites. The first is anthropogenic; sites south of the river have a lower population density and land cover is predominantly agricultural, while northern sites have a greater population density and land cover is largely residential (Figure 4). The second is mineralogy; the aquifer at the northern sites has greater quantities of soluble plagioclase, while the south has higher percentages of weather-resistant quartz (Bonnot et al., 1998). Mineralogy and geology are discussed in greater detail in subsequent sections.

The Torodi region encompasses a population of approximately 13,450 (World Vision Niger Statistics). The communities of Torodi, Koubo, and Sirimbana are rural communities that rely mostly on rain-fed cultivation of staple millet and sorghum. However, subsistence agriculture is extremely challenging because of periods of insufficient rainfall and economic constraints (Zones, 2005). Traditionally, the agricultural cycle in southwest Niger was a 20-year fallow period when the land would be left unsown to restore its fertility followed by a 10-year cropping phase. This cycle has been replaced by 5-year fallow and 10-year cropping sequences because of population growth and the lack of fertilizers (Ibrahim et al., 2014).

An increase in Sahel rainfall has been observed since the 1990s and is attributed to increased greenhouse gas emissions (Rodríguez-Fonseca et al., 2011). Some climate projections for southern Niger show a reduction in annual rainfall, which may result in reduced recharge to groundwater and lowering of groundwater levels (Africa Adaptation Program, 2011). Though the long-term impact of these reductions is expected to be minimal, the greatest vulnerability will result mainly from dynamic withdrawals for irrigation (Africa Adaptation Program, 2011).

2.2 Geology

The geologic complex of southwest Niger, known as the Liptako, marks the northeastern segment of the Paleoproterozoic Leo Rise of West Africa and consists of alternating granitoid-

greenstone belts (Pons et al., 1995; Figure 5). The Liptako is a 2.1-billion-year old zone of crustal growth that formed as a part of the Birimian terranes of West Africa. The Birimian System is divided into the older "Lower Birimian" and the younger "Upper Birimian" (Pons et al., 1995). The Lower Birimian consists of volcano-sedimentary greenstone belts that include metabasalts and metasediments and the Upper Birimian consists of granodioritic plutons (Pons et al., 1995).

Three large granodioritic batholiths from the northwest to southeast of the Liptako are defined: the Tera-Ayorou, Dargol-Gotheye and Torodi batholiths (Figure 5), which underlie about 70 % of the exposed Paleoproterozoic rocks of southwestern Niger (Machens, 1967). These batholiths consist of elliptical, medium-grained granodioritic plutons that range in size from 500 to 5,000 km^2 (Pons et al., 1995). Plutonism of the Liptako lasted about 50 million years, starting with the Tera pluton and ending with the Torodi pluton (Pons et al., 1995).

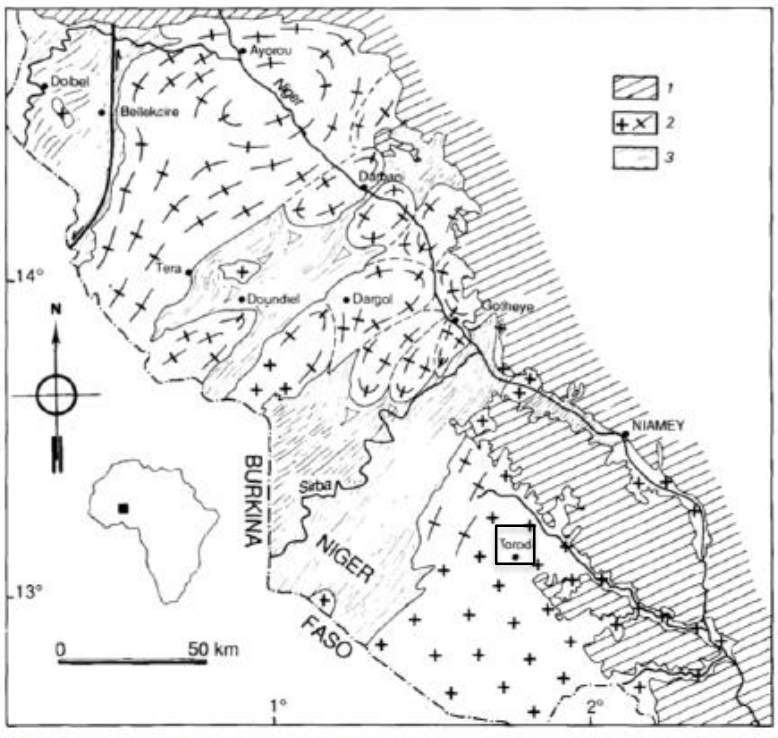

Figure 5. Sketch of the Paleoproterozoic granite-greenstone complex of the Liptako in southwest Niger. The study area is within the black square. 1-Sedimentary cover; 2-granite; 3-greenstone (Modified from Pons et al., 1995)

The study area is located above the Torodi pluton (Figure 5). The geology of the Torodi drainage basin in described in Figure 6. The geology of the northern sites includes tonalites and granodiorites with phenocrysts of plagioclase, amphibole, and biotite, while the southern sites include quartz-bearing tonalitic diorites with amphibole and biotite. Hereafter, the rocks within the study area are referred to as granodiorites. Late Tertiary continental deposits of the Continental Terminal (CT3) Formation are present along much of the eastern perimeter of the basin. These deposits formed from the erosion of the crystalline formations that surround the Iullemeden Basin of western and south-central Niger, and consist of sands, silts, clays, and sandstones including lateritic layers (Le Gal La Salle et al., 2001).

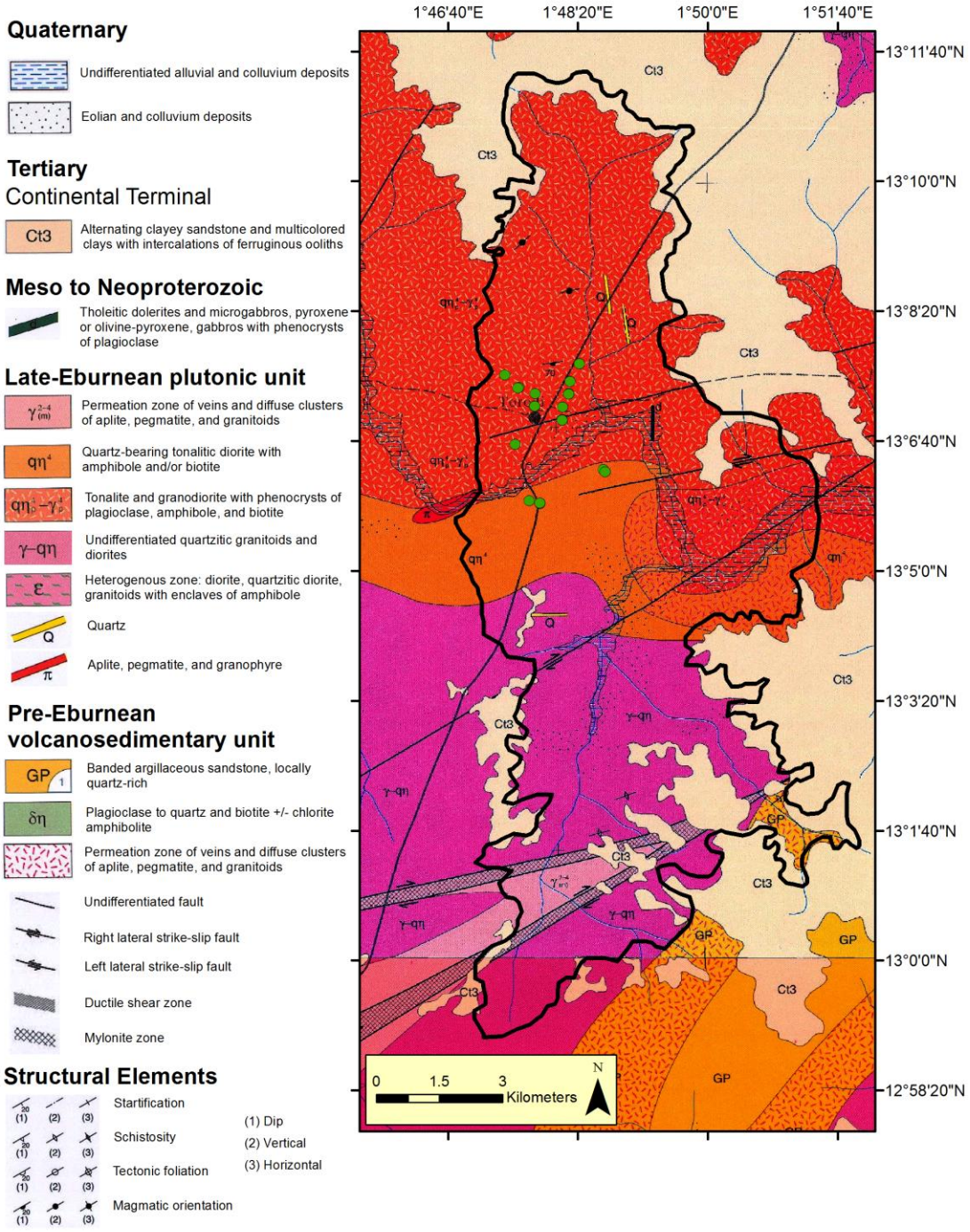

Figure 6. Geology of the Torodi drainage basin (outlined in black) (Modified from Bonnot, 1998). Sampling locations are marked by the green dots.

2.3 Hydrogeology

Birimian basement aquifers are part of a weathering profile that includes multiple layers, each with distinctive hydrogeological properties, resulting in a composite aquifer (Yidana et al., 2012). Most of the groundwater reserve is within fractured bedrock, but the weathered residual of the basement rock may be a part of the aquifer as well (Yidana et al., 2012). Hereafter, this study will refer to the two different aquifer characteristics as fractured and weathered, respectively. The Niger Integrated Water, Sanitation, and Hygiene Project (NI-WASH) borehole logs in section 7.2 of the appendix refer to the weathered layers as "altered." A substantial quantity of groundwater is provided when fractures are expansively connected (Yidana et al., 2012), though even where these aquifers are continuous, permeability is low and groundwater flow systems are relatively localized (Wright, 1992). The fracturing and weathering of the Birimian formations results in a high degree of secondary porosity (Yidana et al., 2012). The recovery of material during drilling, as recorded in the NI-WASH borehole log database, indicates that a weathering profile (Figure 7) exists at each sampling location.

Figure 7. Left: Typical hard-rock weathering profile (Courtois et al., 2010). Right: Hills of well-preserved weathering profiles in southwest Niamey, Niger (55 km northeast of the study area). Erosion has carved out the areas between the hills.

The amount of weathering increases upward through the weathering profile. The fresh granodiorite basement consists mostly of primary silicate minerals like quartz, K-feldspar, plagioclase, biotite and amphibole (Appelo and Postma, 2006). Unaltered granodiorite basement rock has few-to-no fractures and is usually considered impermeable and acts as the base of the aquifer (Marechal et al., 2004).

Above the basement is the fractured granodiorite layer (see Figure 7, fissured layer), where up to 90 % of the groundwater may be found, depending on the thickness of the overlying layers (Wyns et al., 2004). The fractures form from the swelling of certain silicate minerals in the presence of water and fracture density increases upward through the layer (Dewandel et al., 2006). Where fracture density is high, the hydraulic conductivity may reach 2.5×10^{-3} m s^{-1}, thus, the fractured layer regulates the transmissivity of the composite aquifer (Dewandel et al., 2006).

Prolonged chemical weathering of primary minerals in granitoids forms secondary minerals including clays (i.e., kaolinite and montmorillonite) and Fe-oxides that make up much of the weathered layer (see Figure 7, saprolite layer), which is above the fractured zone (Courtois et al., 2010; Appelo and Postma, 2006). The hydraulic conductivity is greatly reduced in this layer (i.e., 5.1×10^{-5} ms^{-1}) because most ancient fractures have been destroyed by recent chemical weathering (Dewandel et al., 2006). The bulk porosity of the weathered layer may reach 30 % because of its sandy-clayey composition (Dewandel et al., 2006; Wyns et al., 1999). Where saturated, this layer contributes to the storage of the composite aquifer (Dewandel et al., 2006).

The top layer of the weathering profile is a highly weathered and Fe-rich laterite that can be up to 3 meters thick (Bromley et al., 1997) or non-existent and may have limited lateral extension depending on erosion rates (Courtois et al., 2010). Because laterite is typically thin and is near the surface, it is not a part of the composite aquifer. Laterite is very hard because of alternating wet-dry sequences, but is permeable, as fractures, joints, termite tunnels, and tree and

shrub root channels provide potential routes for percolation (Bromley et al., 1997). Over time, weathering profiles can be partially carved out by erosion, leaving behind isolated hills (Figure 7).

Aquifer parameters vary depending on the degree of fracture development and weathering. Aquifer parameters of the Torodi region are not well documented; however, Girard (1997) determined that transmissivity values range from 10^{-6} to 10^{-4} m^2 s^{-1} in the Kobio drainage basin, approximately 3 km northwest of Torodi. The transmissivity of the fractured Precambrian basement aquifer in nearby Niamey ranged from 10^{-5} to 10^{-2} m^2 s^{-1} (Girard and Hillaire-Marcel, 1997), while the average measured transmissivity of the fractured granodiorite aquifer in Makalondi (35 km southwest of Torodi) was 1.66 x 10^{-4} m^2 s^{-1} (Garba, 2014).

Groundwater recharge in the region occurs as localized recharge through beds of ephemeral streams and ponds into fractures (Girard et al., 1997) or by widespread, diffuse recharge through the soil (Bromley et al., 1997). Recharge rates vary depending on annual rainfall amount, storm intensity, topography, vegetation cover, land-use, and soil moisture (Valentin and D'Herbès, 1999). Clearing native vegetation for farming enhances runoff, which then concentrates in ephemeral ponds, infiltrates, and potentially reaches the water table (Leduc et al., 2001).

Recharge rates in the region are, thus, highly dependent on land use. Simulations of groundwater recharge in the Wankama catchment, east of Niamey, resulted in rates of 25 mm yr^{-1} at 10 m depth under millet fields and 0 mm yr^{-1} beneath fallowed fields. Increased drainage under millet fields was attributed to relatively low evapotranspiration rates (Ibrahim et al., 2014). Bromley et al. (1997) observed higher groundwater levels under millet and fallow land than beneath neighboring tiger bush vegetation.

In the Kobio Basin, Girard (1997) observed increasing ^{18}O content in groundwater with rising static groundwater levels at the Goroubi-Lomona confluence (Figure 3), concluding that evaporated waters from rivers and streams contribute the majority of recharge to the fractured aquifer. This source of recharge implies that anthropogenic activities that impact river water quality and quantity could impact groundwater (Gibrilla et al., 2011). Girard (1997) also suggested hydraulic continuity within the aquifer where groundwater flows northward, opposite to the direction of flow in the Lomona Kori (Figure 3).

2.4 Groundwater Chemistry

Groundwater chemistry is altered over-time by both natural and anthropogenic factors leading to a complex characterization of groundwater quality. Natural factors include mineral weathering, evaporation, aquifer lithology, cation exchange, soil leaching, recharge water quality, and root-water uptake. Anthropogenic factors include industrialization, urbanization, and leaching of fertilizers (Raju et al., 2016). The degree to which mineral weathering impacts groundwater chemistry depends on groundwater residence time in the rock, temperature, and pH. This process, however, is slow even when desired conditions of low pH and high temperatures are met (Yidana et al., 2012). Birimian granitoid aquifers generally have low concentrations of total dissolved (TDS) (Yidana et al., 2012), typically resulting from low weathering rates or the presence of relatively younger water from a nearby recharge zone (Yidana et al., 2012). TDS represents the amount of dissolved major cations and anions in a solution and the concentration in groundwater may be dictated by the extent of water-rock interaction that has taken place, in addition to anthropogenic activity (Gibrilla et al., 2011).

Referring to the weathering profile (Figure 7), minerals in the parent granodiorite rock dissolve sequentially based on their dissolution rates. For example, plagioclase dissolves first, followed by hornblende, biotite, K-feldspar, muscovite, and finally quartz (Appelo and Postma,

1993). New secondary minerals form because of the insolubility of Al compounds (Appelo and Postma, 1993). When exposed to carbonic acid, feldspars weather first to form gibbsite ($Al(OH)_3$) if sufficient Al is released. If the groundwater becomes oversaturated with gibbsite, clay minerals form beginning with kaolinite ($Al_2Si_2O_5$). With the accumulation of silicic acid (H_4SiO_4), kaolinite can convert to Na and Ca-montmorillonite or other clays (Stumm and Morgan, 1993).

Laterite develops as a result of the prolonged weathering of minerals in the parent rock. Laterites are depleted of soluble minerals, rich in Fe and Al, and may have high Cr, V and Ni content (Hill et al., 2000). The overall impact of silicate mineral weathering on groundwater chemistry is the addition of dissolved cations and SiO_2 (Appelo and Postma, 1993). However, if carbonic acid reacts with the primary minerals, HCO_3 will form as well. Bicarbonate (HCO_3) tends to predominate in groundwater where there is sufficient vegetation (Hem, 1985).

Sources of contamination are not well studied in the Torodi region, but nearby observations have been documented. For example, Smedley et al. (2007) observed high-arsenic groundwater derived from gold mineralization zones in the Birimian volcano-sedimentary rocks of northern Burkina Faso. In Niamey, 10 % of the deep wells exploiting water from the Birimian fractured aquifer were contaminated with NO_3 (Girard and Hillaire-Marcel, 1997). High NO_3 is often attributed to clearing of natural vegetation, which destroys root networks and can trigger the release of NO_3 into the groundwater (Girard and Hillaire-Marcel, 1997). Improper construction and drainage of homemade latrines is also a significant source of NO_3 to groundwater systems in these areas (Girard and Hillaire-Marcel, 1997).

The NI-WASH water-quality database indicates that between 2009 and 2015, NO_3 levels exceeded the WHO guidelines in 17 of 131 boreholes drilled in the south Liptako (Appendix 7.1). For the purposes of this study, all guidelines are discussed with respect to the 2011 WHO drinking water-quality guidelines (Gorchev and Ozolins, 2011). In addition to elevated NO_3

concentrations in the south Liptako, Fe, Mn, and TDS, each exceed their respective guidelines at five of the 131 sites (Appendix 7.1). High Fe and Mn concentrations may be related to the dissolution of Fe and Mn-rich minerals in the sediments and in the aquifer (Yidana et al., 2012). For example, high Fe concentrations were observed in some samples collected near pyrite formations. Of note, these elements were not analyzed in the study area, but could suggest groundwater quality typical in this region.

Figure 8 includes two Piper diagrams demonstrating groundwater types in the south Liptako. The NI-WASH groundwater data from 2009 to 2015 indicate Ca-Mg-HCO_3, Na-K-HCO_3, and Ca-Mg-Cl water types, with the vast majority being the Ca-Mg-HCO_3 type. Groundwater chemistry data collected from different boreholes by Niger's Ministry of Hydraulics from 1981-1984 indicate these same three water types.

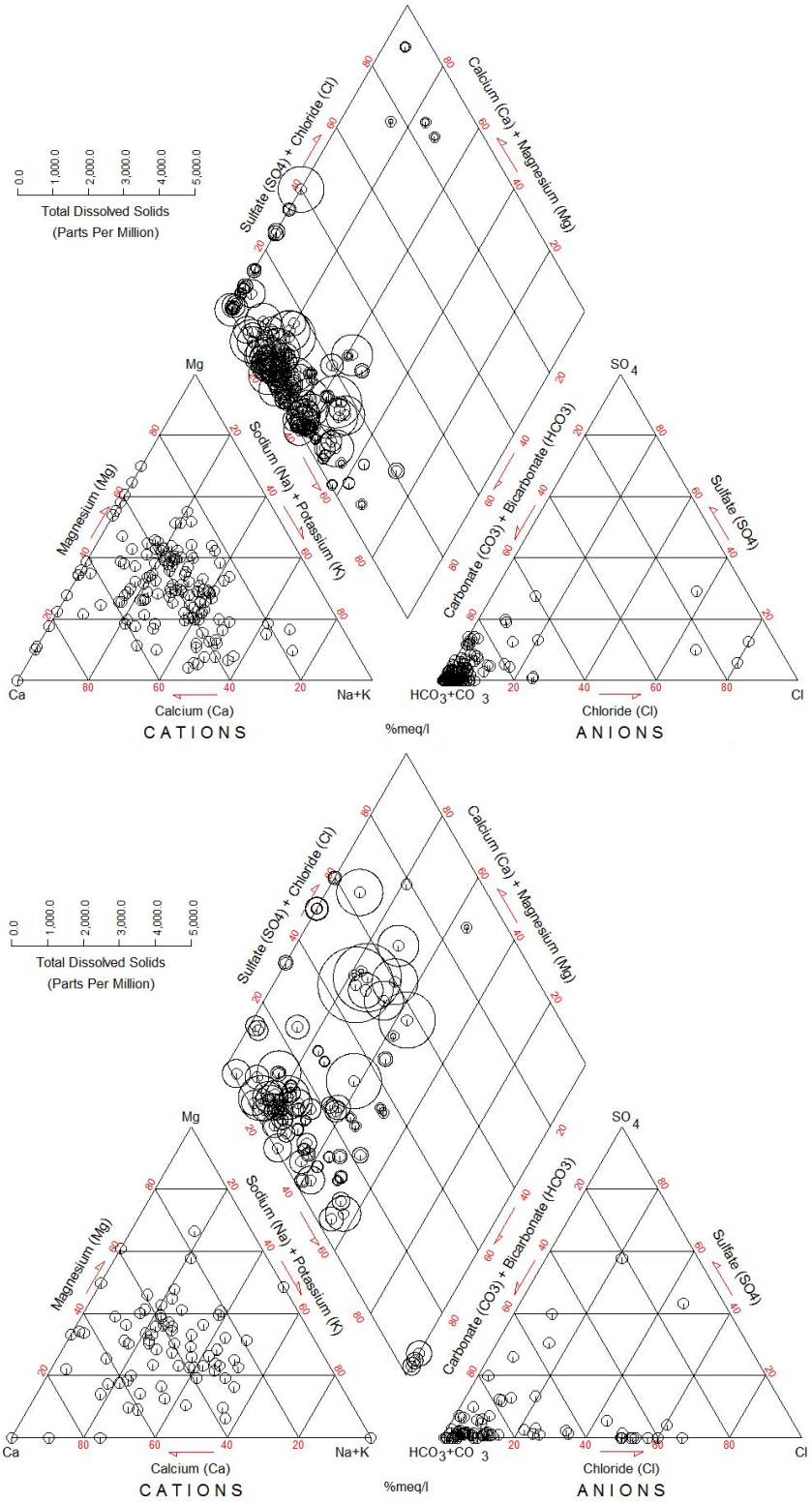

Figure 8. Piper diagrams of major ion concentrations in groundwater samples collected in the south Liptako from 2009 to 2015 by NI-WASH (top) and 1981 to 1984 by Niger's Ministry of Hydraulics (bottom). The radius of a circle in the diamond is proportional to the TDS for that sample.

2.5 Exploratory Data Techniques

Piper, Durov, and Stiff diagrams are three multivariate graphical methods that segregate analytical data into water types. Stability diagrams indicate which minerals are stable in the aquifer based on element activity, dissolved SiO_2 activity, and pH conditions. A Gibbs diagram (Gibbs, 1970) is divided into zones based on the ratio of Na concentrations to the sum of Na and Ca concentrations and the TDS content of typical rainfall/recharge water, water dominated by rock/mineral weathering, and water defined by evaporation/crystallization. This diagram is commonly utilized in groundwater chemistry studies to determine the source of dissolved solids (Yidana et al., 2012).

For purposes of this study, correlation coefficient matrices were generated to show the extent of correlation between each physicochemical variable. Preferred methods exist for calculating correlation coefficients depending on distribution shape, required robustness, and whether the variables contain censored data (Helsel and Hirsch, 2002). Kendall's correlation coefficient (i.e., tau, or Kendall's τ), measures the strength of both the linear and nonlinear monotonic correlations of all variables. Kendall's τ is rank-based, meaning that it determines whether data point a is greater or less than data point b, and is, therefore, resistant to outliers. This method is appropriate for measuring correlation when one or both variables contain censored data values because typically, all values below the detection limit for a given variable are assigned the same rank (Helsel and Hirsch, 2002). Censored data are introduced and defined in section 2.8. Tau values are often lower than those obtained by other correlation coefficient measurements, such as Pearson's r and Spearman's ρ, because it operates on a different scale. For example, a "strong" correlation of r equal to 0.9 equates to a τ of approximately 0.7 (Helsel and Hirsch, 2002).

2.6 Multivariate Statistical Techniques

A spatial groundwater chemistry study is intrinsically a multivariate problem because multiple chemical variables are associated with more than one sampling location (Wanda et al., 2011). Exploratory data analysis techniques used for groundwater geochemistry, such as Piper, Durov, and Stiff diagrams, are not capable of quantitatively analyzing the physicochemical data simultaneously, and thus, the interpretation of results are qualitative.

Multivariate statistical techniques are well-established tools used to examine and compare multiple variables at once, thus, yielding quantitative results that can be used to better understand the sources or processes that control the spatial and temporal variability in groundwater chemistry, and their relative significance (Yidana et al., 2012).

Principal Component Analysis (PCA), specifically, is a variable reduction technique that assists in determination of the sources of dissolved constituents in groundwater (Chowdhury and Al-Zahrani, 2014). Variable reduction is often applied to water-chemistry datasets that include multiple water samples defined by a range of physical (i.e., pH, TDS, temperature) and chemical (i.e., major ions and trace elements) variables. PCA is, thus, useful because the number of variables are reduced, simplifying analyses and interpretations, while maintaining the majority of the information. New variables are constructed, referred to as principal components or PCs that consist of linear combinations of the original physicochemical variables. Each original variable is assigned a "loading" value on the new PC variable, indicating its level of contribution to the PC.

How these original variables are grouped helps to identify the source or process that controls the groundwater chemistry (Chowdhury and Al-Zahrani, 2014). Generally, variables with opposing loading signs (i.e., positive and negative) are less correlated than variables with the same loading sign. If, for example, PCs are computed for four original variables (i.e., Na, Cl, Ca and CO_3) and principal component 1 (or PC1) equals 0.79 Na + 0.8 Cl - 0.75 Ca - 0.93 CO_3, then,

the high positive loadings of Na and Cl on PC1 (i.e., 0.79 and 0.8, respectively) may indicate halite dissolution or saltwater intrusion, depending on the local environment. The significant negative loadings of Ca and CO_3 (i.e., -0.75 and -0.93, respectively) may indicate the dissolution of calcite.

Extending on the above example, each groundwater sample in the analysis is assigned a "score" for the first PC (PC1 score) to demonstrate the impact of PC1 on that sample. Generally, sites with positive PC scores are represented by variables with positive PC loadings and vice versa. If, upon further investigation in this example, the calculated PC1 score for a sample is positive and the sample was collected from a coastal aquifer, salt-water intrusion is likely the main control on the groundwater chemistry. A sample with a negative PC1 score that was collected from an inland location is less impacted by salt-water intrusion and more affected by a processes causing variance in the negatively loaded variables (i.e., Ca and HCO_3), such as the dissolution of calcite.

PCs are uncorrelated (orthogonal) and are constructed with decreasing degree of importance with the first component (PC1) explaining the most variance and each subsequent component (PC2, PC3, etc.) accounting for less variance. It is possible to produce as many principal components as there are original variables, but this would defeat the purpose of a dimension reduction technique (Yidana et al., 2012). The Kaiser criterion (Kaiser, 1960) offers a method to reduce the number of variables by considering only PCs with eigenvalues ≥ 1 as significant. Past water-quality studies have used this this method to reduce data dimensionality (Chowdhury et al., 2008; Varol et al., 2012; Yidana et al., 2012).

PCA is rarely used in isolation and instead interpreted with other graphical techniques to provide meaning to groundwater chemistry analyses (Yidana et al., 2012). Hierarchical Cluster Analysis (HCA) validates the robustness of identified spatial clusters from the PCA and uses

"distance measures" and can be used to assign variables or sample locations to a number of distinct clusters (Yidana et al., 2012; Reimann et al., 2008). The process of clustering sample locations, known as Q-mode HCA, enables the user to distinguish spatial groundwater types (Yidana et al., 2012) based on categories like geology, land cover, or population density. Time-series data for each sampling location can be analyzed in the HCA to determine whether samples collected from the same location cluster together (Steinhorst and Williams, 1985). Euclidean distances indicate the level of similarity of water chemistry between observations in multivariate data space where shorter distances represent samples with more similar chemistry and longer distances indicate samples with disparity (Helsel, 2012).

Both PCA and HCA have been used extensively for spatial and temporal monitoring of groundwater quality around the world. Data collected over several dates from the same wells near a proposed Mo mine in western Colorado were entered as separate samples in an HCA to determine whether they would group in the same cluster (Steinhorst and Williams, 1985). Results suggested that these temporal samples generally grouped in the same cluster, indicating little variation in the groundwater chemistry over time. Raju et al. (2016) used HCA in the Swarnamukhi River Basin in India to illustrate how water chemistry clusters varied from pre-monsoon season to post-monsoon season. HCA and PCA were used in the Fuji River Basin to evaluate the spatial and temporal variations of 12 variables in nearly 15,000 water samples from 13 sites (Shrestha and Kazama, 2007). PCA was used to analyze chemical variations in water samples collected at weekly intervals over a two-year period from the King Fahd Dam Reservoir in southwest Saudi Arabia (Chowdhury and Al-Zahrani, 2014).

2.7 Trend Analysis

Various parametric, nonparametric, and mixed approaches for trend detection have been developed to provide insight into temporal groundwater-quality investigations (Helsel and Hirsch,

2002). To select the appropriate method for evaluating trends, Hirsch et al. (1991) recommends the following be determined: whether the type of trend hypothesis is a step trend or monotonic trend; whether the appropriate statistical method is parametric, nonparametric, or both; and, whether the dataset includes censored data values. Censored values will be introduced and defined in section 2.8.

The nonparametric Regional Kendall test (RKT) is a commonly applied trend analysis in environmental studies (Hirsch et al., 1982). The RKT tests for trends at each observation point and general trends in either a consistent positive or negative direction throughout a particular study area (Helsel and Frans, 2006). Advantages of the RKT nonparametric technique over parametric techniques is that a normal distribution is not required, it is invariant to monotonic power transformations, and it "blocks out" differing borehole characteristics that may impact variable values, such as borehole depth, because no cross-borehole comparisons are made (Helsel and Frans, 2006). However, for the resulting p-values to be correct, errors must be independent and no serial correlation can exist (Helsel and Frans, 2006).

Typically, RKTs are used in water-quality studies to determine whether a trend exists for a single variable or contaminant. Helsel and Frans (2006) used the RKT method to conclude that there was no regional trend for NO_3 concentrations throughout the Columbia Basin in Washington, but trends were significant in two of the three river basin counties. For groundwater management purposes, an RKT was performed to investigate the trends of NO_3, SO_4, and Cl concentrations across various land-use types in the Kangwon Province of Korea. Analysis revealed a significant increasing trend in the NO_3 and SO_4 concentrations in vegetable fields (Kaown et al., 2012).

2.8 Censored Data

Such multivariate statistical analyses (i.e., PCA and HCA) require complete data matrices as input. Environmental studies often include data values known as censored data values, or non-detects, that exist somewhere between zero and a detection limit, complicating any subsequent data analysis (Palarea-Albaladejo and Martín-Fernández, 2015). Estimating values for censored data points is important to accurately calculate basic statistics (i.e., mean, median, and standard deviation) and perform subsequent analyses. Techniques to estimate summary statistics when such censored values exist include substitution (Helsel, 1990), robust regression on order statistics (Helsel, 2012), and distributional methods such as maximum likelihood estimation (MLE), probability plotting, and multiplicative lognormal replacement (Helsel, 1990). Distributional methods are considered unbiased and more accurate than other methods when data fit the assumed distribution (Helsel, 2012; Huston and Juarez-Colunga, 2009). Ultimately, the final choice depends on the study's context and objectives (Palarea-Albaladejo and Martín-Fernández, 2015).

3.0 Methods

A variety of methods facilitated an understanding of characterization of groundwater chemistry. The following sections describe these methods, including procedures used in the field and laboratory, data preparation processes, and techniques used for exploratory, spatial, statistical, and trend analyses.

3.1 Field Methods

To characterize groundwater chemistry in the Torodi region, 71 groundwater samples were collected from 14 boreholes within the communities of Torodi, Sirimbana, and Koubo from December 2016 through May 2017 for trace-element and major-ion analyses. Concentrations of major ions and trace elements are listed in section 7.4 of the appendix. To capture a range of

groundwater conditions, including depletion, steady-state, and recharge, sampling occurred as often as possible through the sampling period. Groundwater samples were obtained from drilled boreholes with hand pumps, as opposed to hand-dug wells (hereafter, sites will be referred to as boreholes). Boreholes were selected to capture the diverse geology, land cover, and population densities to best achieve a representative sampling and to avoid the chance of inadvertently missing trend patterns that occur in the areas not sampled (Helsel and Frans, 2006).

Coordinates (latitude and longitude), elevation, and land cover at each observation point were recorded using a Garmin eTrex 10 global positioning system (GPS) to allow for spatial analysis in ArcMap. Latitudes and longitudes were measured in decimal degrees in the WGS 1984 coordinate system and elevations were measured in masl. To minimize relative error, position and elevation measurements were made in a single day during clear sky conditions when satellite strength is at a maximum. This occurred three times and the average position and elevation for each site was calculated.

Field sampling procedures followed the USGS National Field Manual for the Collection of Water Quality Data (Rounds et al., 2015). Both pH and conductivity meters were calibrated using the manufacturer's instructions. To measure pH and temperature in the field, an Orion 3 Star pH Portable meter was calibrated using a two-buffer calibration to bracket the expected pH range of the respective sampling locations (i.e., either 4.00 and 7.00 or 7.00 and 10.00). An Orion 3 Star Conductivity Portable meter was calibrated using a 250 or 500 $\mu S\ cm^{-1}$ standard, depending on which conductivity was closest to the expected conductivity values for the respective sampling locations.

To ensure that a borehole was adequately purged, pH, conductivity, and temperature were measured before sampling approximately every three to five minutes until stabilized. Groundwater levels were also measured at each borehole prior to sampling using a Waterline

Envirotech Ltd. manual water-level meter. VanEssen Mini-Diver pressure transducers were deployed in six boreholes (Foulan Koira SE2, Fada, Chantier, Zongo, Sirimbana SE1, and Koubo SE2) to make absolute pressure measurements every four hours (12:00, 4:00, etc.) for the duration of the study, providing an accuracy of ± 2.5 cm H_2O. A VanEssen Baro-Diver was placed outside of the World Vision Torodi office to measure atmospheric pressure at the same time interval. Erroneous measurements occurred when a cable likely became tangled around the pipes of the well, leading to false readings. The measurements were corrected by adding 30 cm. In another instance, a logger completely failed to measure after a certain time.

Major-ion samples were collected in 500 or 1,000 milliliter (mL) high-density polyethylene (HDPE) bottles, respectively. Trace-element samples were collected in 35 mL HDPE bottles. Bottles were sterilized with 5 % nitric acid at the Faculté de Science Économique et Juridique de l'Université Abdou Moumouni de Niamey or the Desert Research Institute (DRI). Bottles were rinsed twice with distilled water and then rinsed once with stabilized borehole water immediately prior to sampling. Five trace-element samples were filtered and acidified with 69 % nitric acid for preservation. Remaining trace-element and major-ion samples were unfiltered and not acidified, following DRI's procedure for samples collected at boreholes in Africa. Samples were cooled in a freezer because of the lack of access to a cooler and replaced by another batch after approximately one-hour to avoid freezing. After three cycles, samples were stored at room temperature between one week to three months until being transported to the laboratories.

A modified pump test was performed at the Zongo borehole to measure drawdown, recovery time, and recovery rate of the water table. The pump was locked at night, so no water was pumped for 9 hours before the start of the pump test, allowing a static water level to be measured. All boreholes in this study supply communities, so once pumping commenced, it could not be stopped for long periods to monitor full recovery time. On occasion, pumping would cease

and a partial recovery could be measured. Local men who deliver water to houses and establishments, known locally as ga'ruwa (Youngstedt and Keough, 2016) did the majority of the pumping. When two or more ga'ruwa were at the pump, they had an efficient method to filling their containers and the pumping rate would be held fairly constant. Each ga'ruwa carried ten containers of 20 or 25L per container. Because the volume of each container was known and pumping times were recorded, a pumping rate could be calculated. The Mini-Diver was used to measure the absolute groundwater level every 30 seconds for the duration of the test. Pumping rates and volumes removed from storage were compared to water levels, and recovery data were analyzed.

3.2 Analytical Methods

Samples were analyzed for major and minor ions (i.e., Ca, Mg, Na, K, Cl, SO_4, NO_3, and F), SiO_2, alkalinity, pH, and TDS at the Nevada State Public Health Laboratory (NSPHL). Measured concentrations are listed in section 7.4 of the appendix. Alkalinity was measured by titration following the U.S. Environmental Protection Agency (USEPA) method 2320B; pH was measured with an ion-selective electrode following USEPA method 150.1; and TDS was measured by gravimetry following SM 2540C. Cation concentrations (Ca, Mg, Na, K) were analyzed by inductively coupled plasma optical emission spectrometry (ICP-OES) with USEPA method 200.7 and anions (Cl, SO_4, NO_3, and F) using ion chromatography with USEPA method 300.0.

Trace-element concentrations were determined at DRI; Measured trace element concentrations are listed in section 7.4 of the appendix. Trace elements were measured with an inductively coupled plasma-mass spectrometer (ICP-MS) using standard USEPA procedures. Internal consistency was checked through cation-anion balance and TDS verification (Appendix 7.3).

3.3 Censored Data, Transformations, and Variance

Figure 9 is a flow chart summarizing the steps taken to prepare and analyze the data. Prior to conducting exploratory and statistical analyses, values for censored data were estimated using robust multiplicative lognormal replacement. This is an appropriate method when data are right-skewed with outliers. It is also advantageous because it enables estimation of values for specific observations rather than summary statistics. Thus, non-detected values in the data matrix are replaced so that multivariate statistical procedures can be conducted. Robust replacement estimation was used instead of maximum likelihood because it is less dependent on distributional assumption and is more accurate for "smaller" data sets (Palarea-Albaladejo and Martín-Fernández, 2015).

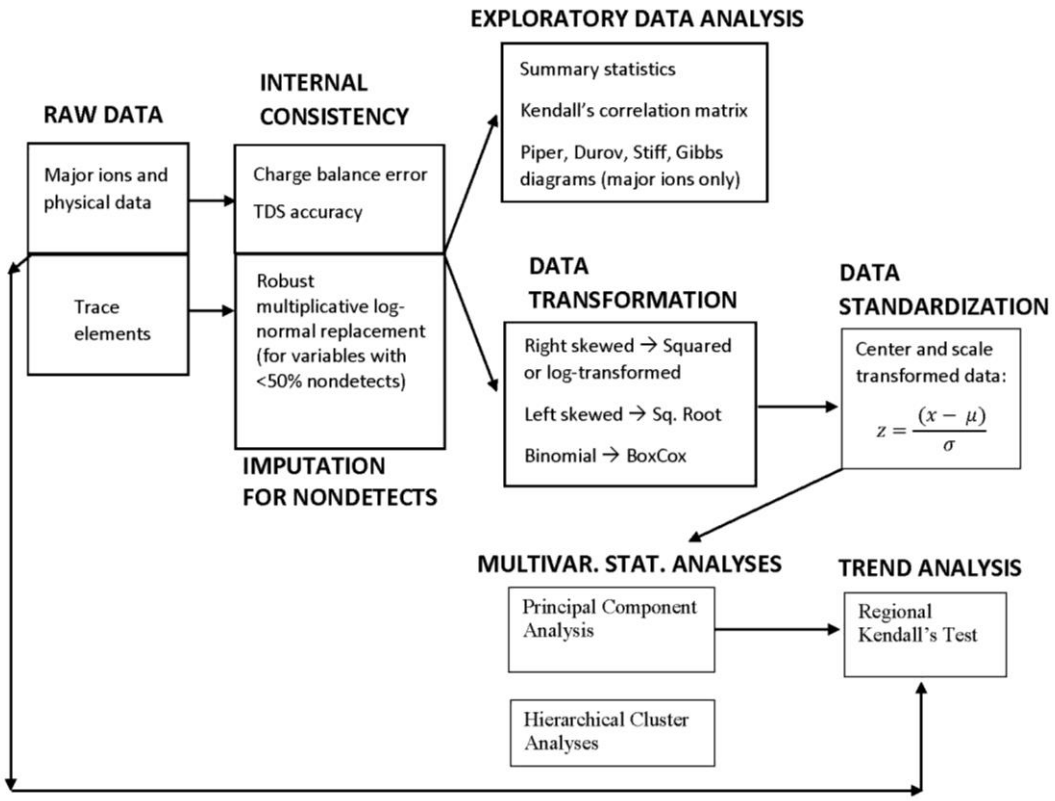

Figure 9. Flow chart summarizing the data preparation and analysis process. Variables with >50 % nondetects were discarded before the imputation for nondetects.

The imputation was carried out using the multLN function of the zCompositions R package (Palarea-Albaladejo and Martín-Fernández, 2015), which relies on robust regression on order statistics (ROS) via the NADA R package. The function computes Weibull-type plotting positions of data that contain censored and uncensored data. Estimates were made in log-space so that methods to compute censored normal variates could be applied (Palarea-Albaladejo and Martín-Fernández, 2015). A linear regression was formed using the plotting positions of the uncensored observations and their normal quantiles. This regression model was then applied to estimate the concentrations of censored data as a function of their normal quantiles.

Although PCA and HCA assume data normality, groundwater chemistry data are typically skewed, requiring data transformations dependent on distribution and skewness. Silica and K concentrations were negatively skewed and squared, while Cl and NO_3 were positively skewed; thus, a square-root transformation was applied. The remaining major ions, F, V, and Cr did not require transformation. Trace elements Al, Mn, Fe, Co, Mo, Zn, Sr, Ba, and Ni were positively skewed and were log-transformed. Se, As, and U were BoxCox transformed using the powerTransform function in R.

Since major ions and trace elements have different scales (mg L^{-1} and μg L^{-1}, respectively), performing PCA or HCA on the raw data would be unproductive because results would favor variables with the greatest variance (i.e., major ions). Each data value was rescaled by the reciprocal of the variable's standard deviation prior to the multivariate analyses so that all variables were weighted equally. The data were also centered on the means of each variable to ensure that data were centered on the origin of the PCs without affecting the variances or spatial relationships. The process of centering and scaling data, referred to as "data standardization", was performed by the equation

$$z = \frac{(x - \mu)}{\sigma}$$

where z is the standardized value, x is the transformed version of the original variable, μ is the mean of that variable, and σ is the variable's standard deviation.

3.4 Exploratory and Spatial Data Analysis

Exploratory data analysis (EDA) utilized boxplots, histograms, and probability plots in RStudio for data observations. Piper, Durov, and Stiff diagrams were created using the AqQA software. Additional information on these diagrams can be found in Helsel and Hirsch (2002). To determine the most stable mineral phase in the groundwater system, silicate mineral stability diagrams were developed (Yidana et al., 2012) using The Geochemist's Workbench software. A Gibbs diagram was made manually according to the section boundaries used by Yidana et al. (2012) and data points were plotted accordingly in RStudio. Saturation indices were calculated with the AqQA software.

A correlation matrix was generated in RStudio using Kendall's correlation coefficient, τ, and accompanying statistics. Helsel and Hirsch's (2002) explanation was followed to calculate τ. First, Kendall's test statistic, S, was calculated by

$$S = P - M$$

where P = the number positive trends (the number of data pairs where the dependent variable, y, increases with the independent variable, x) and M = the number of negative trends (the number of data pairs where the y decreases with x). Then, the null hypothesis (H_o) and alternative hypothesis (H_1) were determined by

$$H_0: \text{probability}[y_j > y_i] = 0.5 \quad \text{where } x_j > x_i$$
$$H_1: \text{probability}[y_j > y_i] \neq 0.5 \quad (\text{two} - \text{sided test})$$
$$\text{for all } i = 1, \ldots, (n-1) \text{ and } j = (i+1), \ldots, n$$

If no correlation exists, and thus, the null hypothesis is confirmed, the number of increasing and decreasing y pairs will be about the same as x continuously increases. In this case, S would be close to zero. Kendall's τ was then calculated to indicate the correlation strength by

$$\tau = \frac{S}{n(n-1)/2}$$

where there are n(n-1)/2 possible comparisons to be made among n data pairs. If all y values increase with increasing x, S = n(n-1)/2, and τ will equal +1. When all y values decrease with increasing x, τ will equal -1. Therefore, τ is in the range of +1 and -1.

Mapping was implicit in this study, so results were geographically displayed using ESRI's ArcGIS to portray groundwater chemistry, groundwater levels, and PC scores at the respective boreholes. Interpolated groundwater-level maps were created using the Empirical Bayesian Kriging method and the land-cover map was made using a supervised image classification technique (Nagi, 2011). Information obtained from the NI-WASH borehole logs was included to aid interpretation of spatial data, including lithology descriptions, layer thicknesses, drilled and equipped depths, air-lift yields, aquifer depths and thicknesses, screen depths, population served, and static water levels.

3.5 Statistical Techniques

Transformed and standardized variables were partitioned into groups based on mineralogy and land cover. An analysis of variance (ANOVA) was used to determine whether or not the means of each variable were significantly different by land cover (i.e., agricultural, residential, and bare soil). A t-test was used to determine if variable means were significantly different between the two mineralogy types (i.e., plagioclase and quartz).

The transformed and standardized data, including both major ions and trace elements, were analyzed as a complete dataset using PCA following other groundwater studies (Qadir et al., 2008; Silliman et al., 2006; Singh et al., 2005; Wanda et al., 2011). The PCA was performed in RStudio using the prcomp function. As described by Holland (2008), with p variables and n samples in a data matrix, the first PC (y_1) was determined by the linear combination of variables $x_1, x_2, \ldots, x_p$ using the equation

$$y_1 = a_{11}x_1 + a_{12}x_2 + \cdots + a_{1p}x_p$$

where the coefficients a_{11}, a_{12}, and a_{1p} are the variable loadings. Recall, these loadings indicate the strength of each variable's contribution to the PC. To limit the variance of PC1, loadings were calculated with the constraint that their sum of squares was equal to 1. The second PC (y_2) was then calculated by

$$y_2 = a_{21}x_1 + a_{22}x_2 + \cdots + a_{2p}x_p$$

This process continued until p PCs had been calculated. Collectively, all of these loadings on the original variables are represented by

$$Y = AX$$

The rows in matrix A are the eigenvectors of the variance-covariance matrix of the original data. The elements in the diagonal of the variance-covariance matrix of the PCs are the eigenvalues, which are equal to the variance explained by each PC.

The position of each water-sample observation in PC space is referred to as the score. Boreholes with similar scores have comparable groundwater chemistry. Time-series data were included in the PCA to determine whether samples from a single borehole have similar scores, or whether they differ. The score of the r^{th} sample on the s^{th} PC is calculated by

$$y_{sr} = a_{s1}x_{s1} + a_{s2}x_{s2} + \cdots + a_{sp}x_{sp}$$

The R package pvclust was used to perform the HCA on transformed and standardized data and assess uncertainty levels for each cluster. The combination of using Euclidean distances to measure observation similarity and the Ward's minimum variance agglomeration method produces optimal HCA results (Yidana, 2010). Ward's agglomeration method ("ward.D2" in R) increases the sensitivity of the approach by squaring the dissimilarities before updating the cluster at each iteration. Euclidean distance measures were appropriate because all data had been standardized and were on the same scale. Euclidean distance is the geometric distance between samples or clusters in multidimensional space and is calculated by the equation

$$d_{jk} = \sqrt{(x_j - x_k)^2}$$

where d_{jk} is the distance between samples j and k, x_j is the vector of water-quality variables for sample j, and x_k is the vector of variables observed on sample k (Reimann et al., 2008). Shorter distances equate to greater similarity between sample chemistry. Similar to the PCA, time-series data from each observation point were added as separate samples to determine whether they group into the same clusters (Steinhorst and Williams, 1985).

Ward's method starts with each groundwater observation as its own cluster (leaf), then the algorithm proceeds iteratively, joining the two most similar clusters (i.e., clusters with the shortest distance between them) into a new bigger cluster (node) at each iteration until there is a single cluster (root). The result is a completed dendrogram (tree) where groundwater samples are clustered by similar chemistry on the x-axis and Euclidean distances are on the y-axis.

The pvclust package uses the hclust function and computes p-values for all clusters via bootstrap resampling. To reduce the standard error of the cluster p-values, 10,000 bootstrap

replications were performed. Two types of p-values were computed for each cluster, an approximately unbiased p-value (AU) and a bootstrap probability value (BP). The AU p-value produces a better approximation because it is computed by multiscale bootstrap resampling, while the BP value is calculated by normal bootstrap resampling and is often reported as biased. The AU p-values were used in the analysis.

To obtain a normal bootstrap probability, a bootstrap replicate of a water sample was produced by randomly drawing with replacement n times (n = the number of water-quality variables) from a parametric probability distribution predicted from the original sample or cluster (Imaizumi et al., 2006). Random sampling with replacement means that the bootstrap replicates consist of values from the original data set, with some appearing zero times, one time, or multiple times (Sohn and Menke, 2002). To form robust estimates of standard error for the p-values and form confidence limits, the number of bootstrap replicates is usually >1,000 (Sohn and Menke, 2002). The p-value for a cluster was then approximated by counting the number of replicates that confirm the null hypothesis of no significant difference between the mean value of the replicate and the mean of the observed sample or cluster (Shimodaira, 2014). The multiscale bootstrap adjusts for bias by extrapolating the normal bootstrapping method and taking more random samples for each replicate.

3.6 Trend Analysis

The RKT tested for trends in PC scores and select variables across the 14 boreholes. To compute the degree of a regional trend, the RKT incorporates the results of the Mann-Kendall test (Helsel and Frans, 2006) performed at each borehole. Kendall's correlation statistics (found in section 3.4) were used for the RKT, however, the independent variable, x, was replaced with time, t. Kendall's S-statistic was first calculated at each sampling location. For a single borehole, the null hypothesis (H_o) was confirmed when the number of increasing pairs over time and

number decreasing were approximately equal, and therefore, no trend was observed. The data indicated a trend in y if S was significantly different from zero (i.e., p-value ≤ 0.05). The median trend was given by the Theil-Sen's (TS) slope, which is a nonparametric estimator based on the median of all pairwise slopes that have been rearranged to have a common origin. For short time-series data, the TS slope is considered more reliable than other methods, like ordinary least squares estimate (Zhang et al. 2017). Kendall's correlation coefficient, τ, was then calculated to measures the strength of the monotonic association between y and t. The RKT computed the overall test statistic, S_R, by summing the individual Kendall's S-statistics, S_L, for each of L = 1 to m locations by

$$S_R = \sum_{L=1}^{m} S_L$$

As previously mentioned, RKT is typically applied in water-quality studies by determining whether a trend exists in individual variables. In this study, a modified approach was used – RKTs were performed on PC scores in addition to individual variables. Groundwater samples were collected sequentially and PCA was conducted on the time-series data, so varying PC scores at each borehole reflect variation over time, and it became possible to determine whether a temporal trend exists in the PC scores. Recall that PC scores are linear combinations of the original variables, so performing an RKT on PC scores can be considered the equivalent of performing the test on multiple variables simultaneously. The purpose of this modified approach was to determine if the degree to which a factor and/or process controls groundwater chemistry shows a trend over time.

4.0 Results and Discussion

Seventy-one groundwater samples collected from 14 boreholes in the Torodi region were analyzed to 1) identify and characterize the natural and anthropogenic factors controlling spatial and temporal variations in groundwater chemistry and 2) determine whether these factors increased or decreased over time. Recall, the aquifer within the study area was divided into northern and southern sections based on mineralogy (Figure 6). Thus, herein, boreholes located in the plagioclase-dominated section in the north are referred to as the northern sites and boreholes in the quartz-dominated section in the south are called the southern sites. The term significant is used to describe a correlation, trend, or difference between group means that is statistically significant and has a p-value ≤ 0.05 or a PC loading ≥ 0.25.

4.1 Field-Laboratory Data Comparison and Accuracy Check

A summary of laboratory-field measurement accuracies is found in section 7.3 of the appendix. All samples showed an increase in pH from the time of field to laboratory measurements, which is not unusual because of the loss of CO_2 to the atmosphere during transport. This phenomenon was caused by not filtering and acidifying in the field, lack of refrigeration, and the length of time from sample collection until analysis.

Hem (1985) states that for waters with moderate dissolved solids concentrations (250-1,000 mg L^{-1}), the CBE will generally not exceed 2 % if the analytical work has been done properly. However, a somewhat larger percent difference can be tolerated for low-TDS water. Mahler (2008) states that charge balances exceeding ±5 % might indicate problems with the analyses. Approximately 83 % of samples (n=59) had CBE values < 2 %, while the remaining 17 % (n=12) of samples had CBE values > 2 % with only one sample > 5 %. Data from all samples were used in the statistical analyses.

Measured and calculated values for TDS should be within a few mg L^{-1} to tens of mg L^{-1} for waters with typical compositions (Hem, 1985). Of the calculated values, 51 % had TDS within 10 mg L^{-1} of the lab-measured values and the greatest difference was 67 mg L^{-1}. Overall, samples demonstrated close matches.

4.2 Imputation for Nondetects

Of the 21 measured trace elements, 15 contained censored data, including: Be, Al, Fe, Mn, Co, Cu, Mo, Ag, Cd, Sb, Tl, Pb, U, As, and Se. The raw trace-element data are provided in section 7.4 of the appendix. The percent of censoring was > 50 % for Be, Cu, Pb, Ag, Cd, Sb, and Tl, so they were removed from the dataset. Trace-element variables with < 50 % censored values are summarized in Figure 29 of Appendix 7.4. Non-detect values were imputed using robust multiplicative log-normal replacement before calculating summary statistics for trace elements (Appendix 7.4) and performing subsequent statistical and trend analyses.

Several major-ion concentrations were below the reporting limit (and thus, considered censored), but were measured above the detection limit of the analytical equipment. These concentrations were assumed to be more accurate than imputing, fabricating, or deleting the censored data altogether, and were, therefore, used in calculating summary statistics and subsequent exploratory and statistical data analyses.

4.3 Exploratory Data

Summary statistics for the 27 physicochemical variables measured in 71 groundwater samples are provided in Table 3. All concentrations existed below the WHO limits and recommendations, indicating that the groundwater was suitable as drinking water. The maximum NO_3 value of 48.7 mg L^{-1}, however, was approaching the WHO drinking water guideline of 50 mg L^{-1}. All other variables existed at concentrations half of their respective guidelines or less.

Table 3. Summary statistics for all measured variables (n = number of observations) and WHO guidelines.

Variable	Units	n	Minimum	Maximum	Median	Mean	SD	WHO Limit	WHO Rec.
Alkalinity	mg L^{-1}	71	65.00	220.00	130.00	128.67	36.56	-	-
pH	-	71	6.34	7.28	6.85	6.84	0.22	-	-
Temp	°C	71	20.90	23.30	22.30	22.14	0.65	-	-
TDS	mg L^{-1}	71	130.00	370.00	210.00	224.93	51.99	-	600
Ca	mg L^{-1}	71	12.20	43.70	22.70	24.44	7.23	-	-
Mg	mg L^{-1}	71	5.70	31.00	15.00	15.32	5.23	-	-
Na	mg L^{-1}	71	6.30	25.00	13.80	14.16	4.51	-	200
K	mg L^{-1}	71	1.60	4.00	3.00	2.92	0.63	-	-
SiO_2	mg L^{-1}	71	66.00	96.00	83.00	81.77	8.16	-	-
HCO_3	mg L^{-1}	71	79.30	268.40	158.60	156.97	44.61	-	-
Cl	mg L^{-1}	71	0.83	15.75	3.53	5.11	4.52	-	250
SO_4	mg L^{-1}	71	3.73	11.52	6.93	6.77	1.61	-	250
NO_3	mg L^{-1}	71	0.18	48.71	13.82	17.80	14.90	50	-
F	mg L^{-1}	71	0.07	0.65	0.36	0.36	0.18	1.5	-
Al	µg L^{-1}	71	0.04	14.08	0.50	1.25	2.29	-	900
Mn	µg L^{-1}	71	0.00	30.93	0.12	1.74	6.08	-	400
Fe	µg L^{-1}	71	0.03	10.38	0.42	1.21	2.00	-	300
Co	µg L^{-1}	71	0.01	0.23	0.03	0.04	0.04	-	-
Mo	µg L^{-1}	71	0.02	11.79	2.09	2.98	3.12	-	-
U	µg L^{-1}	71	0.01	1.12	0.13	0.25	0.32	30	-
Se	µg L^{-1}	71	0.01	0.83	0.02	0.10	0.15	40	-
As	µg L^{-1}	71	0.01	0.09	0.03	0.04	0.03	10	-
V	µg L^{-1}	71	5.62	35.92	26.44	24.16	9.81	-	-
Cr	µg L^{-1}	71	0.03	3.22	0.89	1.08	0.75	50	-
Ni	µg L^{-1}	71	0.11	1.42	0.49	0.56	0.32	70	-
Zn	µg L^{-1}	71	0.99	43.20	7.31	9.06	7.00	-	3000
Sr	µg L^{-1}	71	191.53	669.88	336.64	356.37	110.57	-	-
Ba	µg L^{-1}	71	90.19	358.14	150.73	185.51	76.82	700	-

Major-ions concentrations measured in these samples were plotted in a Piper diagram showing that the Torodi region's groundwater type was Ca-Mg-HCO_3 (Figure 10). The NI-WASH groundwater data from the south Liptako, specifically, contained three water types, with most samples quantified as Ca-Mg-HCO_3 type. The order of cation abundance in all samples,

measured in mg L^{-1}, was Ca > Mg > Na > K. The cation triangle of the Piper diagram shows that all samples had a greater proportion of Ca and Mg ions than Na and K. Based on cation concentrations, the cations were equally dominated by Ca-Mg-Na. The anion triangle demonstrates that all samples were dominated by HCO_3. Anion abundance in 86 % of the samples was $HCO_3 > SO_4 > Cl$. The remaining 14 % included all samples from Sabon Care SE1 and Fada, where Cl concentrations were relatively elevated and the order of abundance was $HCO_3 > Cl > SO_4$. Samples from Fada represent the five points with the highest percentages of Cl.

Proportions of cations and anions were plotted with each sample's pH and TDS presented in a Durov diagram (Figure 10). The TDS concentrations were low throughout the region, ranging from 130 to 370 mg L^{-1} with a mean of 224.9 mg L^{-1}. Samples measured at 360 mg L^{-1} were considered outliers and were all from Sabon Care SE1. Low TDS outliers (< 150 mg L^{-1}) were samples from Koubo SE2. The samples follow a straight line in the TDS column, indicating there was low variation in relative cation abundance. The pH ranged from 6.3 to 7.3 with a mean of 6.8

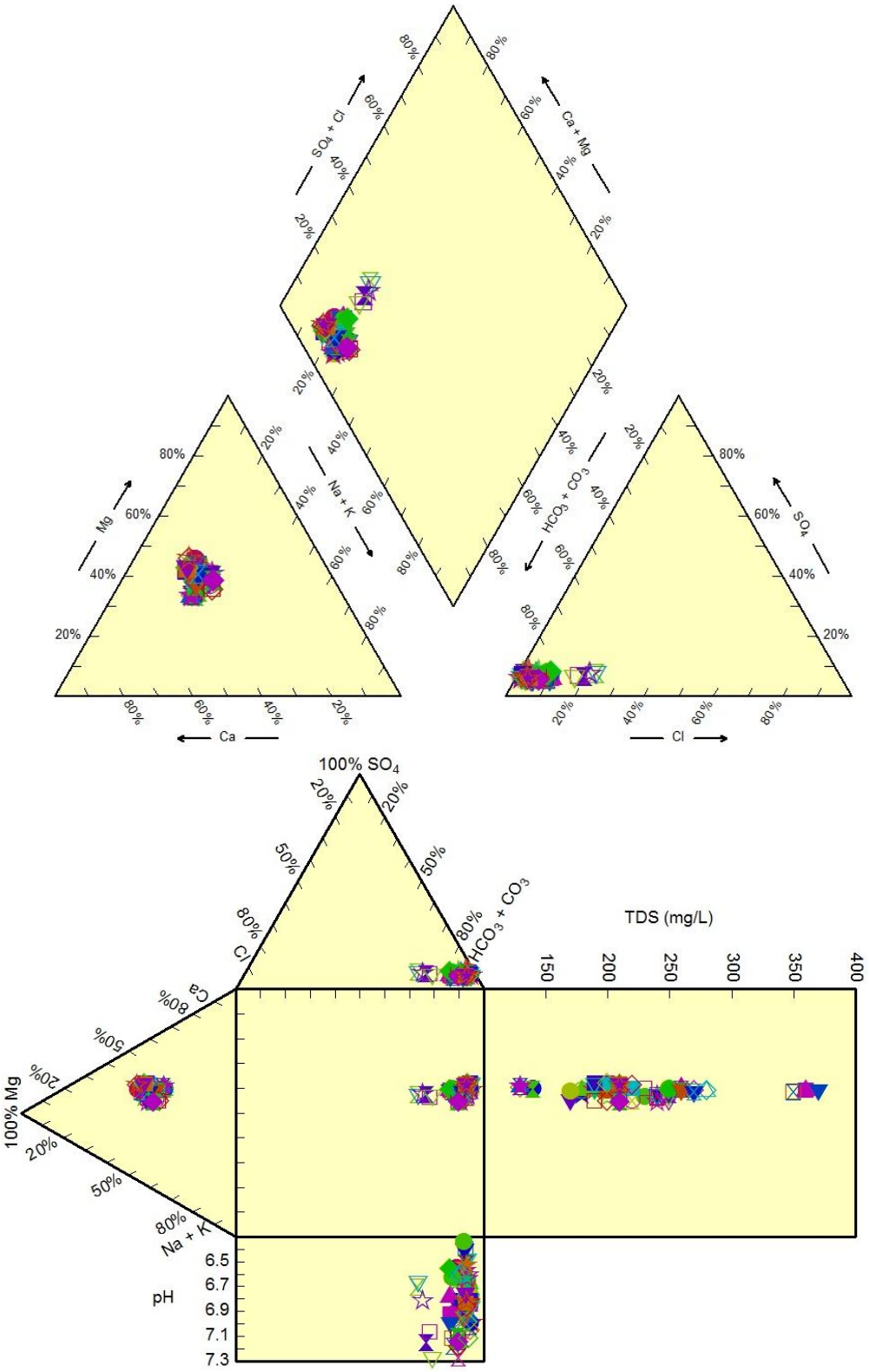

Figure 10. Top: Piper diagram showing the groundwater type of Ca-Mg-HCO_3 for the samples collected during this study. Bottom: Durov diagram showing the same water type, TDS, and pH of groundwater samples collected during this study.

and was acceptable for drinking. Most samples clustered and formed a straight line in the pH box. However, there was some variation in anion proportions to the left because of five samples from Fada with higher Cl percentages.

The Stiff diagrams in Figure 11 were made using the average major-ion concentrations, in meq L^{-1}, for each site. In agreement with the Piper and Durov diagrams, the Stiff diagrams illustrate that HCO_3 was the dominating anion at each site. Sulfate was the second most abundant anion except for boreholes represented by the grey diagrams. The other two groups are defined by cation abundance. Magnesium was the most abundant cation in the red diagrams, whereas the green diagrams were dominated by Ca. Calcium and Mg were more abundant than Na + K at all boreholes. Magnesium was the abundant cation at four of the five boreholes where $Cl > SO_4$ (grey diagrams). Note, relative ion abundances were different in mg L^{-1} and meq L^{-1} because meq L^{-1} accounts for atomic mass and ionic charge. Polygon size for each site is proportional to the total ionic content where Sabon Care SE1 and Sabon Care SE3 have relatively higher TDS concentrations, and Koubo SE2 and Tondobon have relatively lower concentrations.

Figure 12 includes stability diagrams showing which silicate minerals were stable in the aquifer. Each stability diagram in Figure 12 has an inset that zooms into the data points to distinguish between northern and southern sites. A stability diagram for the Na end member of plagioclase (i.e., albite) indicates that pyrophyllite was the most stable mineral in the Na- SiO_2 system. Pyrophyllite has minor amounts of Na (Nesse, 2000) and therefore, is stable under low $[Na^+]/[H^+]$ and high dissolved SiO_2 content. Overall, samples collected at the southern sites plot closest to the kaolinite boundary because of the relatively low $[Na^+]/[H^+]$ and SiO_2 content and northern sites plot nearer the Na-clinoptilolite boundary. Higher $[Na^+]/[H^+]$ in the samples collected from the northern sites may be caused by greater abundances of Na-plagioclase. Three

of these samples (SC1004, SC1005, and F006; Appendix 7.4 for sample ID construction) had high dissolved Na and SiO_2 and plot within Na-clinoptilolite phase.

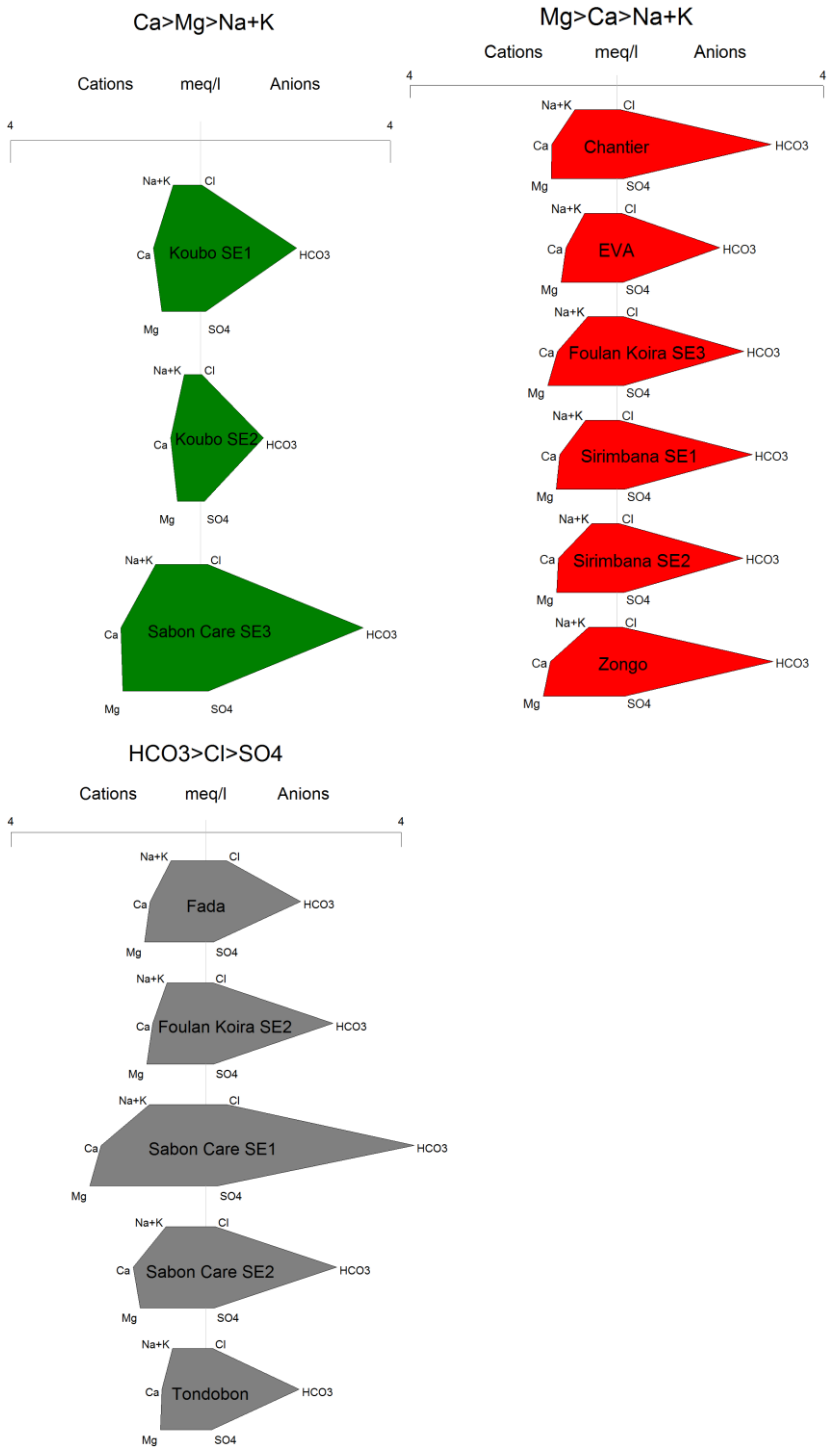

Figure 11. Stiff diagrams showing averaged major-ion concentrations for each sampling location, grouped by select ion abundance.

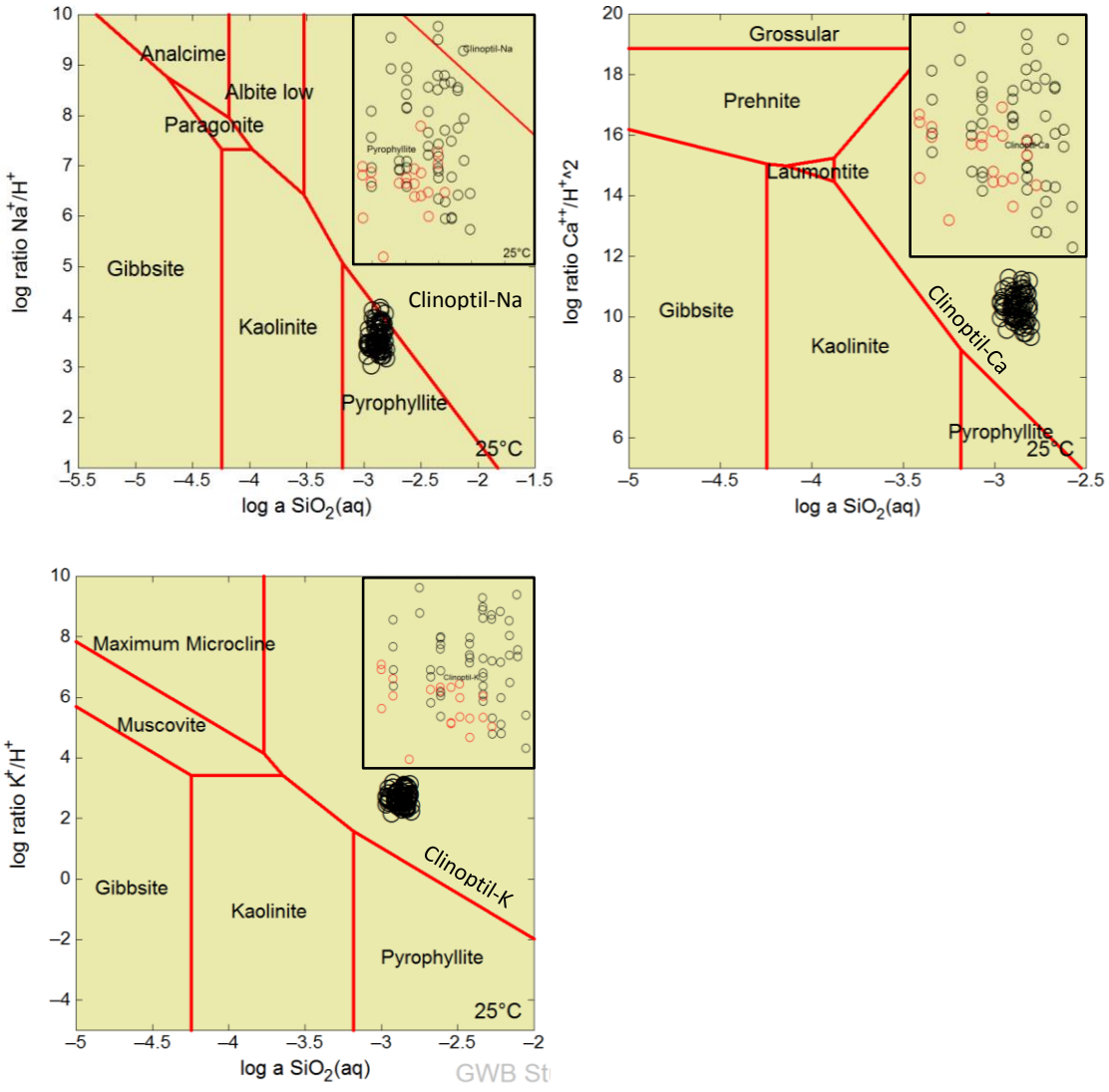

Figure 12. Stability relations of feldspar phases; albite (top-left), anorthite (top-right), and potassium feldspar (bottom). Samples (circles) plot in the stable mineral phase. Zoomed plots in the top right corner of each diagram display southern sites (red circles) and northern sites (black circles).

A stability diagram for the Ca-plagioclase (i.e., anorthite) indicates that Ca-clinoptilolite was the stable species because of moderate $[Ca^{2+}]/[H^+]^2$ and high dissolved SiO_2. Clinoptilolites are in the zeolite group, occupy vesicles, and are sometimes referred to as "clay" because they can comprise a major part of weathered igneous rocks by filling small voids (Nesse, 2000). Calcium clinoptilolite is the weathering product of anorthite, which is abundant in the parent granodiorite. Generally, samples from southern sites plot nearer the kaolinite and pyrophyllite boundaries as a result of lower $[Na^+]/[H^+]$ ratios and SiO_2 content. Greater Ca concentrations in samples collected from the northern sites is likely because of the greater abundance of Ca-plagioclase.

Potassium clinoptilolite was the stable K phase as a result of weathering of the primary mineral, K-feldspar. Similar to the albite and anorthite diagrams, samples from the southern sites had lower $[Na^+]/[H^+]$ ratios and SiO_2 content than the northern sites. All samples were oversaturated with respect to quartz, indicating its precipitation instead of dissolution.

Data plotted on the Gibbs diagram (Figure 13) shows that no samples plot in the rainfall category. This suggests that even at boreholes with the lowest TDS content (i.e., the southern sites), the water chemistry was controlled by mineral weathering.

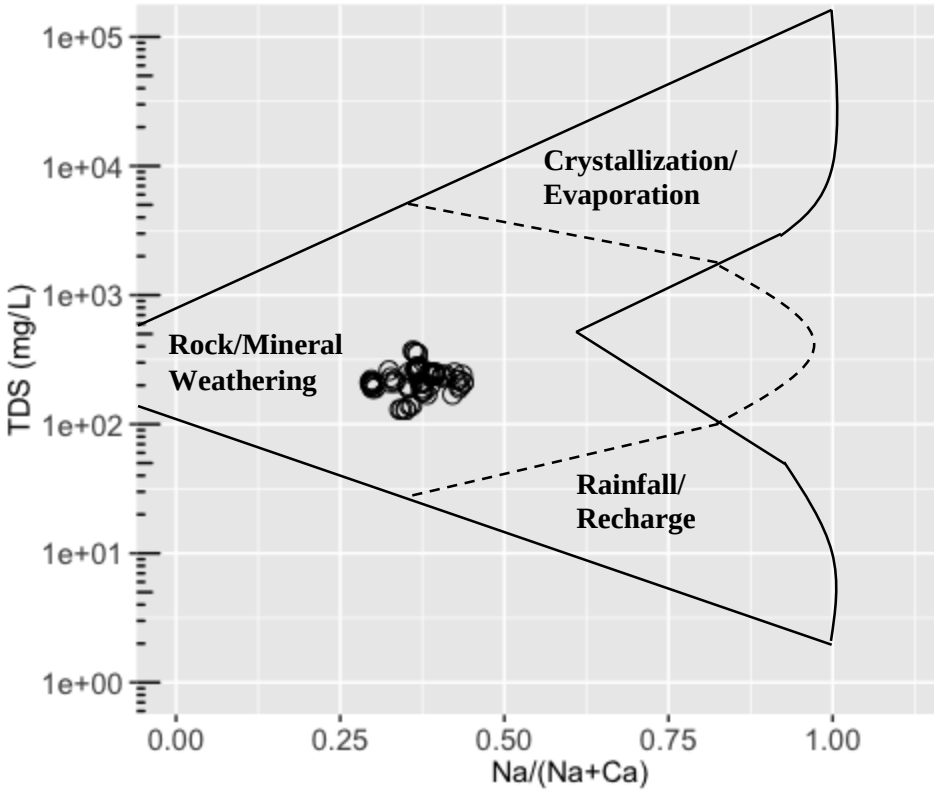

Figure 13. Gibbs diagram displaying that the chemistry of all samples (black circles) was explained by the rock/mineral weathering process.

4.4 Groundwater Chemistry

No element concentrations were present above WHO guidelines (Table 3). However, significant differences in mean concentrations of TDS; major and minor ions K, SiO_2, Cl, NO_3, Na, SO_4, and F; and, trace elements Mo, U, Se, As, V, Sr, and Ba were observed based on mineralogy and land cover (Figure 14). Concentrations of these variables were significantly greater in samples from the northern sites than those collected at the southern sites. These differences may be attributed to the abundance of minerals with higher dissolution rates (i.e., plagioclase), extended water-rock contact, and increased anthropogenic activity in the north (Figure 4). Sometimes, low TDS concentrations are a result of newly recharged water. However, Figure 13 suggests groundwater chemistry to be controlled by mineral weathering and not the

chemistry of rainfall/recharge waters. Therefore, samples with lower TDS concentrations may be the result of less weathering and the presence of less soluble minerals (Figure 15).

Elevated NO_3 concentrations were detected at Sabon Care SE2, Sabon Care SE3, Eglise Vie Abondante, and Tondobon, while concentrations at Fada and Sabon Care SE1 were approaching the limit of 50 mg L^{-1} (Figure 16, Appendix 7.4). Each of these northern sites were located in residential areas. Figure 14 demonstrates the significant difference between mean NO_3 concentrations in residential areas and agricultural land and significant difference between residential areas and bare soil terrain. There was no significant difference in mean concentrations between agricultural and bare soil sites.

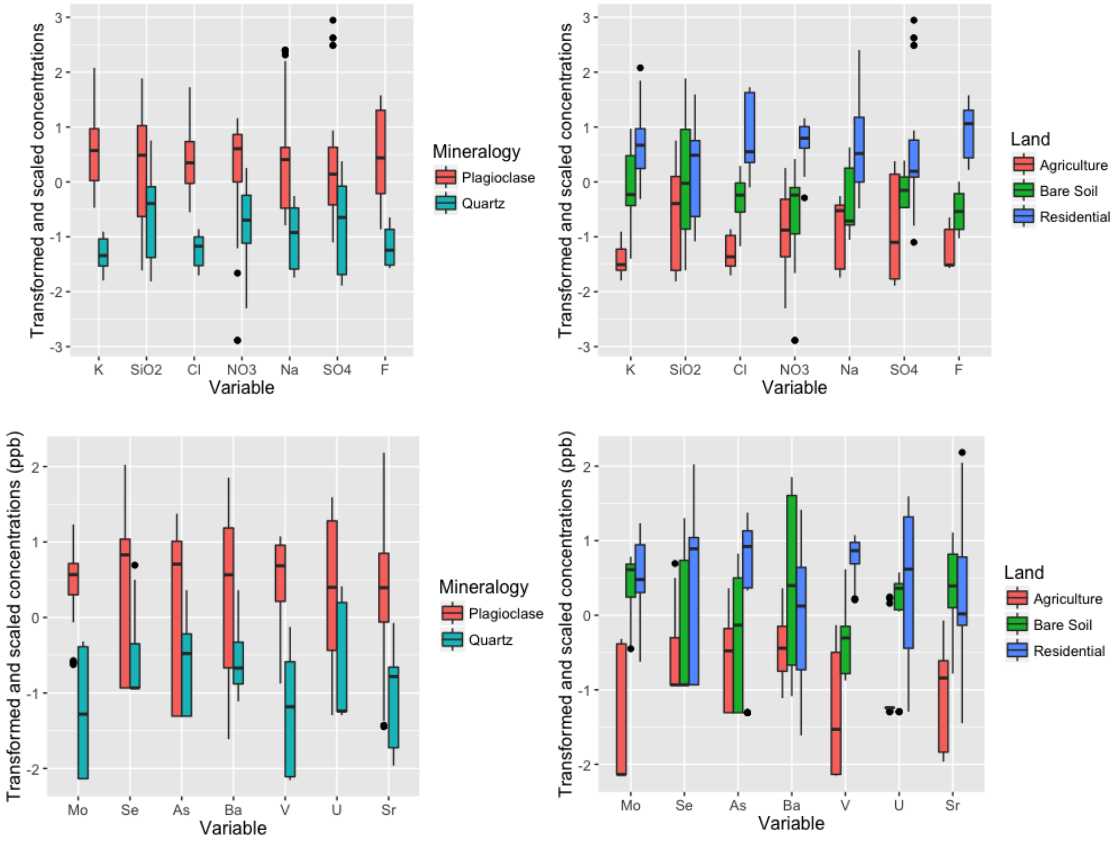

Figure 14. Boxplots of variables that had a significant difference by mineralogy and land cover. Major ions are in the top row and trace elements are in the bottom row.

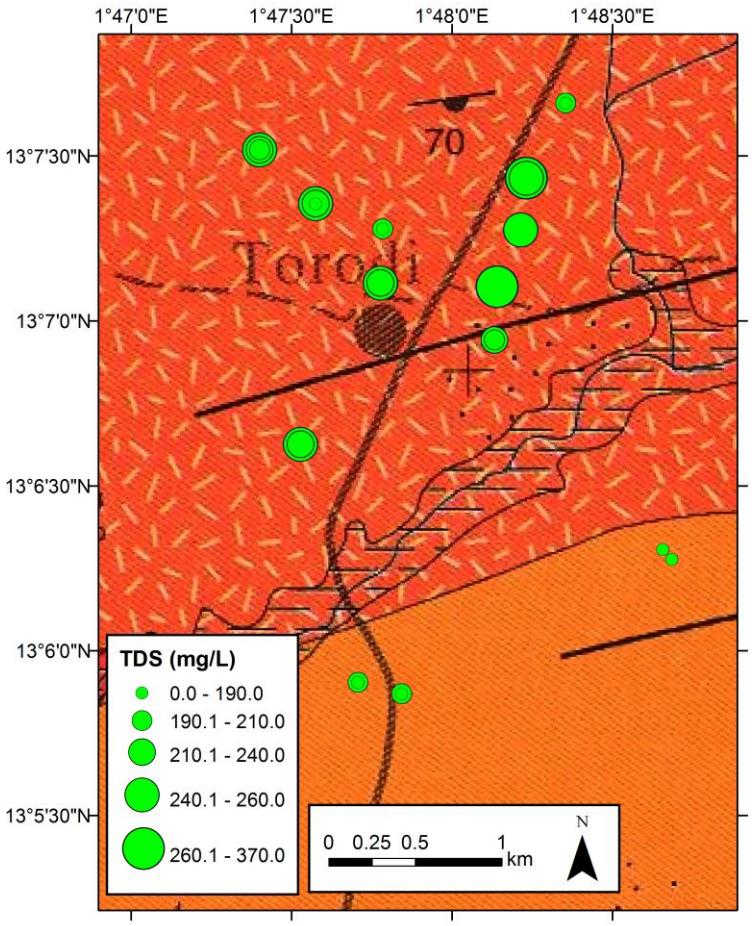

Figure 15. Geology map with observed TDS concentrations at the sampling locations. Concentrations were significantly ($p < 0.05$) greater at the plagioclase-dominated northern sites than the quartz-rich southern sites.

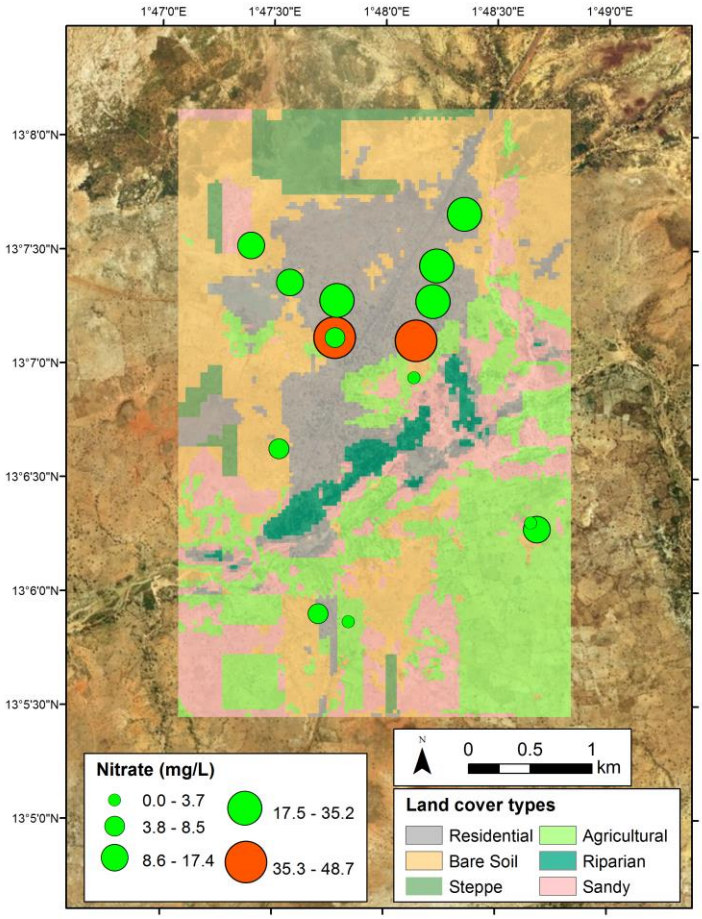

Figure 16. Nitrate concentrations at sampling location in the Torodi study area placed over the land-cover map. Green circles represent concentrations below the WHO guideline (50 mg L^{-1}) and orange circles represent concentrations approaching the guideline.

In such populated, residential areas, high NO_3 can occur where human waste is concentrated. Poorly constructed latrines, shallow boreholes, or insufficient distance between boreholes and latrines are potential explanations of the significant increase in NO_3 in residential areas. Manure from livestock may also contribute to the elevated nitrate concentrations. Thicker weathered zones (i.e., saprolite) tend to minimize the impact of anthropogenic contaminants on groundwater quality (Silliman et al., 2007). NI-WASH borehole logs (Appendix 7.2) show that boreholes in residential areas, including Fada, Sabon Care SE3, and Eglise Vie Abondante have relatively thin weathered zones (23, 15, and 18 m, respectively), making them more vulnerable to anthropogenic contaminants.

Sodium concentrations were significantly greater in samples collected from the northern sites. One possible source of Na is cation exchange (Yidana et al., 2012) where Ca and Mg ions may exchange with sorbed Na as the water moves through clayey material of the saprolite layer. The dissolution of albite, the Na-end member of plagioclase, may also increase the amount of Na ions. In Figure 17 (top left), all samples plot on the Na side of the dissolution line, indicating that albite weathering may have accounted for all of the dissolved Na in the region, but not all of the dissolved SiO_2. Samples from Sabon Care SE1 plot near the dissolution line, suggesting that the dissolution of albite may have explained both the dissolved Na and SiO_2 at that site. The weathering equation for albite and other silicate minerals in the study area (discussed below) are found in section 7.5 of the appendix.

Samples from Sabon Care SE1, SE2, and SE3 plot close to anorthite dissolution line, suggesting the weathering of the Ca-end member of plagioclase. As with albite, all but four samples plot on the SiO_2 side of the anorthite dissolution line (Figure 17), suggesting that weathering of anorthite explained nearly all the dissolved Ca, but not all of the dissolved SiO_2.

The weathering of plagioclase minerals likely accounted for the majority of observed dissolved SiO_2 concentrations. However, an R^2 value of 0.44 indicates that the sum of Ca and Na concentrations were not strong predictors of dissolved SiO_2 (Figure 17). This implies other sources of dissolved SiO_2 in the region, which may have included the weathering of K-feldspar (i.e., orthoclase), biotite, pyroxenes, amphiboles, $SiO_{2(s)}$, and amorphous $SiO_{2(s)}$. Weathering of biotite, pyroxenes, and amphiboles may also have accounted for the dissolved Mg.

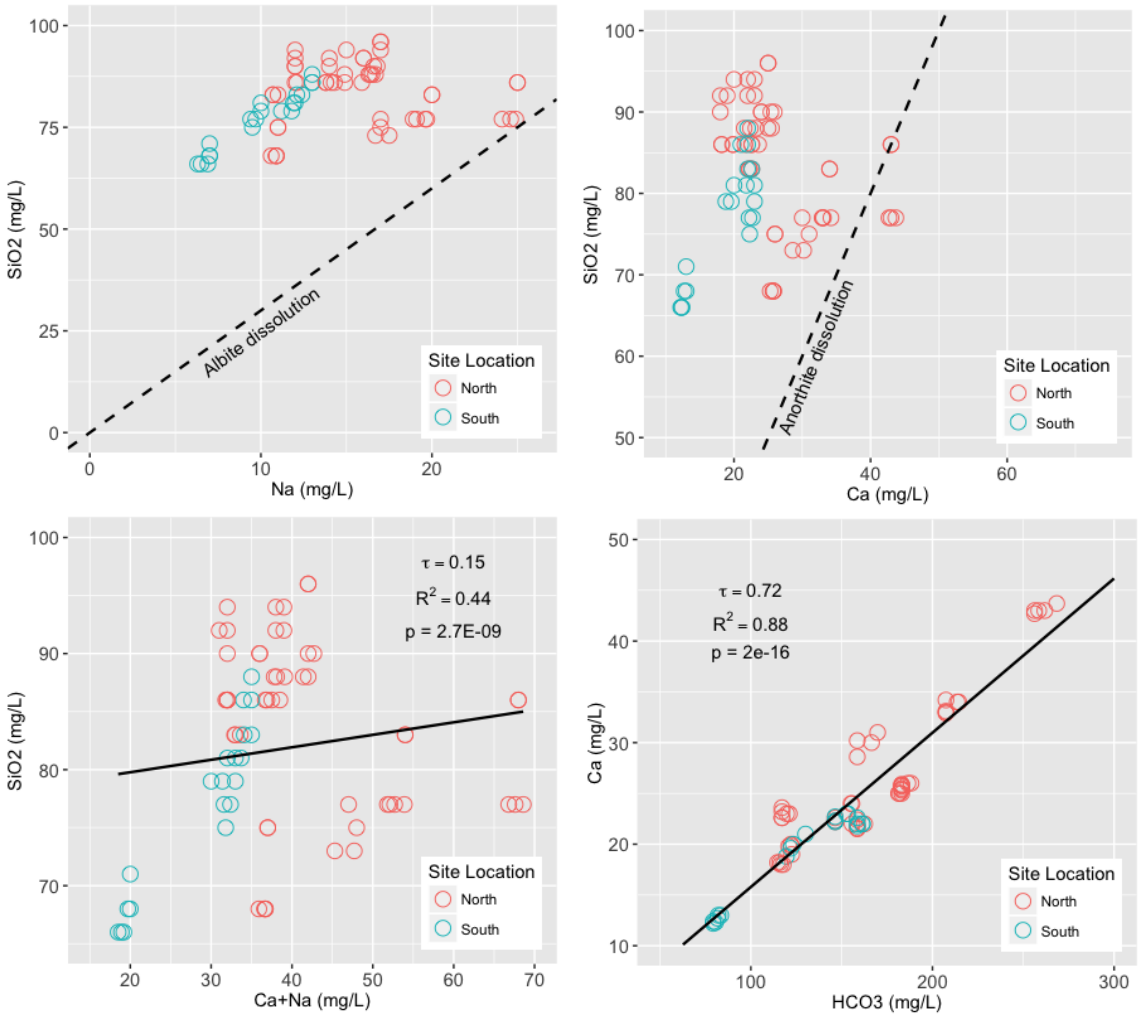

Figure 17. Top left: SiO_2 vs. Na concentrations plotted relative to the albite dissolution line. Top right: SiO_2 vs. Ca concentrations plotted relative to the anorthite dissolution line. Bottom left: Correlation and linear fit of SiO_2 and Ca+Na. Bottom-right: correlation and linear fit between Ca and HCO_3.

A strong relationship ($R^2 = 0.88$) and correlation ($\tau = 0.72$) was identified between Ca and HCO_3 (Figure 17). Calcite is not a common accessory mineral in Birimian granitoid aquifers and did not appear to exist in the region because all samples were undersaturated with respect to calcite. This relationship is likely explained by weathering of anorthite in the presence of water and carbon dioxide.

Though significant spatial variations exist for SO_4, F, and Cl, they each existed at low concentrations (Table 3) and therefore, contributed little to the observed TDS throughout the region. Dissolution graphs for some minerals that contain these elements are found in section 7.5 of the appendix. The main source of SO_4 was likely the oxidation of sulfides in accessory minerals (Hem, 1985). Despite the lack of carbonate rock, a correlation of ($\tau = 0.64$) between Ca and SO_4 may suggest that the dissolution of gypsum accounted for the dissolved SO_4. All samples were undersaturated with respect to gypsum.

Fluorite (CaF_2) is a common F mineral in igneous rocks (Hem, 1985). Greater amounts of fluorite could explain the higher concentrations in samples collected from the northern sites. As expected, all samples had greater Ca concentrations with respect to F, so each sample plots on the Ca side of the fluorite dissolution line. Amphiboles and biotite, which are present throughout the Torodi region (Figure 6), may also contain F that has replaced part of the hydroxide (OH^-) (Hem, 1985).

Though Birimian granitoids do not naturally contain much Cl, the average concentration was 5.11 mg L^{-1} (Table 3), indicating anthropogenic or atmospheric sources. Chloride concentrations were significantly greater in the north than the south, as well as in residential areas over agricultural and bare soil zones (Figure 14). This trend may indicate an anthropogenic source that does not include the use of fertilizers. The underlying geology is not known to contain

much halite (NaCl), but all samples from Fada plot along the halite dissolution line, suggesting that Cl concentrations at that site may have been influenced by the dissolution of halite.

Bicarbonate is especially abundant in groundwater of vegetated areas as a result of the increased carbon dioxide (CO_2) production in the soil zone from plant respiration and biological degradation of dead organic material. Vegetation was sparse throughout the region, but established enough that HCO_3 was the most abundant anion (Figures 10 and 11). Overall, HCO_3 concentrations were greater in the north. This was unexpected because there was less vegetation in the residential north than the south. This may suggest an anthropogenic source of HCO_3.

Uranium concentrations showed a bimodal distribution, which is explained by the elevated U concentrations at the northeast boreholes of Sabon Care SE1, Sabon Care SE2, and Sabon Care SE3 and relatively low concentrations at all other locations. Spatial clustering was evident, as the mean U concentration in the northeast was significantly greater than the other three quadrants. Uranium has a greater solubility in oxidizing environments, thus a sharp rise in the northeast of the study area may indicate localized oxidation or a separate source of U.

Typical surface and groundwater samples rarely contain greater than 10 μg L^{-1} of the trace element V (Hem, 1985). In the Torodi region, however, V concentrations reached 35.92 μg L^{-1}, with a mean of 24.16 μg L^{-1} (Table 3). Like U, V is fairly soluble in oxidizing environments and less so in reducing environments (Hem, 1985). V and U are associated in certain types of ore deposits (Hem, 1985). The data show moderate correlation (τ =0.34) between V and U.

4.5 Groundwater Levels and Recharge

Figure 18 is an interpolated map of the average observed groundwater levels (measured in masl) for the month of February. Though levels varied throughout the study period, February is an accurate representation of the relative spatial differences observed throughout the majority of

the study period. Groundwater levels were highest in the northwest and southeast and lowest in the northeast. Generally, the groundwater levels follow the land-surface elevation.

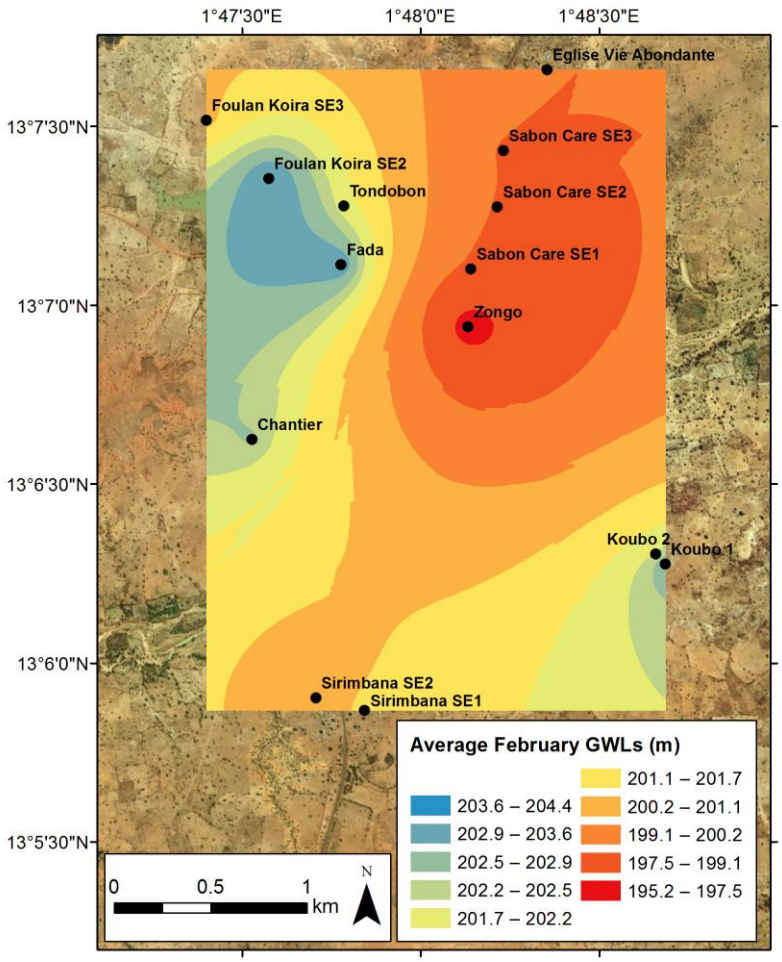

Figure 18. Interpolated map of averaged February groundwater levels. Water flowed perpendicular to lines of equal water level from areas of higher (blue) to lower (red) levels.

Groundwater levels reduced at each site throughout the study period. Figure 19 is an interpolated map illustrating the total decline in groundwater levels throughout the region. The greatest decreases were observed at Zongo and Sabon Care SE1, followed by the four most northwesterly boreholes. Table 4 reports the mean and median groundwater level reduction by land-cover and aquifer type. By land cover, the greatest declines were observed in residential areas, which was likely a result of increased groundwater pumping due to the higher population density. Even though southern sites with fractured aquifers (i.e., Sirimbana SE2, Koubo SE1, and Koubo SE2) had low reductions, the greatest mean and median reduction was observed in fractured aquifer segments. High reductions at Zongo and Tondobon due to increased pumping may explain this observation. These observations were based on comparisons of mean and median values and were not found to be statistically significant ($p > 0.05$). There was also no significant difference of water-table depths by land-cover type ($p > 0.05$).

During the second half of May, groundwater levels were either unchanged or increased at Zongo, Fada, and Sabon Care SE2 (Appendix 7.6). These fluctuations took place shortly after the first observed rain event on May 10, suggesting groundwater recharge occurred. The groundwater level at Zongo decreased throughout the study period until May 15, remained at a constant level of 194 masl for three days (i.e., May 15-17), then increased by 3 cm over the following two days (i.e., May 17-19). While this increase was small, it suggests that recharge occurred only five days after the initial rain event – a considerably shorter lag than anticipated. A recovery rate in the groundwater level of 84 % after 2 minutes without pumping at Zongo (Appendix 7.8) may suggest high fracture density, which may have contribute to the rapid recharge. An increase of 3 cm was also observed at Fada between May 16 and 17 after a fairly stable decreasing trend since the beginning of January. A 7 m laterite layer is present at Fada (Appendix 7.2), which may have a high permeability, explaining the rapid recharge.

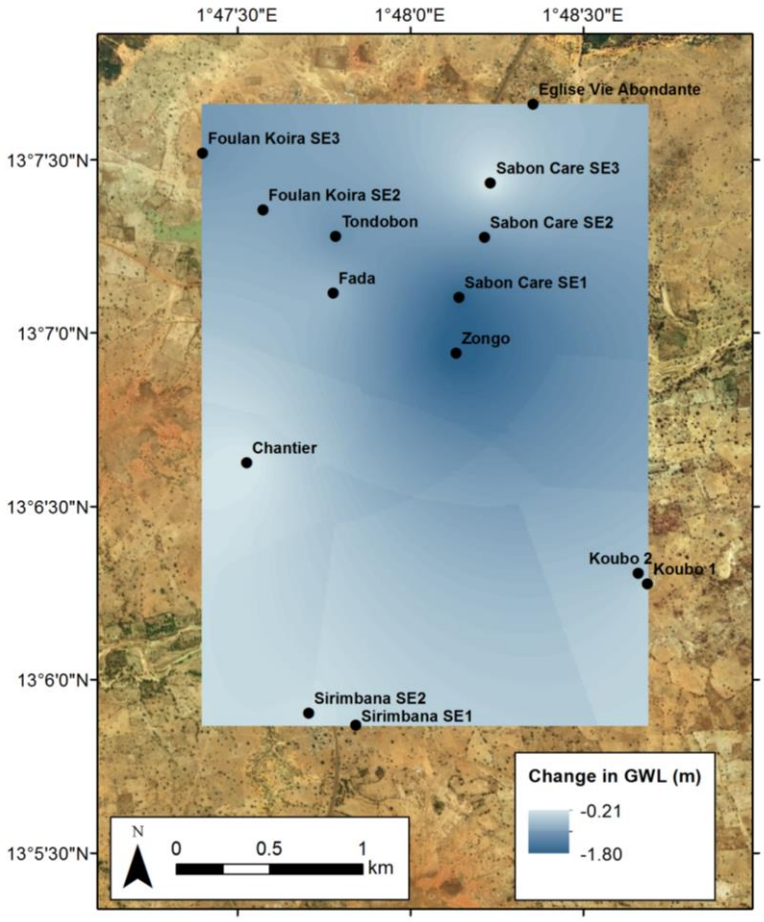

Figure 19. Interpolated total reductions in groundwater levels from November to May, 2016. Dark blue indicates a greater reduction.

Table 4. Mean and median groundwater level reduction by land cover type and aquifer type.

Category	Mean	Median
Land Cover		
Residential	1.55	1.67
Bare	1.12	1.05
Agricultural	1.15	1.27
Aquifer		
Metamorphic	1.14	1.14
Fractured	1.45	1.54
Weathered	1.37	1.25
Sandy	0.63	0.63

Manual measurements were made at approximately monthly intervals at Sabon Care SE2. There was a decreasing trend in the water table from December until April, then between April 18 and May 25, the water level increased by 78 cm. This increase may be explained, in part, by recharge after the May 10 rain event, a reduction in groundwater pumping, or groundwater contribution from an adjacent groundwater basin.

While groundwater declines were observed at all other boreholes locations, the static water level at Chantier rose 19 cm from December 16 until plateauing from January 15 through January 21. Meanwhile, approximately 600 meters south of Chantier, the Goroubi River flowed until at least November 8, 2017 and contained some stagnant water until December 25 as recorded by Landsat 8 image archives. Measured groundwater levels were lower than the Goroubi River levels, suggesting that the Goroubi River was losing to the groundwater system, which may attribute to the observed increase of the water level at Chantier. This finding is consistent with the results of Girard (1996), who determined that waters from the Goroubi-Lomona junction (Figure 3), approximately 3.5 km to the west of the study area, contribute the majority of recharge to the fractured aquifer near the river and streams. Groundwater levels at Chantier decreased by 20 cm from January 21 to April 10, as river flows and rainfall were not available to contribute to recharge.

4.6 Multivariate Statistical Analyses

4.6.1 Principal Component Analysis

A summary of the first seven PCs is found in Section 7.4 of the appendix. The first seven PCs were considered significant with eigenvalues >1 (Kaiser, 1960) and explained a cumulative 86 % of the total variance in the data matrix. Interpretation of PCs became increasingly difficult for those that explained a much smaller percentage of the variance (i.e., PC3, PC4, PC5, PC6, and PC7 only accounted for 9, 8, 7, 6, and 4 % of the original data variance, respectively). For this reason, only the first two PCs, accounting for the majority (i.e., 52 %) of the original data variance, were examined.

Table 5 summarizes the first two PCs and Figure 20 illustrates their loadings and scores. The PC1 variables had relatively low loading values because their contributions in explaining the variance of the dataset were distributed among more than one PC (Seyhan et al., 1985), but Silliman et al. (2006) considered loadings in the range of 0.25 and 0.33 to be significant when they were ranked highly among all loading values. Therefore, variables with absolute value loadings ≥ 0.25 were considered significant. In addition, variables with loadings between 0.20 and 0.24 were considered moderately significant and will also be discussed.

PC1 accounted for 40 % of the original variance and is hypothesized to represent weathered or fractured characteristics of the aquifer. Supporting this hypothesis is that the signage of each PC1 score (i.e., positive or negative) represents two separate aquifer characteristics. For example, the NI-WASH borehole logs show that boreholes with negative PC1 scores were generally located in aquifers with weathered characteristics, while boreholes with positive PC1 scores were in fractures. A comparison of PC1 scores, borehole yields, and aquifer characteristics is presented in Table 6.

Table 5. Summaries of the first two principal components. Significant loading values are in bold.

PRINCIPAL COMPONENT 1		**PRINCIPAL COMPONENT 2**	
% of Variance	40	**% of Variance**	12
Cumulative %	40	**Cumulative %**	52
SD	3.2	**SD**	1.8
Eigenvalue	10.4	**Eigenvalue**	3.1
Variable	**Loading**	**Variable**	**Loading**
Na	**-0.29**	HCO_3	**-0.27**
Ca	**-0.28**	Ca	-0.21
F	**-0.28**	Mg	-0.20
Mg	**-0.27**	Mn	-0.20
SO_4	**-0.27**	Sr	-0.18
Sr	**-0.27**	SO_4	-0.17
Mo	**-0.26**	Co	-0.16
Cl	**-0.26**	Al	-0.13
V	**-0.26**	Temp	-0.09
HCO_3	**-0.25**	Zn	-0.09
U	-0.24	U	-0.07
K	-0.22	Mo	-0.04
NO_3	-0.21	Na	-0.01
Co	-0.18	Ba	0.00
As	-0.14	Fe	0.00
Temp	-0.14	pH	0.09
Ba	-0.11	Cl	0.10
Se	-0.11	Ni	0.14
SiO_2	-0.08	F	0.16
pH	-0.03	K	0.18
Cr	-0.01	V	**0.26**
Al	0.00	As	**0.28**
Zn	0.05	NO_3	**0.28**
Fe	0.06	SiO_2	**0.29**
Ni	0.09	Se	**0.34**
Mn	0.09	Cr	**0.39**

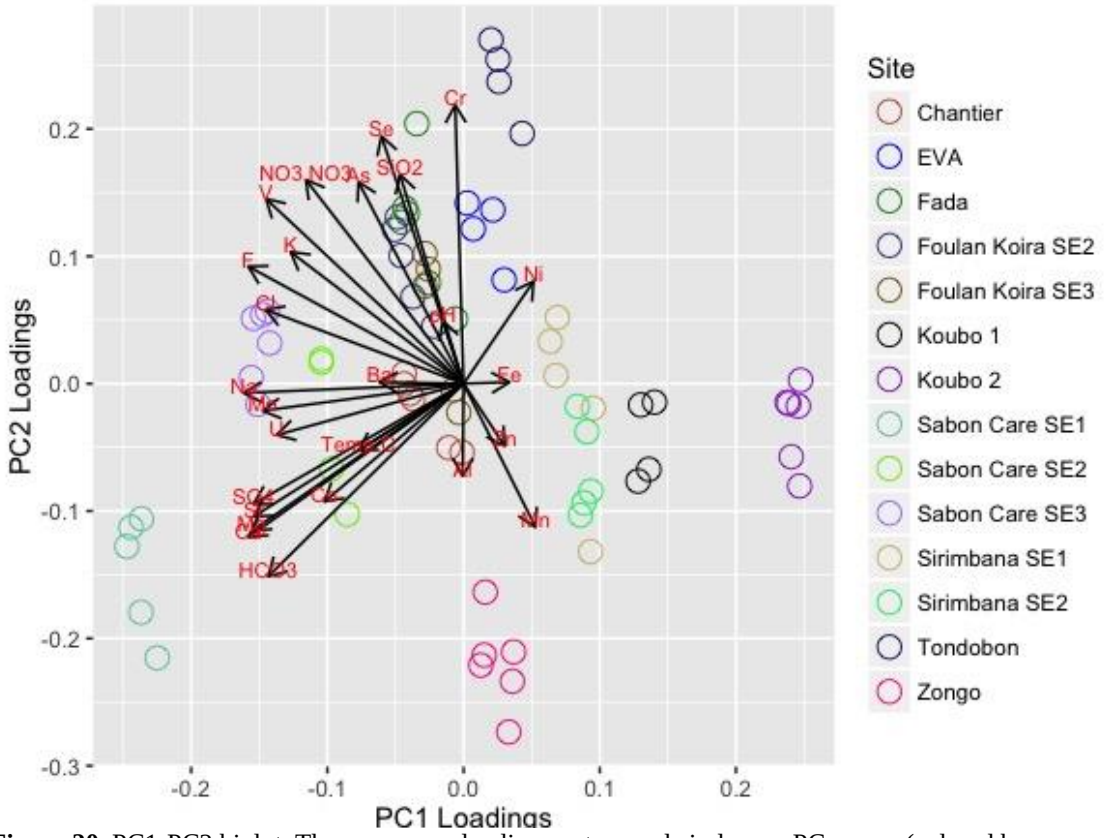

Figure 20. PC1-PC2 biplot. The arrows are loading vectors and circles are PC scores (colored by borehole).

Negative PC1 loadings of major ions and some accessory elements, presented in order of most to least significant include: Na, Ca, F, Mg, SO_4, Sr, Mo, Cl, V, and HCO_3. Several of these negatively loaded PC1 variables are highly soluble, suggesting weathering of the silicate minerals of the granodiorite host rock (Hem, 1985; Hill et al., 2000). These include Ca and Na from plagioclase; Mg from biotite, pyroxenes, and amphiboles; HCO_3 from carbonic acid reacting with a range of silicate minerals; and Sr that has replaced either Ca or K. The significant PC1 loadings of U and V may indicate oxygen-rich groundwater (Hem, 1985).

Table 6. Summary of site characteristics including average PC1 scores, borehole yield, and aquifer type.

PC1 score (mean)	Site	Yield (m^3h^{-1})	Aquifer type
Negative	Sabon Care SE1	3.5	Weathered
	Sabon Care SE2	1	Weathered
	Sabon Care SE3	4	Weathered
	Chantier	3.5	Weathered
	Fada	1.5	Metamorphic
	Foulan Koira SE2	3	Weathered**
	Foulan Koira SE3	3	Fractured
Positive	Eglise Vie Abondante	2	Fractured
	Sirimbana SE2	0.5	Fractured
	Sirimbana SE1	4	Sandy
	Koubo SE1	9	Fractured**
	Koubo SE2	13	Fractured**
	Zongo	5	Fractured**
	Tondobon	3	Fractured*

** Assumed based on PC score and yield.
* Assumed based on PC score.

Borehole logs indicated that six of the seven boreholes with negative PC1 scores have weathered or metamorphosed aquifers with little to no fracturing (Table 6). In the absence of fractures, hydraulic conductivity is relatively low and residence times are high, which promotes weathering. This is supported by significantly greater TDS concentrations in weathered and metamorphic sections than fractured zones. There was no available borehole log for Foulan Koira SE2, however, the air-lift yield of 3 m^3h^{-1} was comparable to the average yield at boreholes with little to no fracturing (2.8 m^3h^{-1}). A low yield suggests a weathered aquifer with a low degree of fracturing. The samples collected at Foulan Koira SE3 were anomalies because they had negative PC1 scores, yet the well screens at this borehole were within fractured granodiorite. However, it is possible that the 6 m layer of weathered granodiorite and clay was controlling the groundwater chemistry (Appendix 7.2).

Samples with positive PC1 scores were collected from boreholes where existing records indicate a known predominance of fractures and were characterized by significantly low EC values (140.3 to 320.0 µS cm^{-1}). These two factors suggest shorter residence times and reduced weathering. The aquifer at Eglise Vie Abondante and Sirimbana SE2 is predominantly fractured granodiorite (Table 6). The aquifer at Sirimbana SE1 is coarse sand with some clay. Sirimbana SE1 had a positive PC1 score because the hydraulic conductivity of sand is comparable to that of fractured granite (Heath, 1983).

There were no available borehole logs that described the lithology or degree of fracturing in the aquifer at Koubo SE1, Koubo, SE2, Zongo, or Tondobon. However, observations suggested that Koubo SE1 and Koubo SE2 had relatively higher yields of 9 m^3h^{-1} and 13 m^3h^{-1}, respectively, which may imply dense fractures. The modified pump test at Zongo recorded a drawdown of 1.22 m after a morning of nearly constant pumping, with an 84 % recovery after 2 minutes (Appendix Section 7.8). This rapid recovery rate implies a high hydraulic conductivity and that the presence of fractures is likely. A relatively low yield of 3 m^3h^{-1} at Tondobon may make this site an anomaly when comparing to the average yield of boreholes with positive PC1 scores (5.21 m^3h^{-1}). A fractured aquifer was assumed for Tondobon based on PC1 scores. The division of PC1 scores by aquifer characteristics based on borehole logs, borehole yields, and PC1 results is illustrated in Figure 21.

The PC2 accounted for 12 % of the variance in the original 27-variable dataset and is hypothesized to represent a presence or absence of a laterite layer. Table 7 shows that boreholes with positive average PC2 scores have a near-surface laterite layer and boreholes with negative PC2 scores do not. Borehole logs illustrate a laterite layer at Fada, Eglise Vie Abondante, Foulan Koira SE3, Sabon Care SE3, and Sirimbana SE1 (Appendix 7.2). These laterites are at or near the land surface and above the composite aquifer, therefore, elements in the laterite may have been

leached to the water table by infiltrating water. Foulan Koira SE2 and Tondobon had positive PC2 scores, suggesting the presence of laterite, though borehole logs were not available for either site.

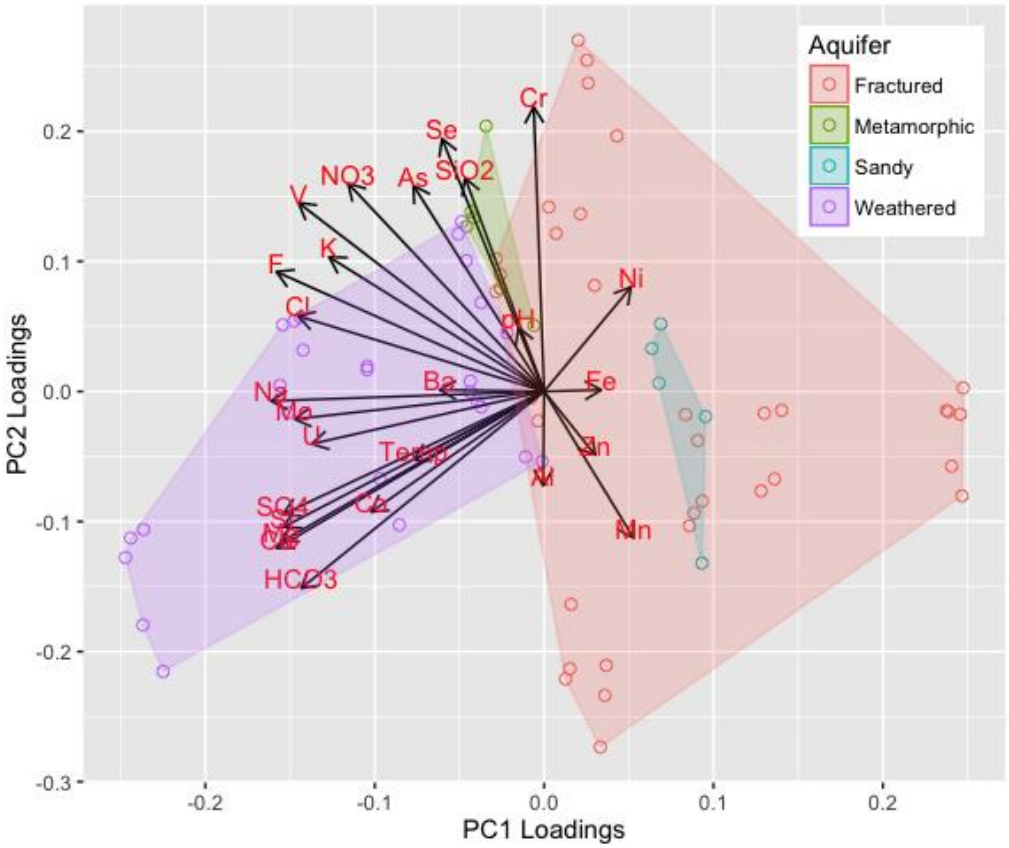

Figure 21. PC1-PC2 biplot with PC scores grouped by aquifer type.

Table 7. Summary of site characteristics based on PC2 scores and whether a laterite layer exists.

PC2 score (mean)	Site	Laterite
Positive	Fada	Yes
	Eglise Vie Abondante	Yes
	Foulan Koira SE3	Yes
	Sabon Care SE3	Yes
	Sirimbana SE1	Yes
	Foulan Koira SE2	Yes*
	Tondobon	Yes*
Negative	Sirimbana SE2	No
	Chantier	No
	Sabon Care SE1	No
	Sabon Care SE2	No
	Koubo SE1	No*
	Koubo SE2	No*
	Zongo	No*

* Assumed based on PC score

In order of significance, Cr, Se, SiO_2, NO_3, As, and V had the greatest positive PC2 loadings. Laterite is the end result of the long-term weathering of granodiorite and is exhausted in unstable elements that deplete rapidly in the early stages of weathering (i.e., the significant PC1 variables) (Hill et al., 2000). Because they are relatively resistant to weathering, Cr, SiO_2, and V percentages may increase in laterites over time (Hill et al., 2000), making them some of the only elements remaining that are available to react with infiltrating water. Chromium can be one of the most strongly enriched elements in laterites (Hill et al., 2000). A significant positive loading of NO_3 may indicate an anthropogenic component to PC2 and possible sources are discussed in Section 4.4. Arsenic and Se are more soluble in oxidizing waters, so the significant PC2 loadings of As and Se may indicate oxygen-rich groundwater (Hem, 1985).

Boreholes with negative average PC2 scores, including Sirimbana SE2, Chantier, Sabon Care SE1, and Sabon Care SE2 do not have a laterite layer (Table 7, Appendix 7.2). The absence of laterite suggests high erosion rates (Courtois et al., 2010). Koubo SE1, Koubo SE2, and Zongo are grouped with negative PC2 scores, suggesting the absence of laterite, but no borehole logs were available for comparison. The significant negative PC2 loading of HCO_3 and moderate negative loadings of and Ca and Mg may indicate that in the absence of laterite, the dissolution of Ca-rich silicate minerals (i.e., anorthite) and Mg-rich silicate minerals (i.e., biotite, amphiboles, and pyroxenes) with carbonic acid may have controlled groundwater chemistry. Recall that HCO_3, Ca, and Mg also had significant loadings on PC1. The lack of separation of parameters with significant loadings in the first two PCs may indicate that the PCs are competing sets of processes or mechanisms that have impacted the groundwater chemistry (Silliman et al., 2006).

The division of PC2 scores by presence or absence of laterite based on descriptions from borehole logs and PC2 results is illustrated in Figure 27. A general trend was observed for boreholes with laterite, whereby these samples had positive PC2 scores. However, five of 26 samples from laterite sites had negative PC2 scores (negative scores highlighted in blue); 2 of 5 samples collected from Sirimbana SE1, 1 of 6 samples collected from Sabon Care SE3, and 2 of 5 samples collected from Foulan Koira SE3. This may be explained by reduced leaching of laterite elements during the dry season or mixing with groundwater from areas without laterite where weathering of Ca and Mg-rich silicate minerals controlled the water chemistry. Sabon Care SE2 does not have a laterite layer, but samples from this site were divided equally between negative and positive PC2 space, suggesting that water from a nearby laterite site may have influenced the groundwater chemistry.

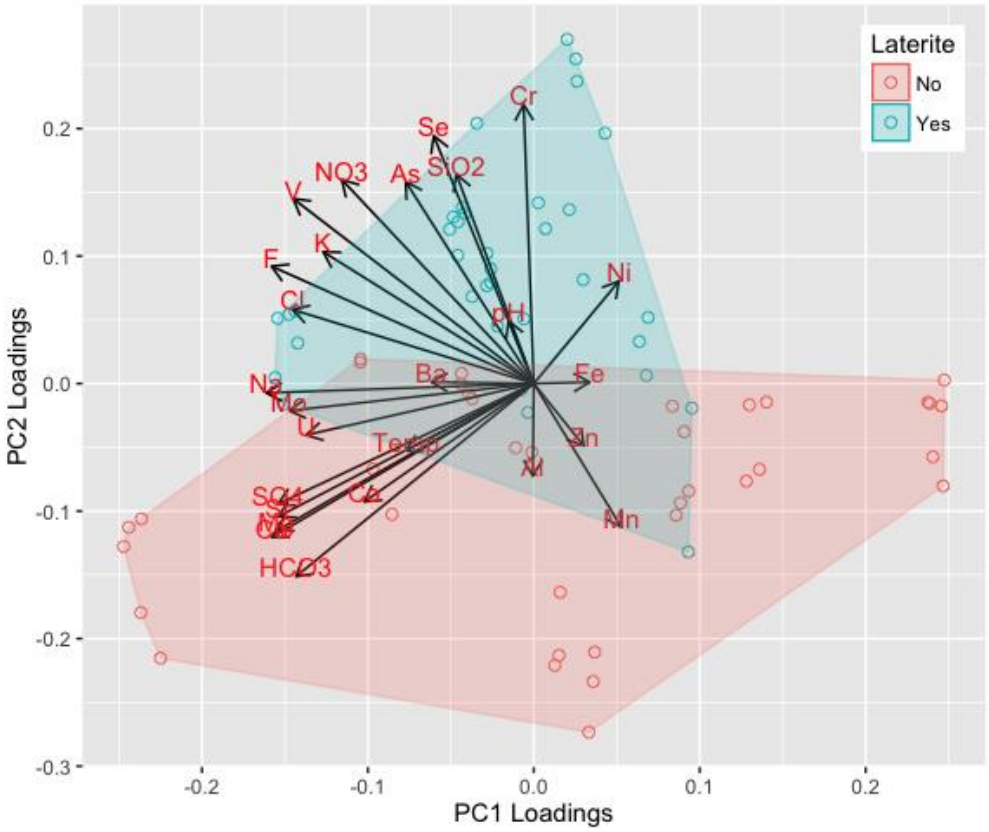

Figure 22. PC1-PC2 biplot with PC scores grouped by presence or absence of laterite.

Principal component scores in the PC1-PC2 biplot were grouped by three types of land cover (Figure 23). Overlap was not observed, suggesting that the observations are distinguishable by land cover. Land cover was not initially defined as a major control on groundwater chemistry by PC1 or PC2. It is noted, however, that there was a bias in sampling with greater number of samples collected from residential areas (i.e., 34 samples were from residential zones compared to only 22 from bare soil terrain and 15 from agricultural lands).

Samples from residential boreholes are highlighted in blue and mostly fall into the negative PC1 space associated with weathered aquifers. As previously mentioned, NO_3 concentrations were significantly greater in residential areas than bare soil zones and agricultural lands. In agreement, the NO_3 loading in Figure 23 goes through the center of the residential group. Samples from agricultural lands are highlighted in red, representing positive PC1 loadings characteristic of fractured aquifers. Samples from boreholes in soil terrain are highlighted in green and are represented mostly by negative PC2 scores associated with the weathering of Ca and Mg-rich silicate minerals in the absence of laterite.

Some samples from bare soil terrain overlap with both agricultural and residential lands. For example, Sirimbana SE2 overlaps with agricultural lands since fields surround this borehole. Groundwater appeared to flow from these higher elevation agricultural zones towards Sirimbana SE2, at a relatively lower elevation (Figure 18 for groundwater levels, Figure 4 for land cover).

The first three samples from Foulan Koira SE3, a site located outside the residential perimeter, overlap with residential samples and thus were likely impacted by nearby residential activity. Groundwater levels were lower than the neighboring residential site Foulan Koira SE2

for the duration of the study period, suggesting that groundwater may have flowed from the residential area to the bare soil zone (Figure 18).

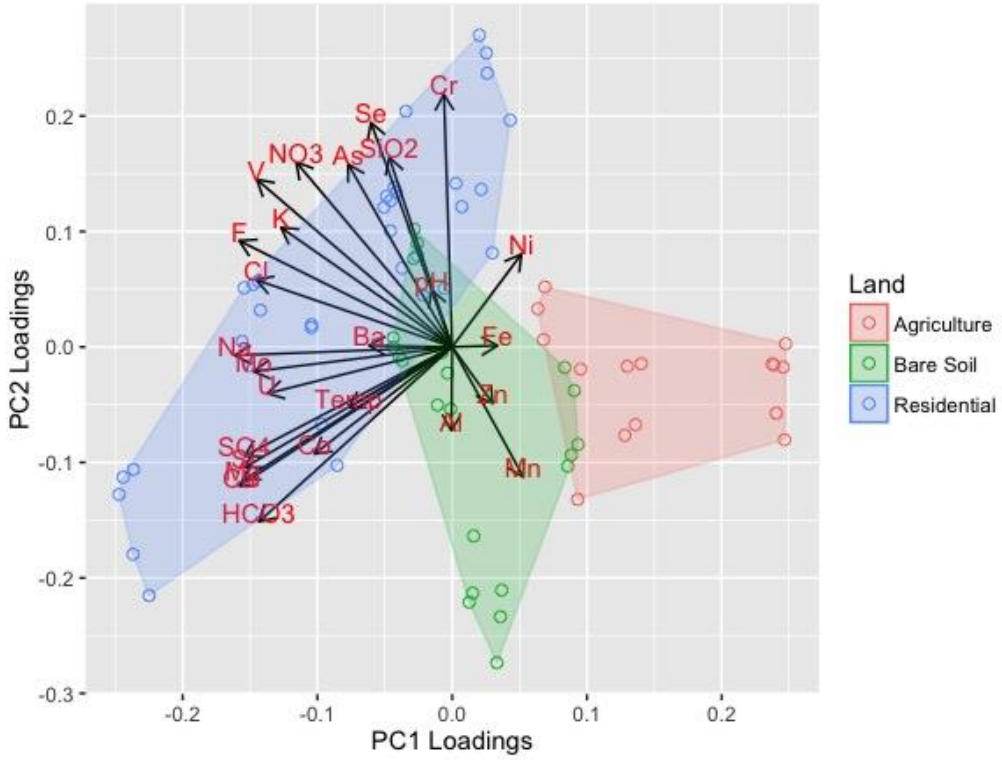

Figure 23. PC1-PC2 biplot with scores groups by land cover

4.6.2 Hierarchical Cluster Analysis

Figure 24 shows the resulting HCA dendrogram of the HCA that was performed for 71 groundwater samples of 26 transformed and standardized variables. Results and discussion are based on the grey "edge" numbers, which provide a label for each cluster, and red AU p-values (see Methods, section 3.5 for more details on AU and BP values). The red boxes outline edges where AU p-values were ≥0.95 and where the null hypothesis was accepted. The null hypothesis states that there are no statistically significant differences between the chemistry of samples within an edge. Samples collected from the same borehole that cluster within an edge indicate a lack of variation in the chemistry over time.

While there were several edges with AU values ≥0.95, only the four largest (i.e., edges 66, 64, 57, and 49) will be discussed in detail. These four edges were projected back into the PC1-PC2 biplot to illustrate their distinguishable characteristics in PC space (Figure 25). The HCA validated the PCA results. Boreholes with PC scores in the "No edge" category in Figure 25 are those that did not cluster into one of the four largest edges. Samples that formed small edges or did not cluster at all suggest unique water chemistry values or variation in chemistry over time.

Edge 66 contains samples from Zongo, Koubo SE1, Sirimbana SE1, and Sirimbana SE2. These boreholes are characterized by the positive PC1 scores (fractures), moderate EC values (ranging from 216 to 320 $\mu S\ cm^{-1}$), and were located in or adjacent to agricultural lands (Figure 4). The first two characteristics indicate that variation of the water chemistry are explained by reduced weathering and short residence times. The high confidence level (96 %) of this edge confirms the null hypothesis that there was no significant difference between the chemistry of the samples collected at these boreholes. This edge is distinguishable in PC space, thus, corroborating the PCA results.

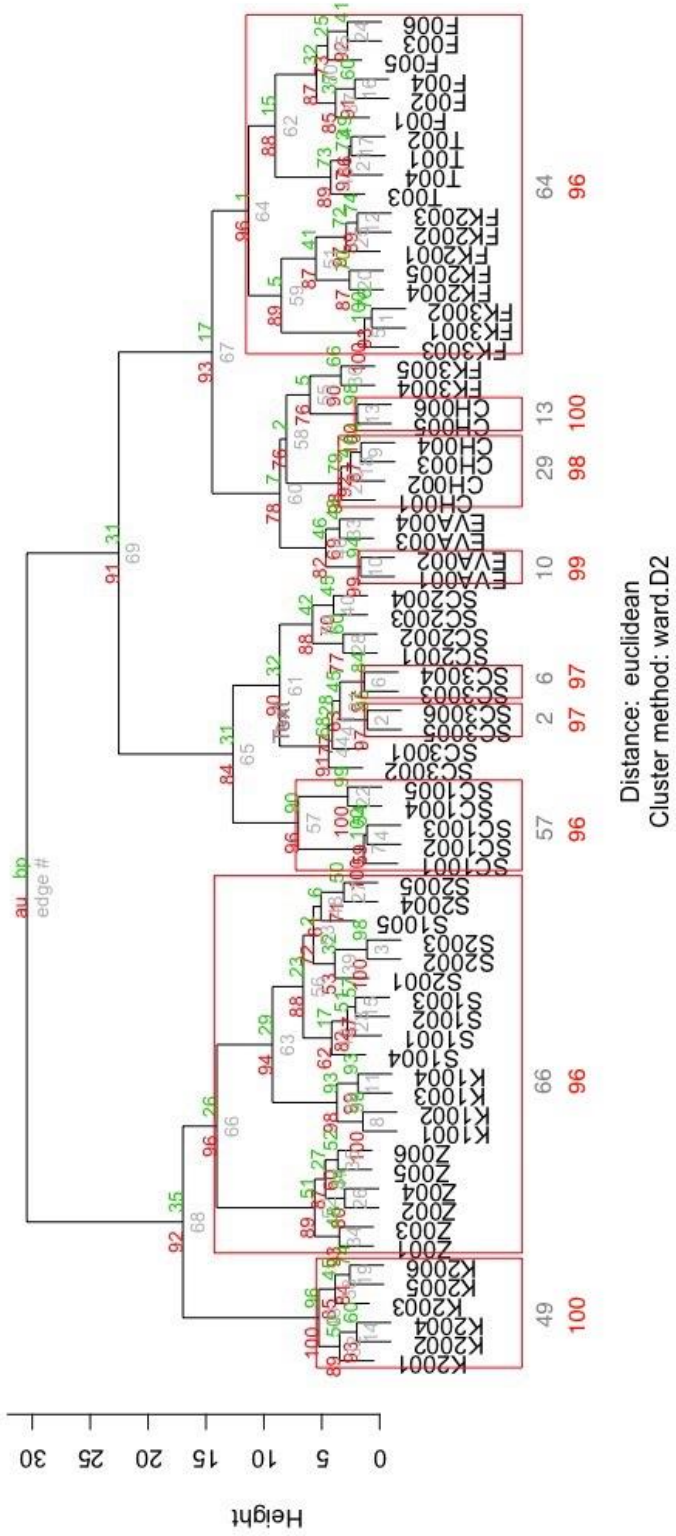

Figure 24. Dendrogram of the HCA. Clusters with AU values >0.95 are shown by the red rectangles. Edge numbers (gray) and AU values (red) are labeled beneath each cluster for clarity.

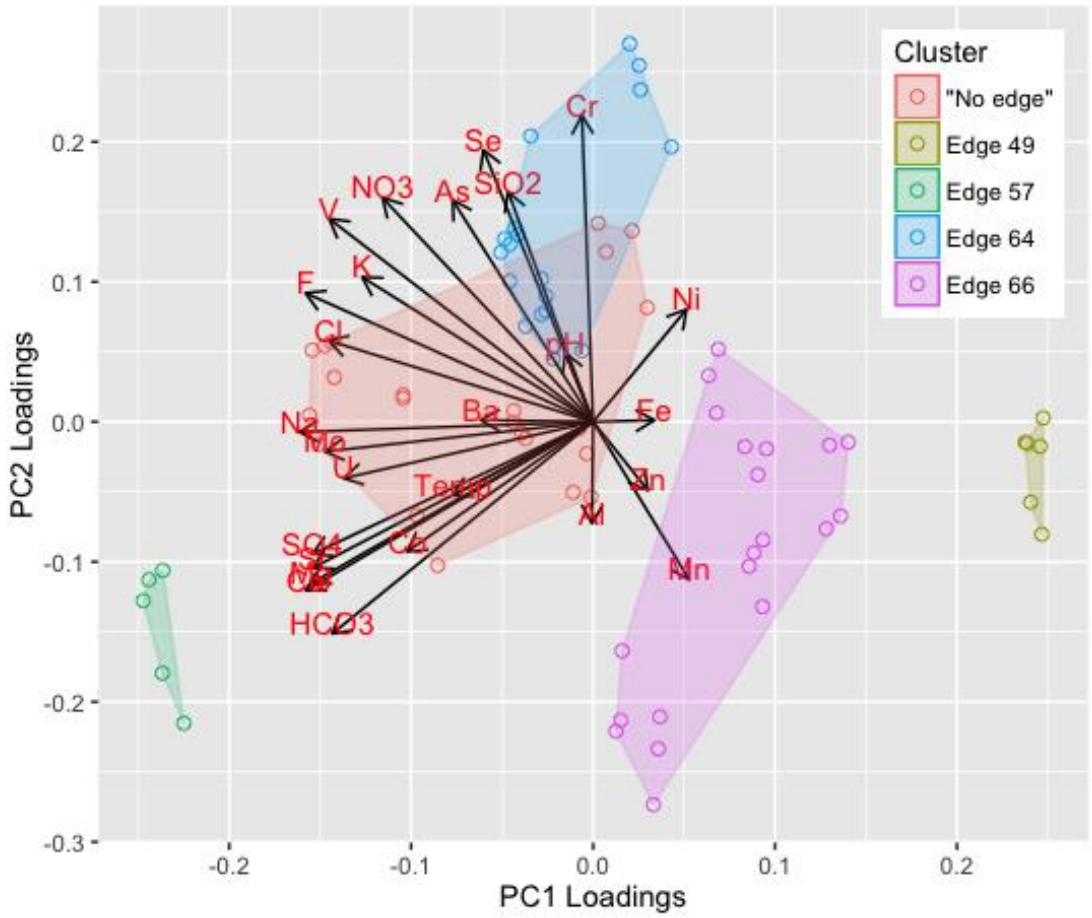

Figure 25. PC1-PC2 biplot with PC scores grouped by clusters or "edges" from the HCA

Edge 64 includes all samples from the most northwesterly boreholes (Figure 1) including Foulan Koira SE2, Tondobon, Fada, and the first three samples from Foulan Koira SE3. With the exception of Tondobon, edge 64 boreholes are characterized by low negative PC1 scores, suggesting weathering of silicate minerals may have accounted for some of the variation in the chemistry. All edge 64 boreholes are characterized by positive PC2 scores, suggesting the variation in water chemistry at these locations was associated with the weathering of near-surface laterite. A confidence level of 96 % indicates a high level of similarity between these samples and the fact that this edge is distinguishable in PC space verifies the PCA results.

The remaining two Foulan Koira SE3 samples did not cluster in edge 64, which is consistent with the PCA results because these samples had negative PC2 scores. The change from positive PC2 scores to negative PC2 scores suggests variation in the water chemistry at Foulan Koira SE3 over time and will be discussed in the following section.

All samples from Sabon Care SE1 form edge 57 with 96 % confidence. This edge is characterized by the greatest negative PC1 scores, a weathered granodiorite aquifer, and the highest EC values (average of 559.9 µS cm^{-1}). These particularly high TDS samples form an independent edge and suggest no significant variations in the chemistry over time at Sabon Care SE1. In support of the PCA, this edge stands alone as an independent group in PC space.

Edge 49 contains all six samples from Koubo SE2. The 100 % confidence level indicates that the water chemistry at this borehole was significantly different from all others and that there exists no significant variation in water chemistry over time. Edge 49 is characterized by the lowest EC of all boreholes (average of 143.3 µS cm^{-1}) and highest borehole yield (Table 6). The division of edges 49 and 66 illustrates the high spatial variation of groundwater chemistry of the fractured aquifer system; Koubo SE1 and Koubo SE2 were approximately 75 meters apart, but did not cluster together. This edge is also distinguishable as an independent group in PC space, supporting the results of the PCA.

4.7 Trend Analysis

When viewing PCA scores by individual boreholes, as shown in Figure 26, variation over time is visually discernible. Yellow circles mark boreholes with negative PC scores, while boreholes with positive scores are marked by black “plus signs.” Symbol size increases as the PC score magnitude increases. A range of symbols and symbol sizes at a borehole suggests that PC scores varied over time, perhaps because of temporal variation in controls on groundwater chemistry, varying groundwater levels, and groundwater mixing. An RKT was employed with the

goal of determining whether a region-wide trend in PC scores could be detected. The results of the RKT of the first two PC scores are presented in Table 8.

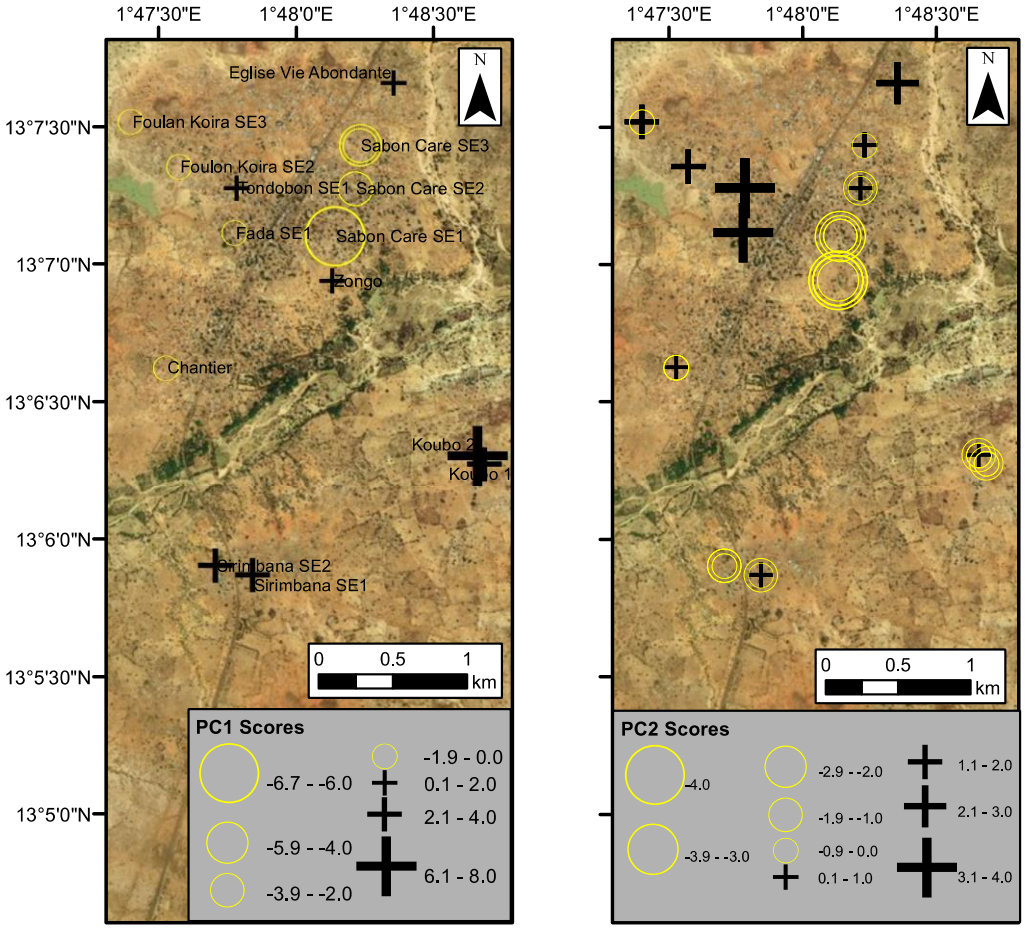

Figure 26. Maps of PC1 and PC2 scores. Varying symbols and symbol sizes at each site indicate temporal variations in PC scores.

Table 8. Results of the Regional Kendall's tests. The p-value with an asterisk (*) is just outside the significance range.

Test	**RKT1**	**RKT2**
PC score number	**PC1**	**PC2**
tau (τ)	0.22	-0.49
Kendall's score (S)	31	-69
p-value	0.06*	<0.05
Theil-Sen's slope	0.94	-2.69

The first test (RKT1) was performed on the regional PC1 scores and the p-value fell just outside the significance range ($p < 0.06$), thus, the null hypothesis stating no regional trend was not rejected. However, the p-value was regarded low enough to explore the remaining results of RKT1. A positive Kendall score (S_1) of 31 indicates that there were 31 more increases in PC1 scores over time than decreases in PC1 scores. In agreement, a TS slope of 0.94 indicates a regional increasing trend of 0.94 over the study period with a strength of $\tau = 0.22$. An increasing trend in PC1 scores throughout the region may indicate that there was an overall reduction in the impact of weathering of silicate minerals on groundwater chemistry throughout the duration of the study. Recall that positive PC1 scores are characterized by lower TDS concentrations, reduced residence times, and lower weathering. Thus, a trend towards positive PC1 space, would typically suggest a reduction in TDS throughout the region. A τ of -0.12 indicates that there was a regional decrease in TDS, but a p-value of 0.24 suggests no significant trend. This discrepancy may suggest that PC1 is not characterized solely by TDS.

Results of RKTs performed on individual major ions, minor ions, and SiO_2 show that there were significant increasing trends in SiO_2, Na, Mg, HCO_3, and Cl. Concurrently, there were significant decreasing trends in K, NO_3, and F. Varying trend directions in these variables, which control TDS, indicate why there is no significant trend direction in TDS.

An S_2 of -69 and slope of -2.69 for RKT2 indicate a significant negative regional trend of the PC2 scores with a strength of $\tau = -0.49$. Recall that positive PC2 scores are characterized by the weathering of a laterite and negative PC2 scores are represented by weathering of Ca and Mg-rich silicate minerals in the absence of laterite. The strong negative-regional trend in PC2 scores may suggest an increased impact of Ca and Mg on groundwater chemistry throughout the study period. This may be the result of the continued weathering of Ca and Mg-silicate minerals in the aquifer or increased concentrations due to declines in groundwater level. In agreement, negatively

loaded PC2 variables, including Mg and HCO_3, had significant increasing regional trends. In addition, at laterite sites (i.e., boreholes with positive PC2 scores), a negative trend in PC2 scores suggests a reduced impact of laterite on groundwater chemistry throughout the study period. This trend may be caused by the reduced leaching of laterite elements during the dry season.

Overall, groundwater levels showed a strong decreasing trend from November until May throughout the region (TS slope = -2.3, τ = -0.77, $p < 0.01$). The lowering of the water table has been observed at similar sites during the dry season (Lutz et al., 2015). Groundwater may have been lost to groundwater pumping, evapotranspiration, and inter-basin flow. By replacing groundwater levels for time in the RKT, it was determined that the variables that had significant trends over time were also correlated to groundwater levels. This was expected because of the strong correlation between water levels and time. As groundwater levels reduced throughout the study, there were significant increases in pH, SiO_2, Na, Mg, HCO_3, and Cl. These elements may have become more concentrated as a result of reduced groundwater levels. Significant reductions in K, NO_3, and F were observed. Nitrate concentrations were likely the highest at the beginning of the study period due to an influx of NO_3 to the water table during the rainy season, which ended two to three months prior to sampling.

5.0 Conclusions

Results of an in-depth exploration of controls on groundwater chemistry suggest that both natural and anthropogenic factors impacted groundwater chemistry in the Torodi aquifer throughout the six-month study period. The local geology accounted for the majority of variations of dissolved constituents in groundwater and the weathering of silicate minerals explains the Ca-Mg-HCO_3 water type. While these observations were expected, the combined PCA and HCA statistical methodology provided additional insight, suggesting that the degree of past weathering of the geologic complexes controlled the majority (i.e., 52 %) of the total variances in

groundwater chemistry. As indicated by PC1, 40 % of the variances were explained by the extent of weathered and fractured layers in the aquifer. Principal component 2 suggests that the presence or absence of laterite accounted for 12 % of the variances. A significant decreasing regional trend in PC2 indicates that the influence of weathering Ca and Mg-rich silicate minerals on groundwater chemistry increased significantly throughout the study period, while in areas of laterite, the impact of laterite decreased. The regional groundwater level also displayed a significant decreasing trend and the greatest mean groundwater level reductions were observed at residential boreholes and boreholes within fractured aquifer segments.

Samples of similar groundwater chemistry cluster by spatial proximity, land cover, aquifer weathering or fracturing, or by presence or absence of laterite. Significant similarities in groundwater chemistry were observed at the most northwesterly boreholes, which may suggest a section of hydraulic connectivity or a homogeneous aquifer segment. However, groundwater chemistry at neighboring boreholes, Koubo SE1 and Koubo SE2, were significantly different, indicating high spatial variation in the groundwater chemistry. Concentrations of NO_3 and Cl were significantly greater in residential areas than agricultural lands and bare soil zones, indicating anthropogenic sources.

6.0 Recommendations

A recommendation for future studies is to evaluate groundwater chemistry over a greater area and more time. To enhance understanding of spatial variations with respect to geology, surface hydrology, land cover, and population density, it would be helpful to analyze water chemistry throughout the entire Torodi drainage basin. Annual observations would be useful to understand long-term trends and variations in relation to climate change and population growth. Furthermore, collecting groundwater samples during periods of recharge would provide insight

into seasonal variations. A water-rock reaction model may reveal how groundwater chemistry changes along flow paths.

Future groundwater chemistry studies and potable water projects would benefit from analyzing groundwater samples for microbial contaminants in addition to chemical constituents. As part of the monitoring and evaluation stage of such projects, sequential groundwater sampling and analyses should be conducted to ensure safe drinking water and to determine whether variables show trends. Nitrate concentrations should be monitored at residential areas, especially where weathered zones are thin and natural filtration of contaminants is reduced. Proper construction, placement, and usage of latrines may help reduce future nitrate concentrations in groundwater.

7.0 Appendix

7.1 Groundwater chemistry of the south Liptako from 2009-2015

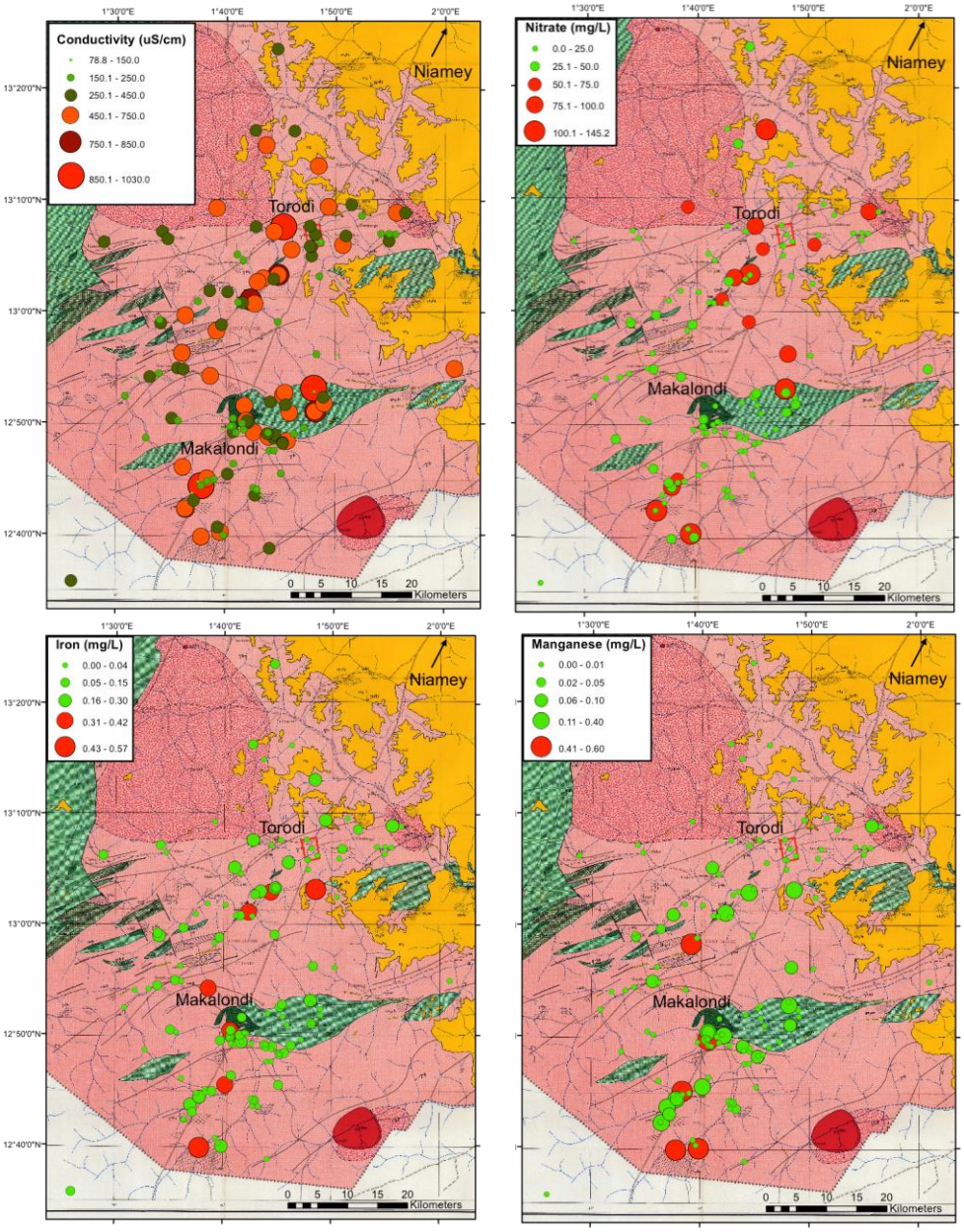

Figure 27. Maps showing EC (top-left), NO_3 (top-right), Fe (bottom-left), and Mn (bottom-right) concentrations of south Liptako groundwater from 2009 to 2015. Green circles indicate concentrations below the WHO guideline and red circles are above the guideline. Orange circles in the EC map indicate concentrations approaching the guideline of 750 µS cm^{-1}. The pink geologic unit represents granitoids (Upper Birimian), green represents greenstones (Lower Birimian), and yellow are continental deposits (late Tertiary). Groundwater data was made available by NI-WASH.

7.2 NI-WASH Borehole Logs

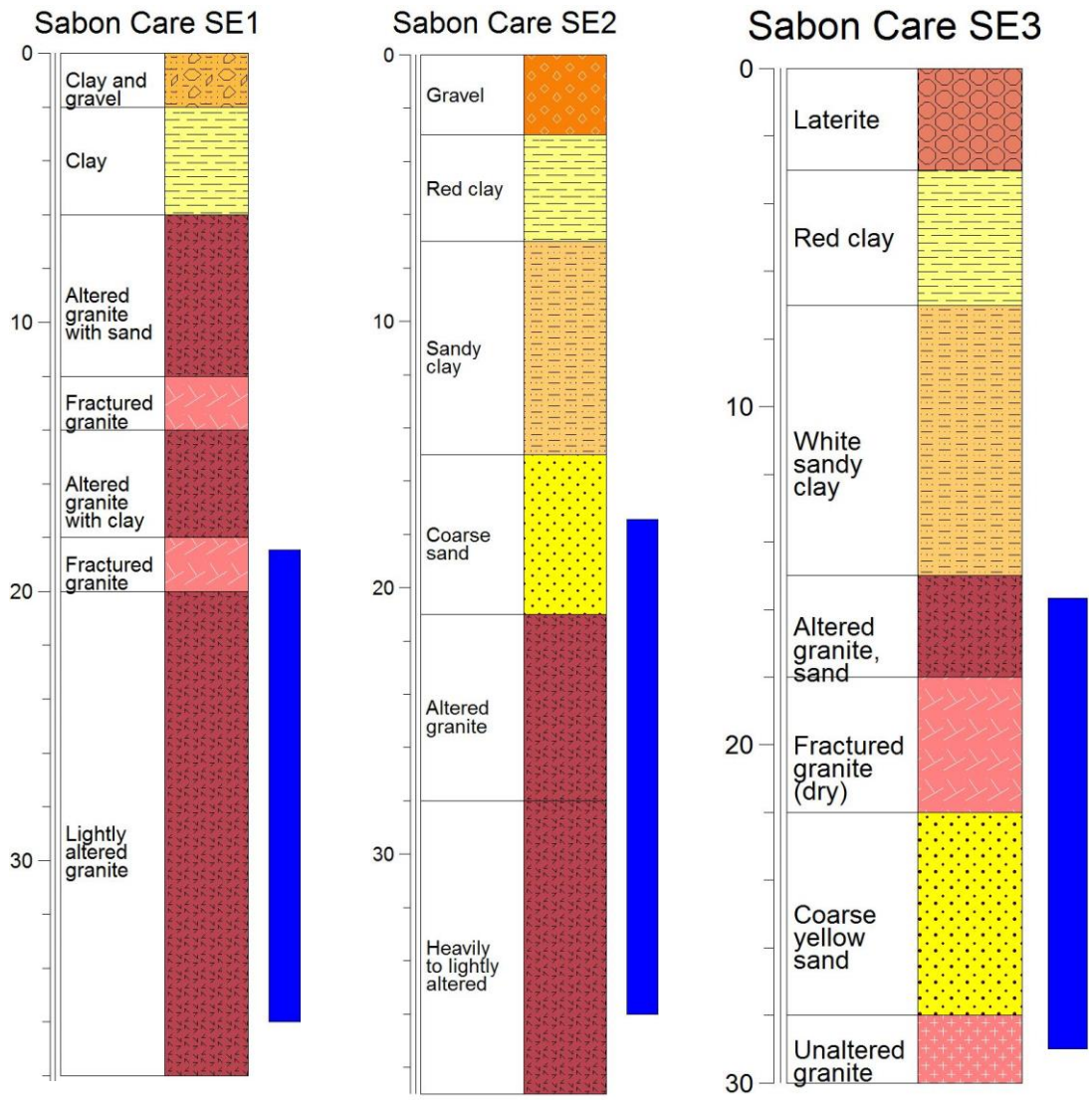

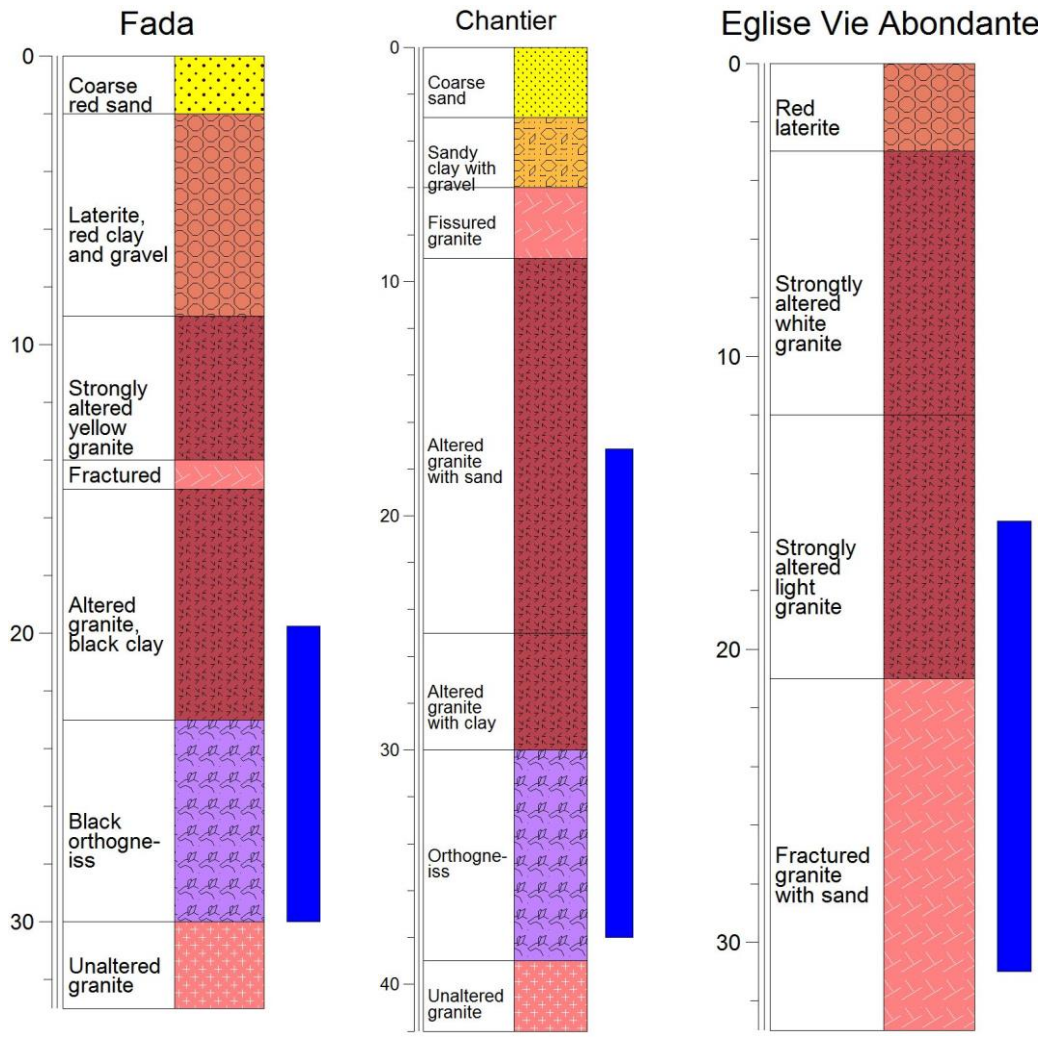
Fada
0
10
20
30
Coarse red sand
Laterite, red clay and gravel
Strongly altered yellow granite
Fractured
Altered granite, black clay
Black orthogne-iss
Unaltered granite
Chantier
0
10
20
30
40
Coarse sand
Sandy clay with gravel
Fissured granite
Altered granite with sand
Altered granite with clay
Orthogne-iss
Unaltered granite
Eglise Vie Abondante
0
10
20
30
Red laterite
Strongly altered white granite
Strongly altered light granite
Fractured granite with sand

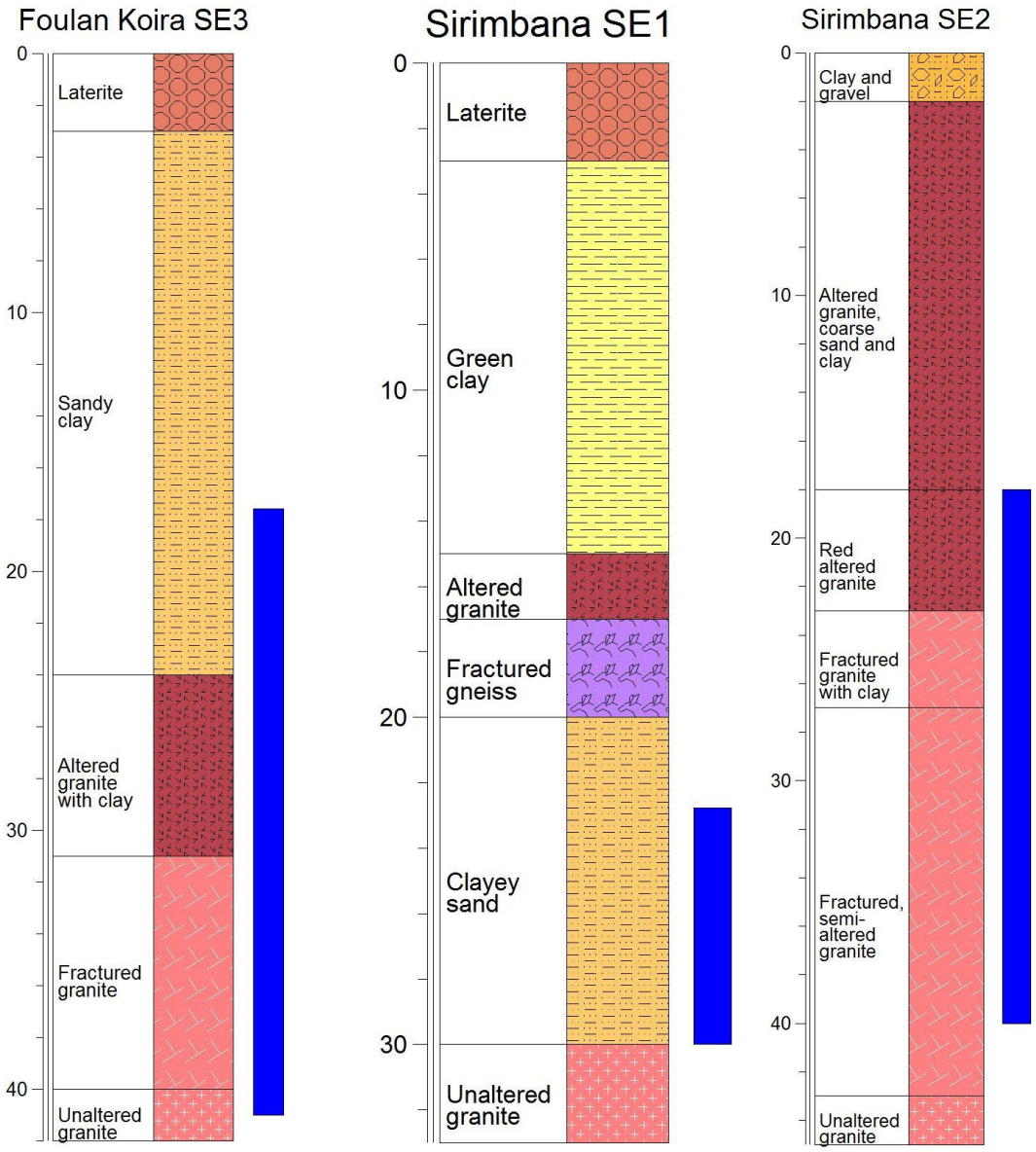

Figure 28. Borehole logs made in RockWare for nine of fourteen sampling locations based on observations made by NI-WASH during drilling. Depth below land surface (in meters) and unit descriptions are found to the left of each log. The aquifer depth and thickness is demonstrated by the blue bar. Borehole logs are not available for Zongo, Koubo SE1, Koubo SE2, Foulan Koira SE2, and Tondobon.

7.3 Internal Consistency

A summary of laboratory-field measurement accuracies is found in Table 9. To check for internal consistency of the chemical analyses, each sample was subjected to a cation-anion balance test by determining the charge balance error (CBE). The CBEs were determined using the RockWare software, then verified with the equation

$$CBE = \frac{\sum cations - \sum |anions|}{\sum cations + \sum |anions|} * 100$$

where Σcations is equal to the sum of the concentrations of cations (i.e., Ca, Mg, Na, and K) in meq L^{-1} and Σ|anions| is equal to the sum of the absolute values of the concentrations of anions (i.e., HCO_3, Cl, SO_4, and NO_3) in meq L^{-1}.

Laboratory-measured TDS were checked for accuracy with the equation

$$TDS = \sum cations + \sum anions + SiO_2$$

where Σcations is the sum of the cation concentrations in mg L^{-1} and Σanions is the sum of the anions in mg L^{-1} plus 0.5 × total alkalinity in mg L^{-1}. Half of the concentration of total alkalinity is used when calculating TDS to compare to the laboratory-measured value because approximately half of the bicarbonate is lost to the atmosphere when the samples are taken to dryness in the laboratory (Hem, 1985). Laboratory-measured TDS includes dissolved SiO_2 concentrations, therefore it is included in the calculation above.

Table 9. Laboratory-field measurement accuracy checks.

Sample ID	Field pH	Lab pH	Dif.	∑Anions	∑Cations	CBE (%)	Lab TDS	Calc. TDS	Dif.
CH001	6.4	7.8	1.4	-3.3	3.3	0.2%	240.0	243.0	-3.0
CH002	6.5	7.7	1.2	-3.3	3.3	-0.1%	250.0	239.3	10.7
CH003	6.6	7.5	0.9	-3.3	3.3	-0.2%	240.0	241.9	-1.9
CH004	6.4	7.4	1.0	-3.3	3.3	-1.0%	240.0	239.2	0.8
CH005	6.5	7.6	1.1	-3.3	3.5	2.9%	240.0	247.9	7.9
CH006	6.3	7.5	1.2	-3.3	3.4	1.6%	230.0	247.6	17.6
EVA001	6.8	8.0	1.2	-2.7	2.6	-1.3%	180.0	222.5	-42.5
EVA002	6.6	8.0	1.3	-2.7	2.6	-1.0%	210.0	222.2	-12.2
EVA003	6.7	7.9	1.2	-2.6	2.7	1.5%	200.0	226.0	26.0
EVA004	6.8	7.9	1.1	-2.7	2.8	2.2%	210.0	230.4	20.4
F001	6.7	7.9	1.2	-2.6	3.1	8.5%	250.0	217.8	32.2
F002	6.7	7.8	1.1	-3.2	3.1	-1.9%	240.0	253.8	-13.8
F003	7.2	8.1	0.9	-3.3	3.1	-2.1%	250.0	261.3	-11.3
F004	6.8	8.0	1.2	-3.2	3.1	-1.3%	250.0	256.4	-6.4
F005	7.1	8.0	0.9	-3.2	3.2	1.0%	240.0	260.2	20.2
F006	7.3	8.1	0.8	-3.1	3.2	0.9%	250.0	260.5	10.5
FK2001	6.9	8.1	1.2	-3.1	3.0	-1.6%	220.0	234.8	-14.8
FK2002	7.1	8.0	0.9	-3.1	3.1	-0.6%	220.0	235.9	-15.9
FK2003	6.7	8.1	1.4	-3.1	3.0	-1.2%	250.0	231.2	18.8
FK2004	6.9	7.9	1.0	-3.1	3.2	1.7%	240.0	241.9	1.9
FK2005	6.9	8.1	1.2	-3.0	3.2	2.8%	170.0	236.8	66.8
FK3001	6.9	7.9	0.9	-2.9	2.9	0.1%	230.0	223.2	6.8
FK3002	7.0	8.2	1.1	-2.9	2.9	-0.7%	210.0	222.5	-12.5
FK3003	6.9	8.0	1.1	-2.9	2.9	-0.3%	260.0	222.7	37.3
FK3004	6.9	8.0	1.1	-3.1	3.2	2.2%	220.0	235.8	15.8
FK3005	6.6	8.1	1.6	-3.1	3.3	3.1%	210.0	238.0	28.0
K1001	6.7	8.0	1.3	-2.3	2.2	-1.3%	180.0	186.5	-6.5
K1002	6.7	8.0	1.3	-2.4	2.3	-0.9%	180.0	192.1	-12.1
K1003	6.8	7.8	1.0	-2.5	2.6	2.2%	170.0	203.8	33.8
K1004	7.0	8.0	1.0	-2.3	2.4	1.3%	190.0	192.0	2.0
K2001	7.0	7.9	0.9	-1.5	1.5	-0.7%	140.0	136.6	3.4
K2002	6.8	8.2	1.4	-1.5	1.4	-1.3%	140.0	133.9	6.1
K2003	7.1	8.2	1.1	-1.4	1.4	0.1%	130.0	131.1	-1.1
K2004	7.0	8.1	1.1	-1.4	1.4	-1.2%	130.0	131.2	-1.2
K2005	7.0	8.1	1.1	-1.5	1.5	1.1%	130.0	134.3	4.3
K2006	6.6	7.8	1.2	-1.5	1.5	0.0%	130.0	138.4	8.4
S1001	6.7	7.8	1.1	-2.8	2.8	-0.2%	200.0	208.8	-8.8
S1002	6.5	7.8	1.2	-2.8	2.8	-0.9%	190.0	211.3	-21.3
S1003	6.7	7.8	1.1	-2.8	3.0	1.9%	190.0	209.8	-19.8

Sample ID	Field pH	Lab pH	Dif.	∑Anions	∑Cations	CBE (%)	Lab TDS	Calc. TDS	Dif.
S1004	6.6	8.3	1.6	-2.9	3.0	1.4%	210.0	215.5	5.5
S1005	6.8	8.1	1.3	-2.7	2.7	0.8%	210.0	215.1	5.1
S2001	6.9	8.0	1.1	-2.7	2.7	0.4%	200.0	199.3	0.7
S2002	6.8	7.9	1.1	-2.8	2.9	2.0%	200.0	200.0	0.0
S2003	6.8	7.9	1.1	-2.7	2.9	2.2%	190.0	197.7	-7.7
S2004	6.9	7.7	0.9	-2.9	2.8	-0.7%	210.0	206.2	-3.8
S2005	6.9	7.8	0.9	-2.7	2.7	0.4%	190.0	204.2	14.2
SC1001	6.8	7.6	0.8	-5.8	5.6	-1.1%	360.0	358.3	1.7
SC1002	6.9	7.8	0.9	-5.6	5.6	-0.2%	360.0	351.6	8.4
SC1003	7.0	7.7	0.7	-5.6	5.6	-0.4%	370.0	353.0	17.0
SC1004	7.1	7.9	0.8	-5.7	5.9	1.9%	350.0	365.7	15.7
SC1005	7.2	7.9	0.7	-5.7	5.9	1.7%	350.0	368.8	18.8
SC2001	7.1	8.1	0.9	-3.5	3.5	-0.3%	260.0	251.5	8.5
SC2002	7.3	8.0	0.7	-3.5	3.6	1.7%	260.0	253.2	6.8
SC2003	6.6	7.9	1.2	-3.7	3.8	2.6%	250.0	260.4	10.4
SC2004	6.6	7.6	1.1	-3.6	3.7	1.4%	250.0	259.9	9.9
SC3001	6.6	7.8	1.1	-4.2	4.1	-0.8%	280.0	280.4	-0.4
SC3002	6.6	7.5	0.9	-4.2	4.1	-0.5%	280.0	277.6	2.4
SC3003	6.9	8.0	1.1	-4.2	4.1	-0.8%	270.0	278.4	-8.4
SC3004	7.0	7.8	0.8	-4.2	4.2	0.1%	260.0	281.9	-21.9
SC3005	6.9	8.0	1.1	-4.3	4.5	2.1%	270.0	291.5	21.5
SC3006	7.0	7.8	0.8	-4.3	4.5	1.9%	270.0	293.0	23.0
T001	7.1	8.1	1.0	-2.5	2.5	-0.4%	190.0	212.4	-22.4
T002	7.2	8.0	0.8	-2.5	2.5	-0.6%	200.0	213.2	-13.2
T003	7.1	8.0	0.9	-2.5	2.6	0.6%	210.0	219.9	9.9
T004	7.2	7.8	0.6	-2.5	2.6	1.5%	210.0	216.8	6.8
Z001	7.1	7.9	0.7	-3.3	3.2	-1.2%	210.0	211.9	-1.9
Z002	7.0	8.0	1.0	-3.3	3.2	-1.5%	200.0	211.8	-11.8
Z003	6.8	7.9	1.0	-3.3	3.2	-1.3%	210.0	210.8	-0.8
Z004	6.8	7.7	0.9	-3.3	3.1	-2.0%	210.0	210.9	-0.9
Z005	6.9	8.1	1.2	-3.3	3.4	1.6%	220.0	220.9	0.9
Z006	6.8	7.9	1.0	-3.3	3.4	1.2%	210.0	221.6	11.6

7.4 Physicochemical datasets

Sample identifications in Tables 10, 11, and 12 were created using site abbreviations and sample numbers. Site abbreviations are CH = Chantier, EVA = Eglise Vie Abondante, F = Fada, FK2 = Foulan Koira SE2, FK3 = Foulan Koira SE3, K1 = Koubo SE1, K2 = Koubo SE2, S1 = Sirimbana SE1, S2 = Sirimbana SE2, SC1 = Sabon Care SE1, SC2 = Sabon Care SE2, SC3 = Sabon Care SE3, T = Tondobon, and Z = Zongo. Samples are numbered in the order in which they were collected, starting with 001 at each site (i.e., CH001 is the first sample collected from Chantier and CH002 is the second sample collected at Chantier).

Table 10. Major ion concentrations, chemical parameters, and physical data.

		Parameter	Alkalinity	pH	Temp	TDS	Ca	Mg	Na	K	SiO_2	Si	HCO_3	Cl	SO_4	NO_3 -N	NO_3	F
		Unit	(mg $CaCO_3$ L^{-1})	-	°C	mg L^{-1}	mg L^{-1}	mg L^{-1}	mg L^{-1}	mg L^{-1}	mg L^{-1}	mg L^{-1}	mg L^{-1}	mg L^{-1}	mg L^{-1}	mg L^{-1}	mg L^{-1}	mg L^{-1}
		Rep. Limit	20	2	15	25	5	5	5	5	1	0.5	-	5	5	0.5	-	0.1
		WHO guide/rec	-	-	-	600	-	-	200	-	-	-	-	250	250	-	50	-
Sample ID	**Sample Date**	**Analysis Date**																
CH001	12/16/16	3/24/17	150.00	8.12	22.20	240.00	25.90	14.90	16.80	3.50	90.00	41.80	183.00	2.24	6.12	1.93	8.55	0.32
CH002	1/11/17	3/24/17	150.00	7.96	22.30	250.00	25.50	14.90	16.50	3.50	88.00	41.40	183.00	2.23	6.08	1.72	7.62	0.32
CH003	2/6/17	3/24/17	150.00	8.03	22.40	240.00	25.40	14.90	16.60	3.50	90.00	41.70	183.00	2.24	6.19	1.83	8.10	0.32
CH004	3/6/17	3/24/17	150.00	7.77	22.60	240.00	25.00	14.70	16.40	3.40	88.00	41.30	183.00	2.24	6.67	1.77	7.84	0.32
CH005	4/10/17	6/9/17	149.05	7.89	22.00	240.00	25.00	17.00	17.00	3.40	96.00	45.00	181.85	2.36	6.00	1.50	6.64	0.30
CH006	5/16/17	6/9/17	148.57	7.71	21.50	230.00	25.00	16.00	17.00	3.30	96.00	45.00	181.26	2.45	6.00	1.70	7.53	0.30
EVA001	2/27/17	3/24/17	100.00	7.81	22.60	180.00	19.90	12.10	12.10	3.90	86.00	39.70	122.00	3.29	5.69	6.66	29.49	0.44
EVA002	3/13/17	3/24/17	99.00	7.77	22.50	210.00	19.80	12.30	12.00	3.80	86.00	40.00	120.78	3.37	5.72	6.71	29.71	0.44
EVA003	4/18/17	6/9/17	100.44	7.77	21.20	200.00	19.00	14.00	12.00	3.80	92.00	43.00	122.53	3.30	6.00	5.80	25.68	0.40
EVA004	5/25/17	6/9/17	100.06	7.63	21.20	210.00	20.00	14.00	12.00	4.00	94.00	44.00	122.07	3.39	6.00	6.10	27.01	0.40
F001	12/16/16	3/24/17	96.00	8.10	22.70	250.00	22.60	15.40	14.10	2.90	86.00	40.50	117.12	15.40	6.93	1.47	6.51	0.47
F002	1/11/17	3/24/17	96.00	7.92	22.30	240.00	22.60	15.00	14.30	2.90	86.00	40.50	117.12	14.81	6.91	9.78	43.31	0.47
F003	2/6/17	3/24/17	96.00	8.07	22.00	250.00	23.20	15.10	14.90	3.00	88.00	40.70	117.12	15.75	7.08	10.45	46.27	0.48
F004	3/6/17	3/24/17	96.00	7.85	22.80	250.00	23.60	14.70	14.90	3.00	86.00	40.50	117.12	14.72	7.02	10.04	44.46	0.47
F005	4/10/17	6/9/17	99.35	7.82	21.30	240.00	23.00	16.00	16.00	2.80	92.00	43.00	121.20	14.32	7.00	8.90	39.41	0.40
F006	5/16/17	6/9/17	98.16	7.74	21.40	250.00	23.00	16.00	15.00	3.00	94.00	44.00	119.76	14.01	7.00	8.90	39.41	0.40
FK2001	1/9/17	3/24/17	130.00	8.08	21.40	220.00	21.50	14.00	16.30	3.30	88.00	41.40	158.60	4.81	7.06	3.34	14.79	0.57
FK2002	1/31/17	3/24/17	130.00	8.03	21.50	220.00	22.40	13.90	16.70	3.50	88.00	40.70	158.60	4.92	7.09	3.26	14.44	0.56
FK2003	2/20/17	3/24/17	130.00	7.95	21.60	250.00	21.60	14.10	15.90	3.50	86.00	40.30	158.60	4.94	7.15	2.93	12.97	0.55
FK2004	4/3/17	6/9/17	133.33	7.89	21.50	240.00	22.00	16.00	17.00	3.20	94.00	44.00	162.67	4.96	7.00	2.50	11.07	0.50
FK2005	5/9/17	6/9/17	127.59	7.85	21.40	170.00	22.00	16.00	16.00	3.40	92.00	43.00	155.66	5.12	7.00	2.60	11.51	0.50
FK3001	1/9/17	3/24/17	120.00	8.10	21.70	230.00	22.60	15.40	11.00	2.90	83.00	39.40	146.40	4.57	6.56	3.88	17.18	0.36
FK3002	1/31/17	3/24/17	120.00	8.05	21.90	210.00	22.20	15.30	10.70	2.80	83.00	39.10	146.40	4.57	6.60	3.92	17.36	0.36
FK3003	2/20/17	3/24/17	120.00	8.02	22.40	260.00	22.30	15.50	10.70	2.80	83.00	39.30	146.40	4.54	6.64	3.90	17.27	0.36
FK3004	4/3/17	6/9/17	127.20	8.05	21.40	220.00	24.00	17.00	12.00	2.70	90.00	42.00	155.18	4.60	6.00	3.60	15.94	0.30
FK3005	5/9/17	6/9/17	127.59	8.02	21.60	210.00	24.00	18.00	12.00	2.80	90.00	42.00	155.66	4.60	6.00	3.80	16.83	0.30
K1001	2/27/17	3/24/17	98.00	7.62	21.20	180.00	18.80	9.00	11.20	2.10	79.00	36.70	119.56	0.96	5.46	2.48	10.98	0.09
K1002	3/13/17	3/24/17	100.00	7.52	21.60	180.00	19.60	9.50	11.80	1.90	79.00	37.30	122.00	1.00	5.46	3.12	13.82	0.09
K1003	4/18/17	6/9/17	106.64	7.88	21.60	170.00	21.00	11.00	13.00	1.80	86.00	40.00	130.10	1.13	5.00	2.60	11.51	0.08
K1004	5/25/17	6/9/17	101.13	7.62	22.30	190.00	20.00	10.00	12.00	1.70	81.00	38.00	123.38	1.11	5.00	2.40	10.63	0.08
K2001	12/16/16	3/24/17	67.00	7.77	20.90	140.00	12.70	5.90	7.00	1.80	68.00	31.60	81.74	0.86	3.94	0.65	2.88	0.08
K2002	1/11/17	3/24/17	66.00	7.68	21.30	140.00	12.30	5.80	6.90	2.00	66.00	31.20	80.52	1.31	3.84	0.63	2.79	0.08

		Parameter	Alkalinity	pH	Temp	TDS	Ca	Mg	Na	K	SiO_2	Si	HCO_3	Cl	SO_4	NO_3 -N	NO_3	F
		Unit	(mg $CaCO_3$ L^{-1})	-	°C	mg L^{-1}	mg L^{-1}	mg L^{-1}	mg L^{-1}	mg L^{-1}	mg L^{-1}	mg L^{-1}	mg L^{-1}	mg L^{-1}	mg L^{-1}	mg L^{-1}	mg L^{-1}	mg L^{-1}
		Rep. Limit	20	2	15	25	5	5	5	5	1	0.5	-	5	5	0.5	-	0.1
		WHO guide/rec	-	-	-	600	-	-	200	-	-	-	-	250	250	-	50	-
Sample ID	**Sample Date**	**Analysis Date**																
K2003	2/6/17	3/24/17	65.00	7.51	21.00	130.00	12.40	5.80	6.50	1.90	66.00	31.00	79.30	0.85	3.91	0.29	1.28	0.08
K2004	3/6/17	3/24/17	65.00	7.37	21.00	130.00	12.20	5.70	6.30	1.90	66.00	30.90	79.30	0.83	4.09	0.38	1.68	0.08
K2005	4/10/17	6/9/17	67.22	7.75	22.40	130.00	13.00	6.00	7.00	1.60	68.00	32.00	82.01	0.96	3.73	0.09	0.40	0.07
K2006	5/16/17	6/9/17	68.41	7.54	22.10	130.00	13.00	6.00	7.00	1.60	71.00	33.00	83.46	0.97	3.87	0.17	0.75	0.07
S1001	1/9/17	3/24/17	130.00	7.93	21.30	200.00	21.80	14.00	11.90	2.40	81.00	38.30	158.60	1.66	7.33	0.84	3.72	0.23
S1002	1/31/17	3/24/17	130.00	7.93	21.20	190.00	22.60	13.50	12.40	2.40	83.00	39.00	158.60	1.53	7.20	0.83	3.68	0.23
S1003	2/20/17	3/24/17	130.00	7.79	21.50	190.00	22.00	13.50	12.10	2.30	83.00	39.00	158.60	1.57	7.38	0.67	2.97	0.24
S1004	4/3/17	6/9/17	132.30	7.96	21.90	210.00	22.00	15.00	13.00	2.20	88.00	41.00	161.41	1.68	7.00	0.10	0.44	0.20
S1005	5/9/17	6/9/17	132.22	7.79	22.30	210.00	22.00	15.00	13.00	2.10	86.00	40.00	161.31	1.71	7.00	0.50	2.21	0.20
S2001	1/9/17	3/24/17	120.00	8.01	21.80	200.00	22.20	13.70	9.40	2.30	77.00	36.10	146.40	1.34	6.43	1.56	6.91	0.17
S2002	1/31/17	3/24/17	120.00	7.95	21.50	200.00	22.70	13.50	9.70	2.40	77.00	35.90	146.40	1.35	6.52	1.55	6.86	0.17
S2003	2/20/17	3/24/17	120.00	7.87	21.30	190.00	22.30	13.60	9.50	2.40	75.00	35.30	146.40	1.31	6.53	1.59	7.04	0.17
S2004	4/3/17	6/9/17	125.81	7.96	22.90	210.00	23.00	15.00	10.00	2.00	81.00	38.00	153.49	1.45	6.00	1.10	4.87	0.20
S2005	5/9/17	6/9/17	125.17	7.82	23.20	190.00	23.00	15.00	10.00	2.20	79.00	37.00	152.71	1.51	6.00	1.10	4.87	0.20
SC1001	1/9/17	3/24/17	220.00	8.16	22.40	360.00	43.70	27.90	24.90	3.40	77.00	36.20	268.40	14.64	10.78	10.39	46.01	0.63
SC1002	1/31/17	3/24/17	210.00	8.04	22.20	360.00	43.00	27.30	24.60	3.50	77.00	35.90	256.20	14.55	11.52	10.19	45.12	0.62
SC1003	2/20/17	3/24/17	210.00	8.03	22.20	370.00	42.70	27.90	24.10	3.30	77.00	36.30	256.20	15.02	10.78	10.67	47.25	0.63
SC1004	4/3/17	6/9/17	214.62	8.11	22.90	350.00	43.00	31.00	25.00	3.20	86.00	40.00	261.84	14.92	11.00	10.00	44.28	0.60
SC1005	5/8/17	6/9/17	211.87	8.04	22.60	350.00	43.00	31.00	25.00	3.20	86.00	40.00	258.48	14.94	11.00	11.00	48.71	0.60
SC2001	2/27/17	3/24/17	130.00	8.02	22.80	260.00	28.60	15.30	16.70	3.20	73.00	34.40	158.60	6.67	7.86	7.94	35.16	0.65
SC2002	3/13/17	3/24/17	130.00	7.92	22.40	260.00	30.20	15.40	17.50	3.30	73.00	34.20	158.60	6.56	7.85	7.76	34.36	0.63
SC2003	4/18/17	6/9/17	139.17	7.98	22.40	250.00	31.00	18.00	17.00	3.10	75.00	35.00	169.79	6.83	8.00	7.20	31.88	0.60
SC2004	5/25/17	6/9/17	136.43	7.76	22.80	250.00	30.00	17.00	17.00	3.10	77.00	36.00	166.44	6.79	8.00	7.40	32.77	0.60
SC3001	12/16/16	3/24/17	170.00	8.16	22.60	280.00	33.10	18.70	19.60	3.70	77.00	35.90	207.40	5.73	8.28	6.62	29.31	0.60
SC3002	1/11/17	3/24/17	170.00	8.17	22.80	280.00	33.00	18.80	19.10	3.70	77.00	36.10	207.40	5.12	7.72	6.37	28.21	0.60
SC3003	2/6/17	3/24/17	170.00	8.09	23.00	270.00	32.90	18.90	18.90	3.50	77.00	36.00	207.40	5.27	7.75	6.59	29.18	0.59
SC3004	3/4/17	3/24/17	170.00	8.07	23.20	260.00	34.20	18.90	19.70	3.60	77.00	36.00	207.40	5.49	7.83	6.81	30.15	0.60
SC3005	4/10/17	6/9/17	175.79	7.85	22.80	270.00	34.00	22.00	20.00	3.40	83.00	39.00	214.46	5.75	8.00	6.20	27.45	0.60
SC3006	5/16/17	6/9/17	175.09	7.96	22.70	270.00	34.00	22.00	20.00	3.40	83.00	39.00	213.61	5.85	8.00	6.60	29.22	0.60
T001	2/27/17	3/24/17	95.00	7.76	22.50	190.00	18.20	10.80	13.80	3.50	86.00	39.70	115.90	4.58	5.49	5.09	22.54	0.43
T002	3/13/17	3/24/17	94.00	7.80	23.00	200.00	18.20	10.70	13.80	3.50	86.00	39.60	114.68	4.58	5.61	5.38	23.82	0.43
T003	4/18/17	6/9/17	96.59	7.86	22.80	210.00	18.00	12.00	14.00	3.10	92.00	43.00	117.84	4.83	6.00	4.90	21.70	0.40
T004	5/25/17	6/9/17	95.48	7.70	23.00	210.00	18.00	12.00	14.00	3.20	90.00	42.00	116.49	4.72	5.00	5.00	22.14	0.40
Z001	12/16/16	3/24/17	150.00	8.25	22.80	210.00	25.70	16.60	10.90	3.10	68.00	32.40	183.00	3.50	7.26	0.42	1.86	0.22

		Parameter	Alkalinity	pH	Temp	TDS	Ca	Mg	Na	K	SiO_2	Si	HCO_3	Cl	SO_4	NO_3 -N	NO_3	F
		Unit	(mg $CaCO_3$ L^{-1})	-	°C	mg L^{-1}	mg L^{-1}	mg L^{-1}	mg L^{-1}	mg L^{-1}	mg L^{-1}	mg L^{-1}	mg L^{-1}	mg L^{-1}	mg L^{-1}	mg L^{-1}	mg L^{-1}	mg L^{-1}
		Rep. Limit	20	2	15	25	5	5	5	5	1	0.5	-	5	5	0.5	-	0.1
		WHO guide/rec	-	-	-	600	-	-	200	-	-	-	-	250	250	-	50	-
Sample ID	**Sample Date**	**Analysis Date**																
Z002	1/11/17	3/24/17	150.00	8.09	22.50	200.00	25.80	16.40	10.90	2.90	68.00	32.40	183.00	3.51	7.19	0.48	2.13	0.22
Z003	2/6/17	3/24/17	150.00	7.95	22.60	210.00	25.80	16.30	10.90	3.00	68.00	32.00	183.00	3.50	7.35	0.22	0.97	0.22
Z004	3/6/17	3/24/17	150.00	7.88	22.60	210.00	25.30	16.40	10.60	2.90	68.00	32.00	183.00	3.47	7.40	0.41	1.82	0.22
Z005	4/10/17	6/9/17	152.86	8.08	23.00	220.00	26.00	19.00	11.00	2.80	75.00	35.00	186.49	3.53	7.00	0.04	0.18	0.20
Z006	5/16/17	6/9/17	154.25	7.86	23.30	210.00	26.00	19.00	11.00	2.80	75.00	35.00	188.19	3.47	7.00	0.04	0.18	0.20

Table 11. Trace-element concentrations before imputation.

	Parameter	Be	Al	V	Cr	Mn	Fe	Co	Ni	Cu	Zn	Sr	Mo	Ag	Cd	Sb	Ba	Tl	Pb	U	As	Se
	Unit	µg L^{-1}	µg L^{-1}	µg L^{-1}	µg L^{-1}	µg L^{-1}	µg L^{-1}	µg L^{-1}	µg L^{-1}	µg L^{-1}	µg L^{-1}	µg L^{-1}	µg L^{-1}	µg L^{-1}	µg L^{-1}	µg L^{-1}	µg L^{-1}	µg L^{-1}	µg L^{-1}	µg L^{-1}	µg L^{-1}	µg L^{-1}
	Det. Limit	0.097	0.064	0.008	0.011	0.007	0.060	0.007	0.009	0.013	0.011	0.168	0.030	0.008	0.008	0.008	0.176	0.023	0.009	0.021	0.009	0.014
	WHO Guide:	-	-	-	50	-	-	-	70	2000	-	-	-	-	3	20	700	-	10	30	10	40
Sample ID	Sample Date	Analysis Date																				
CH001	12/16/16	4/14/17	BDL	2.46	19.57	0.89	1.28	6.36	0.04	0.63	0.16	10.77	463.20	3.71	0.43	0.02	0.01	352.33	BDL	0.75	0.19	0.05	0.26
CH002	1/11/17	4/14/17	BDL	0.25	20.63	0.47	0.05	0.24	0.03	0.72	BDL	8.49	475.45	3.76	BDL	BDL	BDL	345.01	BDL	BDL	0.17	0.04	0.21
CH003	2/6/17	4/14/17	BDL	0.29	20.16	0.53	1.12	0.37	0.04	0.66	BDL	4.78	465.69	3.74	BDL	0.01	BDL	349.77	BDL	BDL	0.18	0.04	0.25
CH004	3/6/17	4/14/17	BDL	0.54	19.96	0.81	1.48	1.62	0.04	0.77	0.04	4.17	446.15	3.68	BDL	0.01	BDL	336.18	BDL	BDL	0.17	0.04	0.26
CH005	4/10/17	6/5/17	BDL	0.68	20.49	0.71	0.22	2.51	0.03	0.68	BDL	3.01	476.07	3.87	BDL	BDL	BDL	358.14	BDL	BDL	BDL	BDL	BDL
CH006	5/16/17	6/5/17	BDL	0.46	20.14	0.79	0.28	1.08	0.03	0.50	BDL	7.31	459.04	3.80	BDL	BDL	BDL	349.19	BDL	BDL	BDL	BDL	BDL
EVA001	2/27/17	4/14/17	BDL	0.50	25.37	1.70	0.64	1.23	0.03	0.69	BDL	18.52	306.82	1.13	BDL	BDL	BDL	289.69	BDL	BDL	0.05	0.03	0.25
EVA002	3/13/17	4/14/17	BDL	2.03	25.19	1.53	1.35	1.10	0.05	0.85	0.37	17.39	300.42	1.05	BDL	BDL	BDL	279.02	BDL	BDL	0.03	0.04	0.34
EVA003	4/18/17	6/5/17	BDL	0.66	26.44	1.21	0.04	1.29	0.02	0.68	BDL	12.34	320.08	1.13	BDL	BDL	BDL	300.64	BDL	BDL	BDL	BDL	BDL
EVA004	5/25/17	6/5/17	BDL	2.30	25.79	1.65	0.88	1.88	0.03	0.69	BDL	20.33	296.82	1.10	BDL	BDL	BDL	278.96	BDL	0.04	BDL	BDL	0.44
F001	12/16/16	4/14/17	BDL	2.71	34.36	1.40	0.60	6.52	0.04	0.52	0.13	6.34	325.43	2.09	0.34	0.01	0.01	91.83	BDL	0.58	0.09	0.07	0.16
F002	1/11/17	4/14/17	BDL	0.34	35.69	1.08	0.07	0.17	0.03	0.48	BDL	2.55	326.96	2.09	BDL	BDL	BDL	90.19	BDL	BDL	0.08	0.06	0.13
F003	2/6/17	4/14/17	BDL	0.33	35.75	1.01	0.62	0.39	0.04	0.64	BDL	5.38	331.45	2.10	BDL	BDL	BDL	91.62	BDL	BDL	0.08	0.07	0.17
F004	3/6/17	4/14/17	BDL	0.45	35.42	1.20	0.72	1.01	0.04	0.63	BDL	1.84	325.99	2.08	BDL	BDL	BDL	90.53	BDL	BDL	0.08	0.07	0.16
F005	4/10/17	6/5/17	BDL	0.52	35.63	0.89	0.09	1.29	0.03	0.32	BDL	6.76	334.42	2.17	BDL	BDL	BDL	93.47	BDL	BDL	BDL	BDL	BDL
F006	5/16/17	6/5/17	BDL	0.63	35.92	1.18	0.07	1.29	0.03	0.40	BDL	4.42	331.61	2.16	BDL	BDL	BDL	90.91	BDL	BDL	BDL	0.09	0.83
FK2001	1/9/17	4/14/17	BDL	BDL	35.01	0.53	0.01	0.14	0.01	0.47	BDL	6.79	334.30	2.96	BDL	BDL	BDL	176.75	BDL	BDL	0.27	0.05	0.12
FK2002	1/31/17	4/14/17	BDL	0.13	34.55	0.63	0.10	0.51	0.02	0.74	0.01	3.79	336.64	2.85	BDL	BDL	BDL	174.81	BDL	BDL	0.25	0.05	0.11
FK2003	2/20/17	4/14/17	BDL	0.38	34.37	0.67	0.12	0.42	0.02	0.89	BDL	4.77	338.85	2.88	BDL	BDL	BDL	178.96	BDL	BDL	0.25	0.05	0.14
FK2004	4/3/17	6/5/17	BDL	0.47	34.93	0.60	BDL	0.55	0.02	1.09	BDL	0.99	351.85	2.90	BDL	BDL	BDL	184.58	BDL	BDL	0.20	BDL	BDL
FK2005	5/9/17	6/5/17	BDL	0.44	34.65	0.69	0.06	0.69	0.01	0.85	BDL	3.71	342.95	2.83	BDL	BDL	BDL	180.84	BDL	BDL	0.14	BDL	BDL
FK3001	1/9/17	4/14/17	BDL	0.10	29.47	1.39	0.01	BDL	0.01	0.19	0.07	8.33	382.01	1.91	BDL	BDL	0.02	274.60	BDL	0.02	0.24	0.05	0.11
FK3002	1/31/17	4/14/17	BDL	0.09	30.01	1.47	0.01	BDL	0.01	0.18	0.02	6.93	390.01	1.92	BDL	BDL	BDL	272.97	BDL	0.03	0.21	0.05	0.12

	Parameter	Be	Al	V	Cr	Mn	Fe	Co	Ni	Cu	Zn	Sr	Mo	Ag	Cd	Sb	Ba	Tl	Pb	U	As	Se
	Unit	µg L^{-1}	µg L^{-1}	µg L^{-1}	µg L^{-1}	µg L^{-1}	µg L^{-1}	µg L^{-1}	µg L^{-1}	µg L^{-1}	µg L^{-1}	µg L^{-1}	µg L^{-1}	µg L^{-1}	µg L^{-1}	µg L^{-1}	µg L^{-1}	µg L^{-1}	µg L^{-1}	µg L^{-1}	µg L^{-1}	µg L^{-1}
	Det. Limit	0.097	0.064	0.008	0.011	0.007	0.060	0.007	0.009	0.013	0.011	0.168	0.030	0.008	0.008	0.008	0.176	0.023	0.009	0.021	0.009	0.014
	WHO Guide:	-	-	-	50	-	-	-	70	2000	-	-	-	-	3	20	700	-	10	30	10	40
Sample ID	**Sample Date**	**Analysis Date**																				
FK3003	2/20/17	4/14/17	BDL	0.16	28.90	1.42	0.02	BDL	0.01	0.20	0.01	7.15	381.47	1.84	BDL	BDL	BDL	274.79	BDL	BDL	0.21	0.05	0.10
FK3004	4/3/17	6/5/17	BDL	1.15	29.77	1.42	0.03	0.21	0.01	0.16	BDL	7.40	403.40	2.06	BDL	BDL	BDL	291.84	BDL	BDL	0.20	BDL	BDL
FK3005	5/9/17	6/5/17	BDL	2.90	28.98	1.30	0.05	8.32	0.01	0.20	BDL	3.63	392.57	1.98	BDL	BDL	BDL	284.77	BDL	0.03	0.20	BDL	BDL
K1001	2/27/17	4/14/17	0.04	0.24	9.15	0.63	0.40	0.32	0.03	0.44	0.02	7.22	293.84	BDL	BDL	BDL	BDL	172.92	BDL	BDL	BDL	0.02	0.07
K1002	3/13/17	4/14/17	0.04	0.29	9.42	0.64	0.51	1.28	0.04	0.46	0.03	4.40	307.81	BDL	BDL	BDL	BDL	182.15	BDL	BDL	BDL	0.02	0.10
K1003	4/18/17	6/5/17	BDL	0.42	9.59	0.21	0.08	0.42	0.03	0.49	BDL	7.11	331.81	BDL	BDL	BDL	BDL	197.72	BDL	BDL	BDL	BDL	BDL
K1004	5/25/17	6/5/17	BDL	0.40	9.56	0.78	0.14	0.53	0.03	0.44	BDL	7.77	314.84	BDL	BDL	BDL	BDL	187.77	BDL	BDL	BDL	BDL	BDL
K2001	12/16/16	4/14/17	0.05	1.67	5.69	1.24	0.95	4.73	0.01	0.38	0.10	23.46	201.30	BDL	0.29	0.04	BDL	127.72	BDL	0.35	BDL	0.02	0.02
K2002	1/11/17	4/14/17	0.04	0.20	5.70	1.16	0.38	0.13	BDL	0.31	BDL	31.00	195.88	BDL	BDL	BDL	BDL	126.25	BDL	0.05	BDL	0.01	0.01
K2003	2/6/17	4/14/17	0.05	14.08	5.62	1.18	0.44	0.28	BDL	0.37	0.03	5.47	192.05	BDL	BDL	BDL	BDL	123.34	BDL	0.02	BDL	0.01	0.02
K2004	3/6/17	4/14/17	0.05	0.45	5.70	1.27	0.58	0.28	BDL	0.35	0.02	20.17	191.52	BDL	BDL	BDL	BDL	121.53	BDL	0.03	BDL	0.01	0.03
K2005	4/10/17	6/5/17	BDL	3.00	5.90	1.28	0.40	0.53	BDL	0.32	BDL	18.29	206.03	BDL	BDL	BDL	BDL	134.13	BDL	0.05	BDL	BDL	BDL
K2006	5/16/17	6/5/17	BDL	6.99	5.73	1.18	0.02	0.40	BDL	0.32	BDL	11.96	195.76	BDL	0.19	0.80	BDL	128.34	BDL	0.02	BDL	BDL	BDL
S1001	1/9/17	4/14/17	BDL	0.08	21.04	1.54	0.17	0.25	0.01	1.22	0.06	8.46	268.75	0.63	BDL	BDL	BDL	144.36	BDL	BDL	0.14	0.03	BDL
S1002	1/31/17	4/14/17	0.06	0.37	21.52	1.88	0.18	0.21	0.01	1.05	BDL	2.29	263.95	0.58	BDL	BDL	BDL	150.22	BDL	BDL	0.12	0.03	BDL
S1003	2/20/17	6/5/17	BDL	0.52	21.10	1.72	0.02	0.29	BDL	0.90	BDL	5.69	272.15	0.65	BDL	BDL	BDL	143.63	BDL	BDL	BDL	BDL	BDL
S1004	4/3/17	6/5/17	BDL	2.07	21.24	1.88	0.78	4.99	0.03	0.89	BDL	7.36	264.19	0.57	BDL	BDL	BDL	150.73	BDL	BDL	BDL	BDL	BDL
S1005	5/9/17	4/14/17	BDL	0.23	14.98	0.17	2.12	0.27	0.03	1.04	BDL	10.97	266.92	0.55	BDL	BDL	BDL	110.04	BDL	BDL	0.18	0.02	BDL
S2001	1/9/17	4/14/17	BDL	0.16	15.26	0.09	2.55	0.30	0.01	0.56	BDL	6.51	270.36	0.54	BDL	BDL	BDL	111.17	BDL	BDL	0.18	0.02	BDL
S2002	1/31/17	6/5/17	BDL	0.44	15.36	0.12	0.15	0.09	BDL	0.63	BDL	7.71	284.90	0.55	BDL	BDL	BDL	118.06	BDL	BDL	0.12	BDL	BDL
S2003	2/20/17	6/5/17	BDL	0.38	15.81	0.33	0.05	0.65	BDL	0.64	BDL	4.89	276.74	0.59	BDL	BDL	BDL	113.89	BDL	BDL	0.13	BDL	BDL
S2004	4/3/17	4/14/17	0.04	BDL	21.59	1.98	0.02	0.17	0.01	1.05	0.03	8.80	271.82	0.62	BDL	0.01	0.01	147.52	BDL	BDL	0.13	0.03	0.02
S2005	5/9/17	4/14/17	BDL	BDL	14.60	0.22	0.02	0.10	BDL	0.64	BDL	8.58	268.84	0.51	BDL	BDL	BDL	111.26	BDL	BDL	0.17	0.02	BDL
SC1001	1/9/17	4/14/17	BDL	0.81	32.75	0.48	0.02	BDL	0.08	0.31	0.76	10.06	669.88	3.41	0.09	0.01	BDL	231.53	BDL	0.07	1.12	0.05	0.13

	Parameter	Be	Al	V	Cr	Mn	Fe	Co	Ni	Cu	Zn	Sr	Mo	Ag	Cd	Sb	Ba	Tl	Pb	U	As	Se
	Unit	µg L^{-1}	µg L^{-1}	µg L^{-1}	µg L^{-1}	µg L^{-1}	µg L^{-1}	µg L^{-1}	µg L^{-1}	µg L^{-1}	µg L^{-1}	µg L^{-1}	µg L^{-1}	µg L^{-1}	µg L^{-1}	µg L^{-1}	µg L^{-1}	µg L^{-1}	µg L^{-1}	µg L^{-1}	µg L^{-1}	µg L^{-1}
	Det. Limit	0.097	0.064	0.008	0.011	0.007	0.060	0.007	0.009	0.013	0.011	0.168	0.030	0.008	0.008	0.008	0.176	0.023	0.009	0.021	0.009	0.014
	WHO Guide:	-	-	-	50	-	-	-	70	2000	-	-	-	-	3	20	700	-	10	30	10	40
Sample ID	**Sample Date**	**Analysis Date**																				
SC1002	1/31/17	4/14/17	BDL	0.43	31.98	0.46	0.02	BDL	0.08	0.28	0.28	11.44	633.88	3.54	BDL	BDL	BDL	215.90	BDL	0.03	1.05	0.05	0.12
SC1003	2/20/17	4/14/17	BDL	0.34	32.14	0.47	0.04	BDL	0.07	0.28	0.41	7.44	626.73	3.40	BDL	0.01	BDL	218.62	BDL	0.04	1.04	0.05	0.15
SC1004	4/3/17	6/5/17	BDL	1.39	31.87	0.46	BDL	0.70	0.07	0.27	BDL	5.55	640.53	3.58	BDL	BDL	BDL	220.22	BDL	0.05	0.97	BDL	BDL
SC1005	5/8/17	6/5/17	BDL	11.37	32.62	0.43	0.09	1.94	0.06	0.24	BDL	10.17	629.48	3.77	BDL	BDL	BDL	214.56	BDL	0.03	0.92	BDL	BDL
SC2001	2/27/17	4/14/17	BDL	1.14	31.74	0.80	0.10	BDL	0.02	0.19	2.14	9.23	399.08	6.88	BDL	0.02	BDL	134.19	BDL	0.04	0.74	0.07	0.13
SC2002	3/13/17	4/14/17	BDL	4.71	31.38	0.74	0.12	0.86	0.02	0.17	2.72	3.28	402.02	6.88	BDL	0.01	BDL	130.89	BDL	0.03	0.81	0.07	0.14
SC2003	4/18/17	6/5/17	BDL	0.69	30.69	0.51	0.05	10.38	0.02	0.11	BDL	3.86	406.28	7.24	BDL	BDL	BDL	122.80	BDL	0.06	0.91	BDL	BDL
SC2004	5/25/17	6/5/17	BDL	1.28	30.30	0.57	0.13	0.13	0.02	0.11	BDL	6.90	400.06	7.21	BDL	BDL	BDL	117.92	BDL	0.02	0.76	0.06	BDL
SC3001	12/16/16	4/14/17	BDL	3.13	33.78	2.33	0.20	3.45	0.04	0.34	0.39	10.08	423.00	10.73	0.34	0.02	0.01	215.88	BDL	0.25	0.68	0.09	0.17
SC3002	1/11/17	4/14/17	BDL	BDL	34.60	2.19	0.08	0.13	0.04	0.30	1.16	24.10	426.34	10.99	BDL	0.02	BDL	219.00	BDL	BDL	0.72	0.09	0.20
SC3003	2/6/17	4/14/17	BDL	0.67	34.43	2.43	0.10	0.09	0.04	0.32	2.13	5.99	431.21	10.88	BDL	0.02	BDL	222.32	BDL	BDL	0.73	0.09	0.18
SC3004	3/4/17	4/14/17	BDL	0.71	33.61	2.45	0.06	0.08	0.04	0.32	1.52	13.44	432.56	10.60	BDL	0.02	BDL	221.41	BDL	BDL	0.74	0.09	0.17
SC3005	4/10/17	6/5/17	BDL	0.82	33.94	2.01	0.12	0.27	0.04	0.32	BDL	9.01	465.98	11.79	BDL	BDL	BDL	236.28	BDL	BDL	0.67	0.09	BDL
SC3006	5/16/17	6/5/17	BDL	0.85	35.40	2.40	0.06	0.12	0.04	0.31	BDL	10.93	474.70	11.71	BDL	BDL	BDL	240.65	BDL	BDL	0.74	0.08	BDL
T001	2/27/17	4/14/17	BDL	0.29	30.37	2.45	0.09	0.28	0.02	1.13	0.01	6.91	221.79	0.39	BDL	BDL	BDL	128.08	BDL	BDL	0.04	0.06	0.14
T002	3/13/17	4/14/17	BDL	0.55	30.88	3.22	0.14	4.45	0.03	1.42	0.04	9.76	222.95	0.41	BDL	BDL	BDL	127.97	BDL	0.03	0.04	0.06	0.15
T003	4/18/17	6/5/17	BDL	0.70	30.61	2.15	0.02	0.85	0.01	0.75	BDL	1.86	226.72	0.37	BDL	BDL	BDL	131.69	BDL	BDL	BDL	0.09	0.69
T004	5/25/17	6/5/17	BDL	0.57	31.09	2.65	0.10	0.83	0.02	1.36	BDL	9.37	230.02	0.39	BDL	BDL	BDL	134.18	BDL	BDL	BDL	0.06	BDL
Z001	12/16/16	4/14/17	BDL	2.35	14.71	0.17	30.93	3.11	0.23	0.74	0.21	14.40	349.76	4.50	0.15	0.02	BDL	132.49	BDL	0.55	0.12	0.03	BDL
Z002	1/11/17	4/14/17	BDL	0.21	14.94	0.06	1.29	0.17	0.04	0.41	BDL	3.22	353.83	4.46	BDL	0.01	BDL	132.11	BDL	BDL	0.10	0.02	BDL
Z003	2/6/17	4/14/17	BDL	0.47	14.48	0.03	11.71	0.66	0.04	1.15	BDL	43.20	352.50	4.48	BDL	0.02	BDL	130.97	BDL	BDL	0.11	0.02	BDL
Z004	3/6/17	4/14/17	BDL	0.42	14.59	0.06	28.11	0.49	0.21	0.69	BDL	3.32	349.28	4.37	BDL	0.02	BDL	128.70	BDL	BDL	0.10	0.02	BDL
Z005	4/10/17	6/5/17	BDL	0.75	15.32	0.09	0.19	0.34	0.03	0.23	BDL	8.72	368.22	4.85	BDL	BDL	BDL	135.60	BDL	BDL	BDL	BDL	BDL
Z006	5/16/17	6/5/17	BDL	0.87	15.65	0.08	29.89	0.67	0.14	0.59	BDL	4.74	385.99	5.11	BDL	BDL	BDL	141.73	BDL	BDL	BDL	BDL	BDL

Table 12. Trace-element concentrations with imputed values for nondetects. The percent of censoring was greater than 50% for Be, Cu, Pb, Ag, Cd, Sb, and Tl, so they were removed from the dataset and not used in subsequent analyses.

		Parameter	Al	Mn	Fe	Co	Mo	U	Se	As	V	Cr	Ni	Zn	Sr	Ba
		Unit	µg L^{-1}	µg L^{-1}	µg L^{-1}	µg L^{-1}	µg L^{-1}	µg L^{-1}	µg L^{-1}	µg L^{-1}	µg L^{-1}	µg L^{-1}	µg L^{-1}	µg L^{-1}	µg L^{-1}	µg L^{-1}
Sample ID	**Sample Date**	**Analysis Date**														
CH001	12/16/16	4/14/17	2.46	1.285	6.356	0.043	3.71	0.186	0.259	0.046	19.573	0.885	0.634	10.771	463.203	352.328
CH002	1/11/17	4/14/17	0.251	0.051	0.238	0.035	3.758	0.168	0.208	0.038	20.629	0.472	0.72	8.49	475.449	345.009
CH003	2/6/17	4/14/17	0.294	1.117	0.369	0.04	3.736	0.178	0.248	0.038	20.163	0.525	0.659	4.776	465.688	349.773
CH004	3/6/17	4/14/17	0.537	1.479	1.616	0.044	3.68	0.172	0.259	0.041	19.963	0.812	0.767	4.17	446.153	336.183
CH005	4/10/17	6/5/17	0.683	0.225	2.507	0.033	3.867	0.01	0.007	0.006	20.491	0.707	0.678	3.014	476.066	358.141
CH006	5/16/17	6/5/17	0.458	0.276	1.081	0.03	3.799	0.01	0.007	0.006	20.144	0.786	0.501	7.305	459.036	349.189
EVA001	2/27/17	4/14/17	0.497	0.638	1.232	0.027	1.126	0.046	0.25	0.032	25.37	1.702	0.69	18.521	306.82	289.695
EVA002	3/13/17	4/14/17	2.031	1.348	1.096	0.046	1.049	0.026	0.338	0.037	25.189	1.526	0.854	17.387	300.417	279.024
EVA003	4/18/17	6/5/17	0.655	0.044	1.289	0.022	1.131	0.011	0.007	0.006	26.443	1.207	0.681	12.339	320.08	300.64
EVA004	5/25/17	6/5/17	2.303	0.884	1.876	0.03	1.101	0.01	0.44	0.006	25.785	1.647	0.691	20.326	296.818	278.959
F001	12/16/16	4/14/17	2.71	0.601	6.517	0.041	2.093	0.093	0.155	0.073	34.356	1.399	0.519	6.339	325.426	91.833
F002	1/11/17	4/14/17	0.344	0.067	0.174	0.032	2.089	0.082	0.132	0.063	35.693	1.083	0.477	2.546	326.961	90.189
F003	2/6/17	4/14/17	0.328	0.618	0.392	0.041	2.103	0.082	0.168	0.065	35.753	1.012	0.644	5.382	331.453	91.616
F004	3/6/17	4/14/17	0.451	0.72	1.014	0.042	2.082	0.084	0.16	0.067	35.423	1.203	0.63	1.844	325.988	90.528
F005	4/10/17	6/5/17	0.52	0.094	1.289	0.028	2.168	0.01	0.007	0.006	35.629	0.89	0.325	6.763	334.424	93.465
F006	5/16/17	6/5/17	0.634	0.069	1.293	0.029	2.162	0.01	0.831	0.093	35.924	1.18	0.403	4.417	331.608	90.912
FK2001	1/9/17	4/14/17	0.04	0.008	0.139	0.014	2.961	0.266	0.123	0.048	35.009	0.527	0.474	6.794	334.304	176.753
FK2002	1/31/17	4/14/17	0.128	0.103	0.506	0.021	2.853	0.251	0.107	0.05	34.548	0.629	0.736	3.791	336.643	174.806
FK2003	2/20/17	4/14/17	0.378	0.123	0.416	0.023	2.877	0.253	0.14	0.051	34.373	0.673	0.894	4.766	338.846	178.963
FK2004	4/3/17	6/5/17	0.467	0.003	0.555	0.016	2.896	0.203	0.007	0.006	34.934	0.602	1.086	0.986	351.854	184.577
FK2005	5/9/17	6/5/17	0.439	0.058	0.695	0.012	2.834	0.144	0.007	0.006	34.648	0.694	0.851	3.71	342.945	180.837
FK3001	1/9/17	4/14/17	0.104	0.012	0.03	0.014	1.907	0.235	0.107	0.045	29.469	1.392	0.187	8.334	382.014	274.6
FK3002	1/31/17	4/14/17	0.094	0.007	0.03	0.014	1.923	0.21	0.116	0.053	30.012	1.468	0.185	6.925	390.009	272.973
FK3003	2/20/17	4/14/17	0.162	0.018	0.03	0.015	1.844	0.214	0.095	0.051	28.896	1.42	0.197	7.152	381.467	274.793
FK3004	4/3/17	6/5/17	1.148	0.029	0.212	0.013	2.058	0.203	0.007	0.006	29.765	1.418	0.163	7.398	403.397	291.844
FK3005	5/9/17	6/5/17	2.903	0.055	8.322	0.013	1.977	0.205	0.007	0.006	28.982	1.299	0.197	3.632	392.574	284.771
K1001	2/27/17	4/14/17	0.245	0.398	0.324	0.035	0.022	0.011	0.071	0.019	9.146	0.63	0.439	7.218	293.84	172.919
K1002	3/13/17	4/14/17	0.291	0.506	1.282	0.041	0.022	0.011	0.097	0.019	9.42	0.637	0.463	4.395	307.806	182.149
K1003	4/18/17	6/5/17	0.42	0.08	0.424	0.035	0.023	0.011	0.007	0.006	9.593	0.206	0.494	7.109	331.81	197.718
K1004	5/25/17	6/5/17	0.404	0.136	0.533	0.032	0.022	0.011	0.007	0.006	9.559	0.781	0.441	7.768	314.837	187.77
K2001	12/16/16	4/14/17	1.669	0.946	4.731	0.014	0.022	0.01	0.021	0.017	5.692	1.238	0.383	23.46	201.3	127.723
K2002	1/11/17	4/14/17	0.202	0.376	0.129	0.005	0.023	0.011	0.007	0.014	5.704	1.155	0.312	30.998	195.881	126.252
K2003	2/6/17	4/14/17	14.078	0.437	0.277	0.005	0.022	0.01	0.018	0.014	5.619	1.181	0.371	5.467	192.052	123.344

		Parameter	Al	Mn	Fe	Co	Mo	U	Se	As	V	Cr	Ni	Zn	Sr	Ba
		Unit	µg L^{-1}	µg L^{-1}	µg L^{-1}	µg L^{-1}	µg L^{-1}	µg L^{-1}	µg L^{-1}	µg L^{-1}	µg L^{-1}	µg L^{-1}	µg L^{-1}	µg L^{-1}	µg L^{-1}	µg L^{-1}
Sample ID	**Sample Date**	**Analysis Date**														
K2004	3/6/17	4/14/17	0.45	0.583	0.283	0.005	0.022	0.011	0.025	0.014	5.701	1.27	0.351	20.169	191.525	121.534
K2005	4/10/17	6/5/17	2.999	0.396	0.535	0.005	0.022	0.011	0.007	0.006	5.895	1.284	0.323	18.289	206.028	134.131
K2006	5/16/17	6/5/17	6.99	0.019	0.398	0.005	0.022	0.011	0.007	0.006	5.727	1.181	0.321	11.961	195.761	128.34
S1001	1/9/17	4/14/17	0.041	0.018	0.166	0.005	0.623	0.134	0.018	0.029	21.04	1.536	1.217	8.459	268.752	144.364
S1002	1/31/17	4/14/17	0.078	0.17	0.249	0.013	0.634	0.139	0.007	0.032	21.521	1.88	1.048	2.289	263.951	150.223
S1003	2/20/17	4/14/17	0.37	0.176	0.21	0.009	0.583	0.121	0.007	0.033	21.099	1.721	0.9	5.691	272.145	143.626
S1004	4/3/17	6/5/17	0.516	0.023	0.288	0.005	0.654	0.011	0.007	0.006	21.24	1.878	0.888	7.358	264.19	150.734
S1005	5/9/17	6/5/17	2.066	0.776	4.99	0.034	0.571	0.01	0.007	0.006	14.984	0.165	1.043	10.969	266.921	110.039
S2001	1/9/17	4/14/17	0.042	0.017	0.1	0.005	0.511	0.167	0.007	0.018	15.256	0.091	0.561	6.513	270.36	111.168
S2002	1/31/17	4/14/17	0.234	2.117	0.268	0.026	0.548	0.182	0.007	0.017	15.358	0.123	0.635	7.71	284.903	118.061
S2003	2/20/17	4/14/17	0.162	2.552	0.296	0.015	0.544	0.182	0.007	0.016	15.813	0.334	0.636	4.894	276.74	113.892
S2004	4/3/17	6/5/17	0.441	0.155	0.093	0.005	0.554	0.125	0.007	0.006	21.592	1.983	1.049	8.801	271.825	147.519
S2005	5/9/17	6/5/17	0.38	0.048	0.65	0.005	0.592	0.127	0.007	0.006	14.603	0.219	0.643	8.575	268.839	111.263
SC1001	1/9/17	4/14/17	0.815	0.022	0.03	0.076	3.408	1.116	0.125	0.047	32.749	0.478	0.313	10.057	669.876	231.526
SC1002	1/31/17	4/14/17	0.429	0.016	0.03	0.076	3.539	1.047	0.121	0.049	31.979	0.461	0.282	11.439	633.876	215.905
SC1003	2/20/17	4/14/17	0.342	0.043	0.03	0.071	3.404	1.039	0.149	0.05	32.14	0.468	0.283	7.437	626.735	218.62
SC1004	4/3/17	6/5/17	1.392	0.003	0.7	0.07	3.576	0.969	0.007	0.006	31.872	0.463	0.268	5.547	640.532	220.222
SC1005	5/8/17	6/5/17	11.373	0.091	1.937	0.064	3.77	0.917	0.007	0.006	32.618	0.425	0.245	10.174	629.483	214.559
SC2001	2/27/17	4/14/17	1.139	0.097	0.03	0.024	6.88	0.738	0.129	0.071	31.744	0.795	0.191	9.231	399.083	134.186
SC2002	3/13/17	4/14/17	4.715	0.124	0.864	0.024	6.877	0.814	0.135	0.066	31.385	0.743	0.175	3.277	402.017	130.891
SC2003	4/18/17	6/5/17	0.693	0.055	10.38	0.021	7.242	0.912	0.007	0.006	30.692	0.51	0.11	3.862	406.282	122.797
SC2004	5/25/17	6/5/17	1.279	0.13	0.128	0.02	7.207	0.76	0.007	0.061	30.304	0.565	0.111	6.899	400.055	117.921
SC3001	12/16/16	4/14/17	3.13	0.201	3.451	0.041	10.734	0.678	0.171	0.089	33.781	2.326	0.337	10.079	423.005	215.88
SC3002	1/11/17	4/14/17	0.039	0.08	0.131	0.041	10.987	0.72	0.2	0.087	34.596	2.191	0.298	24.099	426.343	218.999
SC3003	2/6/17	4/14/17	0.667	0.099	0.086	0.043	10.881	0.734	0.177	0.086	34.431	2.427	0.319	5.988	431.215	222.317
SC3004	3/4/17	4/14/17	0.715	0.056	0.08	0.041	10.604	0.741	0.172	0.089	33.61	2.453	0.319	13.437	432.563	221.411
SC3005	4/10/17	6/5/17	0.817	0.12	0.269	0.037	11.789	0.667	0.007	0.088	33.94	2.013	0.318	9.008	465.984	236.283
SC3006	5/16/17	6/5/17	0.849	0.057	0.123	0.039	11.715	0.736	0.007	0.083	35.399	2.403	0.311	10.929	474.695	240.646
T001	2/27/17	4/14/17	0.288	0.09	0.281	0.023	0.386	0.041	0.139	0.06	30.369	2.449	1.127	6.914	221.792	128.082
T002	3/13/17	4/14/17	0.551	0.138	4.455	0.027	0.406	0.044	0.147	0.061	30.876	3.223	1.419	9.763	222.953	127.971
T003	4/18/17	6/5/17	0.702	0.019	0.851	0.014	0.369	0.01	0.688	0.087	30.609	2.15	0.751	1.86	226.721	131.686
T004	5/25/17	6/5/17	0.573	0.102	0.83	0.022	0.389	0.011	0.007	0.057	31.085	2.652	1.358	9.374	230.015	134.179
Z001	12/16/16	4/14/17	2.354	30.931	3.11	0.231	4.496	0.122	0.007	0.027	14.714	0.173	0.736	14.398	349.761	132.491
Z002	1/11/17	4/14/17	0.208	1.294	0.168	0.037	4.458	0.101	0.007	0.024	14.937	0.055	0.409	3.22	353.832	132.115
Z003	2/6/17	4/14/17	0.47	11.713	0.66	0.043	4.476	0.108	0.007	0.022	14.483	0.028	1.153	43.198	352.5	130.97
Z004	3/6/17	4/14/17	0.419	28.112	0.487	0.207	4.372	0.104	0.007	0.024	14.59	0.062	0.693	3.323	349.282	128.701

		Parameter	Al	Mn	Fe	Co	Mo	U	Se	As	V	Cr	Ni	Zn	Sr	Ba
		Unit	µg L^{-1}	µg L^{-1}	µg L^{-1}	µg L^{-1}	µg L^{-1}	µg L^{-1}	µg L^{-1}	µg L^{-1}	µg L^{-1}	µg L^{-1}	µg L^{-1}	µg L^{-1}	µg L^{-1}	µg L^{-1}
Sample ID	**Sample Date**	**Analysis Date**														
Z005	4/10/17	6/5/17	0.748	0.195	0.337	0.033	4.847	0.01	0.007	0.006	15.323	0.086	0.226	8.718	368.222	135.598
Z006	5/16/17	6/5/17	0.87	29.888	0.674	0.142	5.108	0.01	0.007	0.006	15.647	0.082	0.589	4.74	385.994	141.73

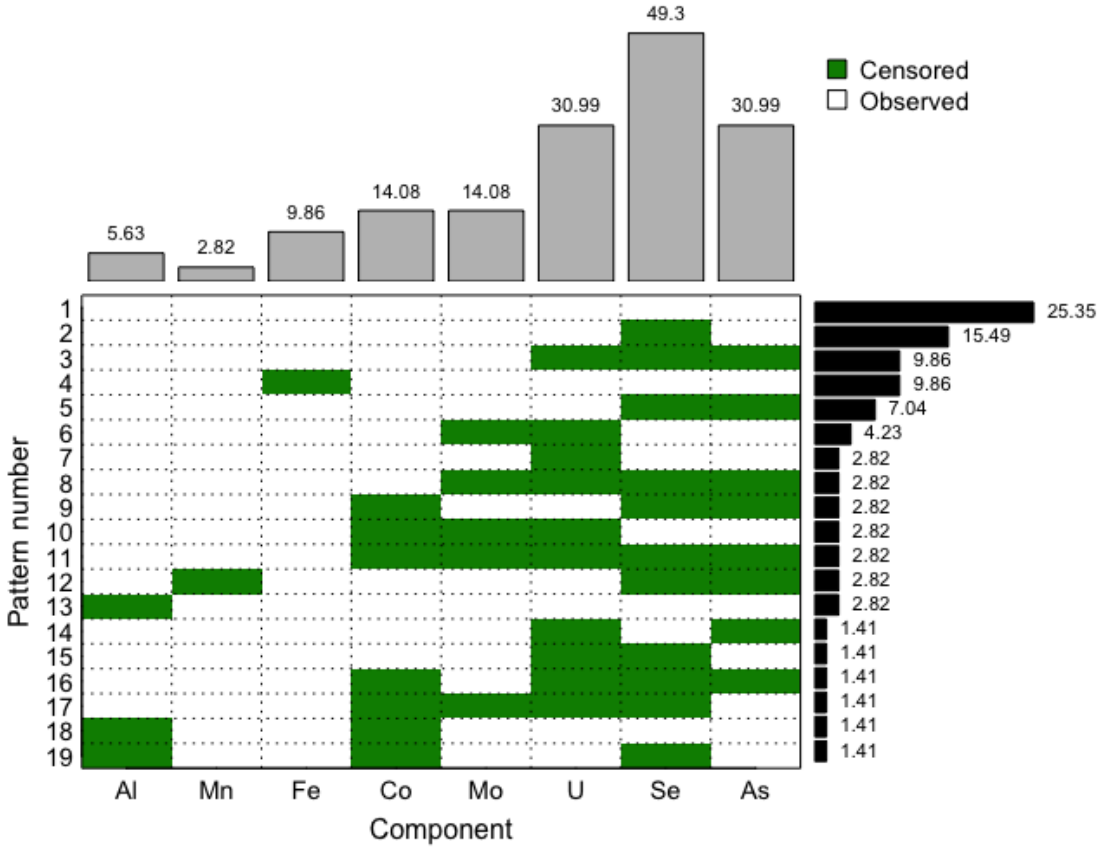

Figure 29. Diagram summarizing the percent censored values by variable and percent of samples that follow a particular detect-nondetect pattern. The barplot on the top indicates percentage number of censored values by variable (e.g., 30.99% of all As values are censored). Green cells in the grid indicate non-detected or censored variables within a pattern. There were 19 observed patterns, as indicated by the listed *pattern numbers* to the left of the grid. The barplot on the right (black bars) displays frequency of these censoring patterns (e.g., 7.04% of observations contain nondetected Se and As values). This figure was produced using the *zPatterns* function of the *zCompositions* package in R.

7.5 Mineral Dissolution

Table 13. Weathering equations for some minerals present in the study area. Dissolved silica, which is mentioned in the text, figures, and appendix as SiO_2 equates to H_4SiO_4 by the first equation.

$SiO_2 + 2H_2O \rightarrow H_4SiO_4$ silica dissolved silica (silicic acid)
$2NaAlSi_3O_8 + 2CO_2 + 11H_2O \rightarrow Al_2Si_2O_5(OH)_4 + 2Na^+ + 2HCO_3^- + 4H_4SiO_4$ albite kaolinite
$CaAl_2Si_2O_8 + 2CO_2 + 3H_2O \rightarrow Al_2Si_2O_5(OH)_4 + Ca^{2+} + 2HCO_3^-$ anorthite kaolinite
$CaAl_2Si_2O_8 + 2H^+ + 6H_2O \rightarrow 2Al(OH)_3 + Ca^{2+} + 2H_4SiO_4$ anorthite gibbsite
$2KAlSi_3O_8 + 2CO_2 + 11H_2O \rightarrow Al_2Si_2O_5(OH)_4 + 2K^+ + 2HCO_3^- + 4H_4SiO_4$ orthoclase kaolinite
$2KMg_3AlSi_3O_{10}(OH)_2 + 14CO_2 + 10H_2O \rightarrow Al_2Si_4O_{10}(OH)_2 + 2K^+ + 6Mg^{2+} + 14HCO_3^- + 2H_4SiO_4$ biotite montmorillonite
$CaMgSi_2O_6 + 4CO_2 + 6H_2O \rightarrow Ca^{2+} + Mg^{2+} + 4HCO_3^- + 2H_4SiO_4$ diopside (pyroxene)
$Ca_2Mg_4Al_2Si_7O_{22}(OH)_2 + 12CO_2 + 12H_2O \rightarrow Al_2Si_4O_{10}(OH)_2 + 2Ca^{2+} + 4Mg^{2+} + 12HCO_3^- + 3H_4SiO_4$ tremolite (amphibole) montmorillonite
$CaSO_4{\cdot}2H_2O \rightarrow Ca^{2+} + SO_4^{2-} + 2H_2O$ gypsum

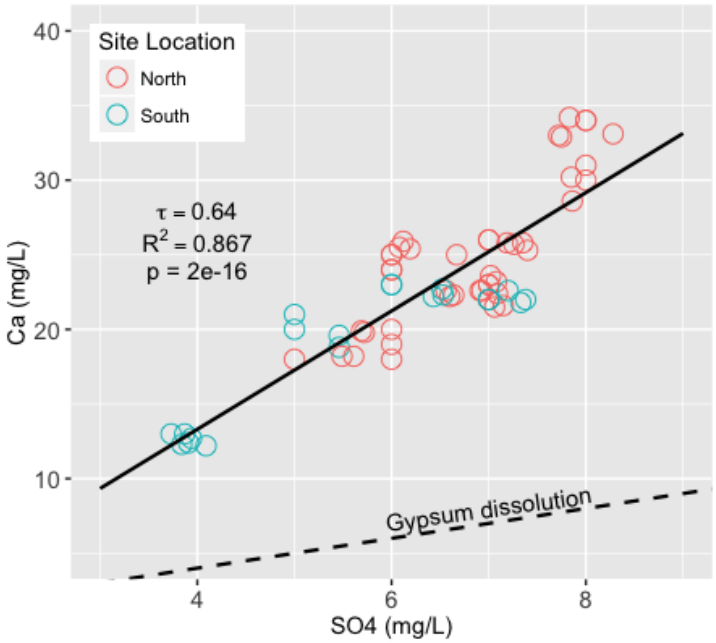

Figure 30. Correlation and linear fit of Ca and SO_4 concentrations. Concentrations are plotted relative to the gypsum dissolution line. All samples had excess Ca with respect to SO_4 and were undersaturated with respect to gypsum.

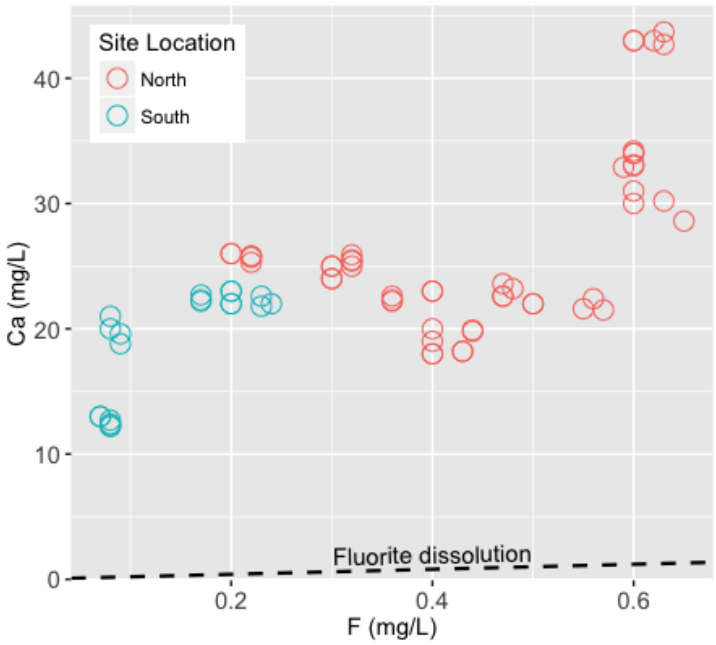

Figure 31. Calcium vs. F concentrations plotted relative to the fluorite dissolution line demonstrating a relative excess of Ca.

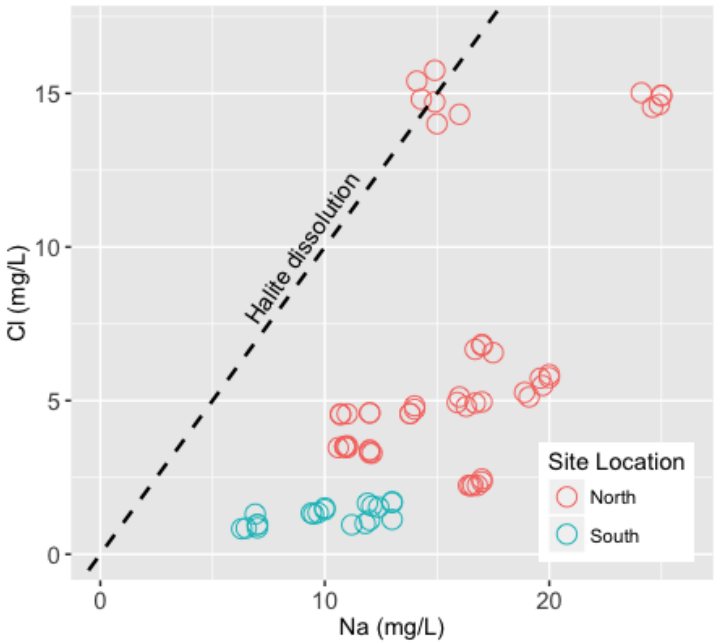

Figure 32. Chloride vs. Na concentrations plotted relative to the halite dissolution line. Six samples from Fada plotted along the halite dissolution line, while the remaining samples had excess Na.

7.6 Recharge

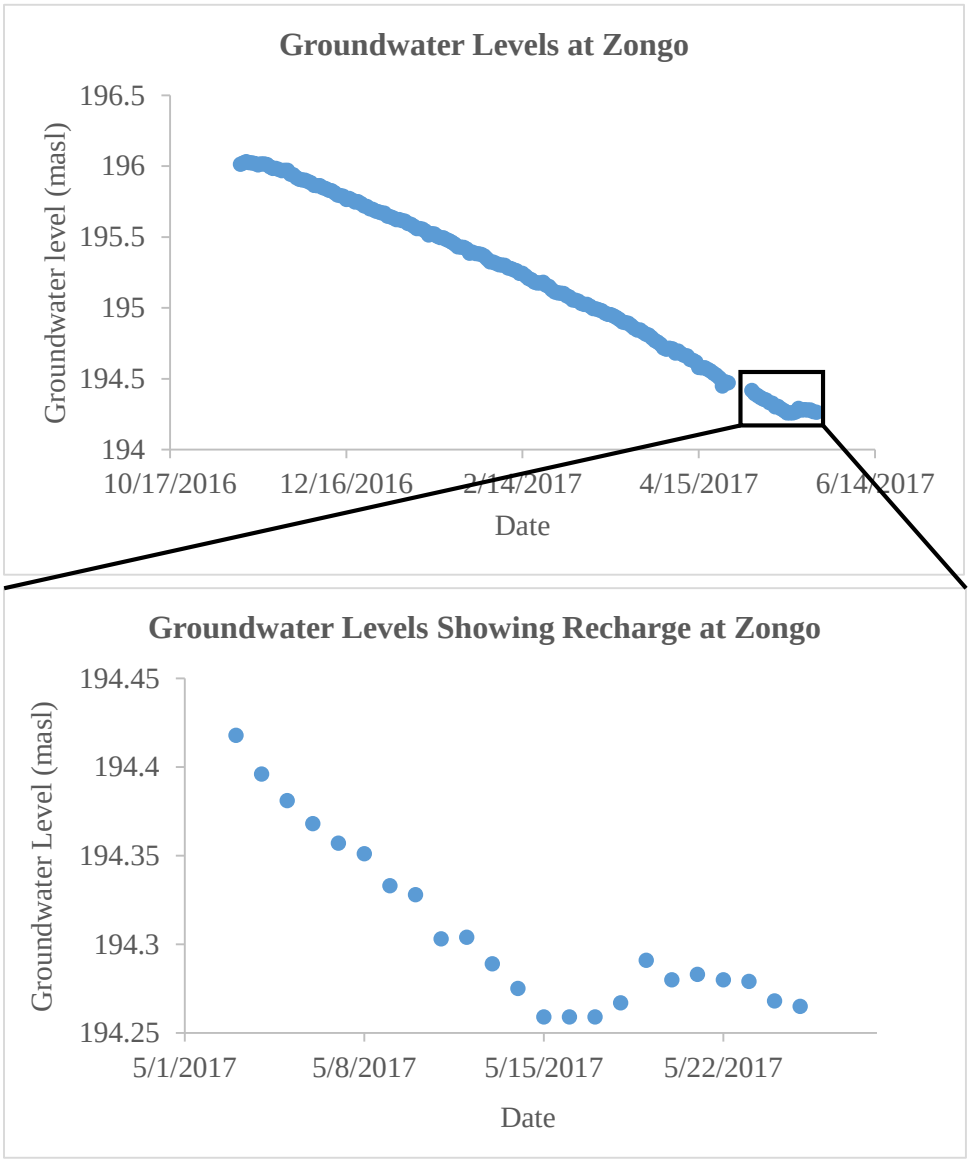

Figure 33. Top: Observed static water levels at Zongo from November 10, 2016 to May 25, 2017. Bottom: Zoom-in of the static water levels illustrating a change in trend direction from May 15 to 19, which indicates that recharge had occurred.

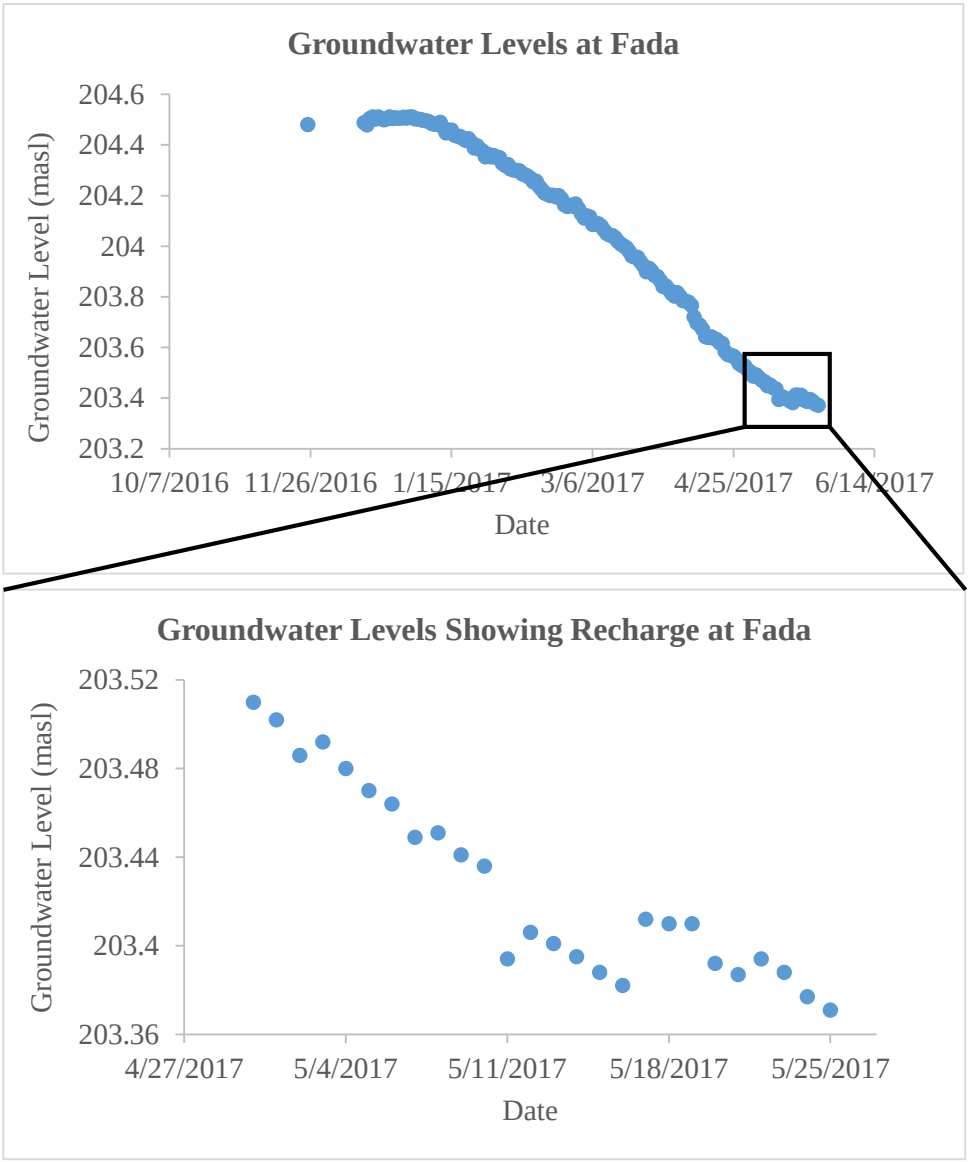

Figure 34. Top: Observed static water levels at Fada from December 16, 2016 to May 25, 2017 (observation on November 25, 2016 was a manual measurement of the dynamic water level). Bottom: Zoom-in of the static water levels illustrating a change in trend direction between May 15 and 16, indicating that recharge had occurred.

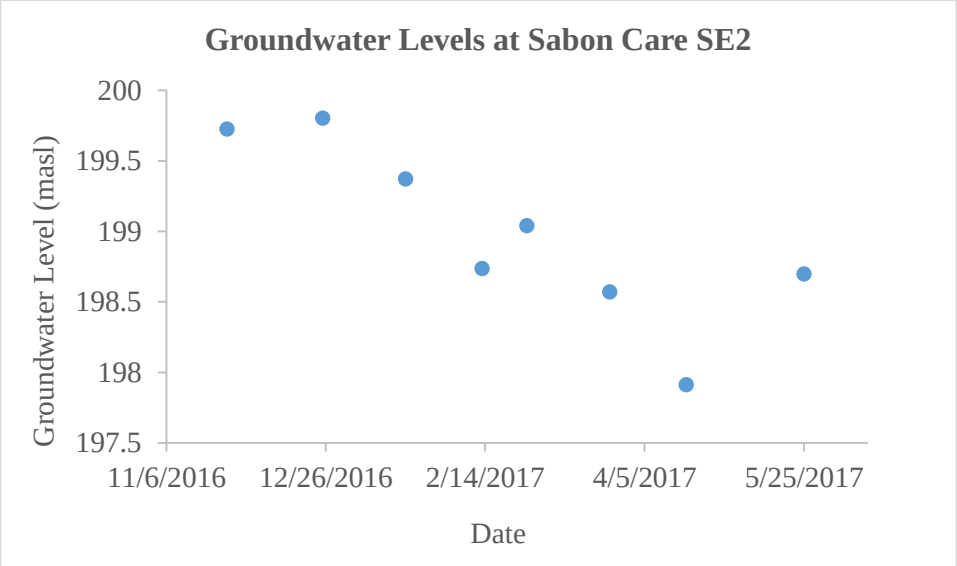

Figure 35. Observed water levels at Sabon Care SE2 from November 25, 2016 to May 25, 2017. An increase of 78 cm in the water level between April 18 and May 25 may indicate that recharge occurred.

7.7 Principal Component Summaries

Table 14. Summaries of PCs with eigenvalues > 1, including percent of variance, cumulative percent of variance, standard deviation, eigenvalue, and loadings for each PC.

Principal Component	**PC1**	**PC2**	**PC3**	**PC4**	**PC5**	**PC6**	**PC7**
Percent of Variance (%)	40	12	9	8	7	6	4
Cumulative Percent (%)	40	52	61	69	76	82	86
Standard Deviation	3.217	1.751	1.511	1.440	1.297	1.201	1.012
Eigenvalue	10.346	3.065	2.283	2.074	1.682	1.442	1.024
Na	-0.285	-0.013	0.036	-0.069	-0.051	0.066	0.009
F	-0.279	0.163	-0.036	0.067	-0.068	0.077	0.025
Ca	-0.279	-0.213	-0.064	-0.001	0.016	0.042	0.042
Mg	-0.274	-0.204	-0.016	-0.066	-0.094	0.014	0.114
SO_4	-0.273	-0.167	-0.098	0.000	-0.092	-0.105	0.035
Sr	-0.272	-0.184	0.069	-0.141	0.079	0.032	-0.164
Mo	-0.261	-0.038	0.110	0.020	0.027	-0.147	0.147
Cl	-0.257	0.103	-0.014	0.138	-0.269	-0.018	-0.075
V	-0.256	0.256	0.004	-0.031	-0.158	-0.060	0.122
HCO_3	-0.254	-0.268	0.004	-0.093	0.115	-0.052	0.158
U	-0.242	-0.071	-0.225	0.005	0.116	-0.027	0.041
K	-0.224	0.183	0.268	0.043	0.173	0.051	0.014
NO_3	-0.205	0.283	-0.048	-0.038	-0.076	0.132	-0.269
Co	-0.181	-0.164	0.303	0.238	0.043	-0.147	-0.251
As	-0.136	0.280	-0.125	0.316	0.274	-0.201	-0.110
Temp	-0.136	-0.093	0.065	0.352	0.066	0.004	0.440
Ba	-0.109	0.002	0.212	-0.353	0.410	0.280	-0.066
Se	-0.107	0.343	0.063	0.181	0.245	-0.030	-0.383
SiO_2	-0.083	0.290	0.317	-0.368	-0.195	-0.022	0.055
pH	-0.027	0.087	-0.251	0.335	-0.347	0.073	-0.028
Cr	-0.011	0.387	-0.033	0.110	0.145	0.267	0.461
Al	-0.001	-0.128	0.228	0.235	-0.251	0.545	-0.019
Zn	0.053	-0.086	-0.032	0.194	0.392	0.407	0.111
Fe	0.060	0.002	0.498	0.084	-0.286	0.162	-0.013
Ni	0.091	0.142	0.313	-0.004	0.034	-0.421	0.382
Mn	0.093	-0.199	0.342	0.369	0.144	-0.205	-0.142

7.8 Pump Test at Zongo

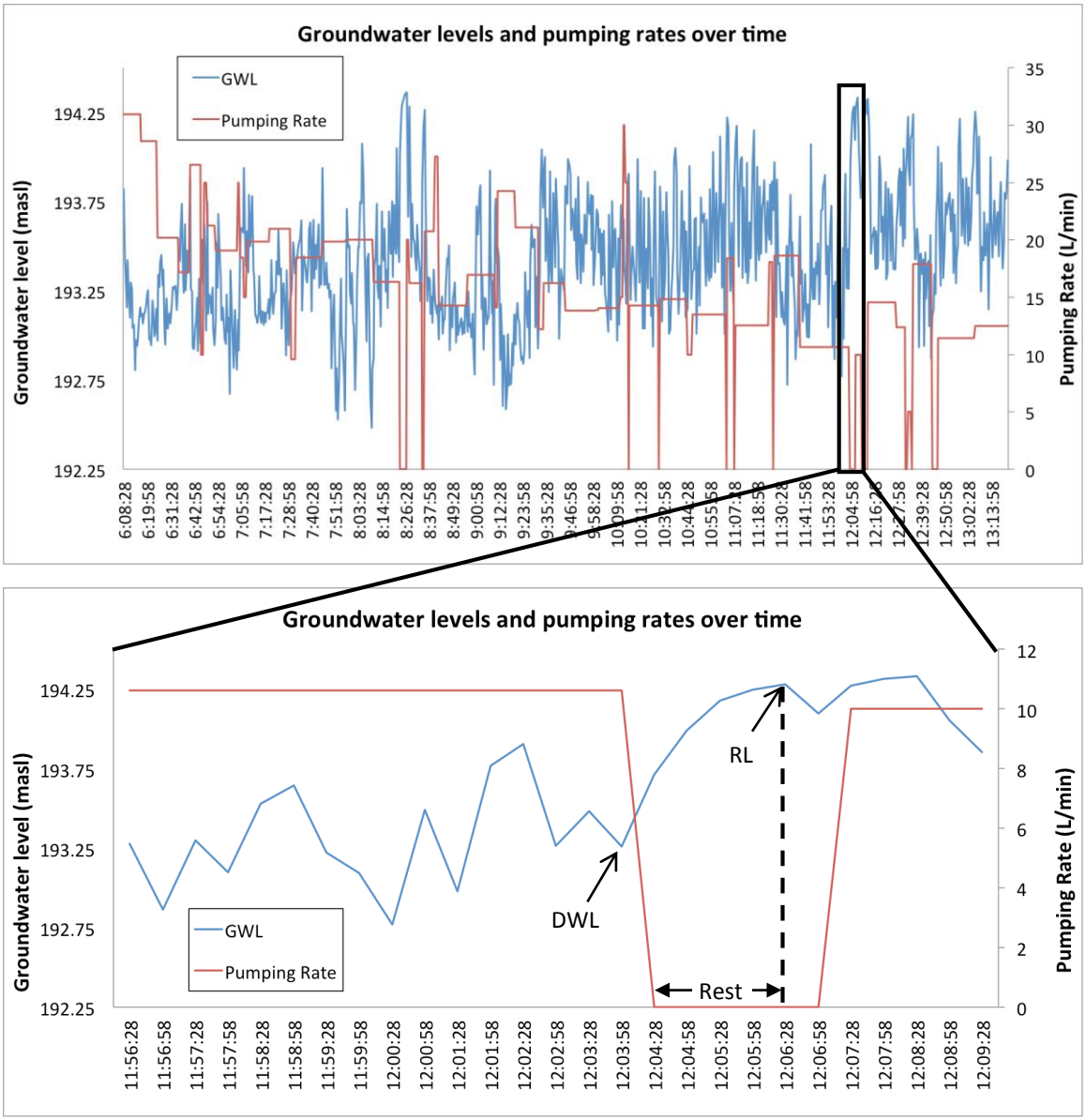

Figure 36. Top: Groundwater levels and pumping rates recorded during the pump test at Zongo. Bottom: Zoom-in indicating the dynamic water level, recovery level, and rest from pumping duration values used for calculations.

Table 15. Pump test values. All units are in meters, except percent recovery (%) and rest (minutes).

Static water level (SWL)	194.48
Dynamic water level (DWL)	193.26
Drawdown = SWL - DWL	1.22
Recovery level (RL)	194.28
Recovery = RL - DWL	1.02
% Recovery = Recovery/Drawdown	84%
Rest from pumping	2 minutes

8.0 References

Africa Adapatation Programme. (2011). Improving access, understanding, and application of climate data and information. Discussion Paper Series, 2.

Appelo, C. A. J., & Postma, D. (2006). Geochemistry, Groundwater and Pollution. *Vadose Zone Journal*, *5*(1), 510. https://doi.org/10.2136/vzj2005.1110br

Bonnot, H., Abdou, A., Bory Kadey, D., Chalamet, D., Saint Martin, M., Younfa, L. (1998). Carte geologique du Niger a 1/200 000, feuille Niamey. Ministere des Mines du Niger, Direction de la Recherche Geologique et Miniere et Ministere francais de la Cooperation.

Bromley, J., Brouwer, J., Barker, A. P., Gaze, S. R., & Valentin, C. (1997). The role of surface water redistribution in an area of patterned vegetation in a semi-arid environment, south-west Niger. *Journal of Hydrology*, *198*(1–4), 1–29. https://doi.org/10.1016/S0022-1694(96)03322-7

Bromley, J., Edmunds, W. M., Fellman, E., Brouwer, J., Gaze, S. R., Sudlow, J., & Taupin, J. D. (1997). Estimation of rainfall inputs and direct recharge to the deep unsaturated zone of southern Niger using the chloride profile method. *Journal of Hydrology*, *188–189*(1–4), 139–154. https://doi.org/10.1016/S0022-1694(96)03157-5

Chowdhury, S., & Al-Zahrani, M. (2014). Water quality change in dam reservoir and shallow aquifer: analysis on trend, seasonal variability and data reduction. *Environmental Monitoring and Assessment*, *186*(10), 6127–6143. https://doi.org/10.1007/s10661-014-3844-0

Chowdhury, S., Champagne, P., & James McLellan, P. (2008). Factors influencing formation of trihalomethanes in drinking water: Results from multivariate statistical investigation of the Ontario drinking water surveillance program database. *Water Quality Research Journal of Canada*, *43*(2–3), 189–199.

Courtois, N., Lachassagne, P., Wyns, R., Blanchin, R., Bougaïré, F. D., Somé, S., & Tapsoba, A. (2010). Large-scale mapping of hard-rock aquifer properties applied to Burkina Faso. *Ground Water*, *48*(2), 269–283. https://doi.org/10.1111/j.1745-6584.2009.00620.x

Dewandel, B., Lachassagne, P., Wyns, R., Marechal, J. C., & Krishnamurthy, N. S. (2006). A generalized 3-D geological and hydrogeological conceptual model of granite aquifers controlled by single or multiphase weathering. *Journal of Hydrology*, *330*(1–2), 260–284. https://doi.org/10.1016/j.jhydrol.2006.03.026

Fry, L. M., Cowden, J. R., Watkins, D. W., Clasen, T., & Mihelcic, J. R. (2010). Quantifying health improvements from water quantity enhancement: An engineering perspective applied to rainwater harvesting in West Africa. *Environmental Science and Technology*, *44*(24), 9535–9541. https://doi.org/10.1021/es100798j

Garba, M. (2014). *Caractérisation hydrogéologique du socle cristallin et cristallophyllien dans la commune rurale de Makalondi*. Université Abdou Moumouni.

Gibbs, R. J. (1970). Mechanisms Controlling World Water Chemistry. *Science*, *170*(3962), 1088–1090. https://doi.org/10.1126/science.170.3962.1088

Gibrilla, A., Bam, E. K. P., Adomako, D., Ganyaglo, S., Osae, S., Akiti, T. T., … Agyeman, E.

K. (2011). Application of Water Quality Index (WQI) and Multivariate Analysis for Groundwater Quality Assessment of the Birimian and Cape Coast Granitoid Complex: Densu River Basin of Ghana. *Water Quality, Exposure and Health*, *3*(2), 63–78. https://doi.org/10.1007/s12403-011-0044-9

Girard, P., & Hillaire-Marcel, C. (1997). Determining the source of nitrate pollution in the niger discontinuous aquifers using the natural 15N/14N ratios. *Journal of Hydrology*, *199*(3–4), 239–251. https://doi.org/10.1016/S0022-1694(96)03318-5

Girard, P., Hillaire-Marcel, C., & Oga, M. S. (1997). Determining the recharge mode of sahelian aquifers using water isotopes. *Journal of Hydrology*, *197*(1–4), 189–202. https://doi.org/10.1016/S0022-1694(96)03261-1

Gorchev, H. G., & Ozolins, G. (2011). *WHO guidelines for drinking-water quality. WHO chronicle* (Vol. 38). https://doi.org/10.1016/S1462-0758(00)00006-6

Graham, J. P., Hirai, M., & Kim, S. S. (2016). An analysis of water collection labor among women and children in 24 sub-Saharan African countries. *PLoS ONE*, *11*(6), 1–14. https://doi.org/10.1371/journal.pone.0155981

Heath, R. C. (1983). *Basic Ground-Water Hydrology*. *U.S. Geological Survey Water-Supply Paper 2220*. https://doi.org/10.1614/0890-037X(2000)014[0451:]2.0.CO;2

Helsel, D. (1990). Less than obvious, *24*(12).

Helsel, D. R. (2012). *Statistics for Censored Environmental Data Using Minitab and R*. (M. Scott & V. Barnett, Eds.) (2nd ed.). Wiley.

Helsel, D. R., & Frans, L. M. (2006). Regional Kendall test for trend. *Environmental Science and Technology*, *40*(13), 4066–4073. https://doi.org/10.1021/es051650b

Helsel, D. R., & Hirsch, R. M. (2002). Statistical Methods in Water Resources. *Book 4, Hydrologic Analysis and Interpretation*, *36*(3), 510. https://doi.org/10.2307/1269385

Hem, D. (1985). Study and Interpretation the Chemical of Natural of Characteristics Water. *Text*, *2254*(2254), 263. Retrieved from http://pubs.usgs.gov/wsp/wsp2254/pdf/wsp2254a.pdf

Hemson, D. (2007). "The Toughest of Chores": policy and practice in children collecting water in South Africa. *Policy Futures in Education*, *5*(3), 315. https://doi.org/10.2304/pfie.2007.5.3.315

Hill, I. G., Worden, R. H., & Meighan, I. G. (2000). Geochemical evolution of a palaeolaterite: The Interbasaltic formation, Northern Ireland. *Chemical Geology*, *166*(1–2), 65–84. https://doi.org/10.1016/S0009-2541(99)00179-5

Hirsch, R. M. (1982). A comparison of four streamflow record extension techniques. *Water Resources Research*, *18*(4), 1081–1088. https://doi.org/10.1029/WR018i004p01081

Hirsch, R. M., Alexander, R. B., & Smith, R. A. (1991). Selection of methods for the detection and estimation of trends in water quality. *Water Resources Research*, *27*(5), 803–813. https://doi.org/10.1029/91WR00259

Huston, C., & Juarez-Colunga, E. (2009). Guidelines for computing summary statistics for data-sets containing non-detects, 177. Retrieved from http://bvcentre.ca/files/research_reports/08-03GuidanceDocument.pdf

Ibrahim, M., Favreau, G., Scanlon, B. R., Seidel, J. L., Le Coz, M., Demarty, J., & Cappelaere, B. (2014). Augmentation sur le long terme de la recharge diffuse des aquifères suite à l'expension des cultures pluviales dans le Sahel, Afrique de l'Ouest. *Hydrogeology Journal*, *22*(6), 1293–1305. https://doi.org/10.1007/s10040-014-1143-z

Imaizumi, Y., Suzuki, N., & Shiraishi, H. (2006). Bootstrap methods for confidence intervals of percentiles from dataset containing nondetected observations using lognormal distribution. *Journal of Chemometrics*, *20*(1–2), 68–75. https://doi.org/10.1002/cem.987

Kaiser, H. F. (1960). The application of electronic computers to factor analysis. *Educational and Psychological Measurement*, *20*, 141–151. https://doi.org/10.1177/001316446002000116

Kaown, D., Hyun, Y., Bae, G. O., Oh, C. W., & Lee, K. K. (2012). Evaluation of spatio-temporal trends of groundwater quality in different land uses using Kendall test. *Geosciences Journal*, *16*(1), 65–75. https://doi.org/10.1007/s12303-012-0009-4

Le Gal La Salle, C., Marlin, C., Leduc, C., Taupin, J. D., Massault, M., & Favreau, G. (2001). Renewal rate estimation of groundwater based on radioactive tracers (3H, 14C) in an unconfined aquifer in a semi-arid area, Iullemeden basin, Niger. *Journal of Hydrology*, *254*(1–4), 145–156. https://doi.org/10.1016/S0022-1694(01)00491-7

Leduc, C., Favreau, G., & Schroeter, P. (2001). Long-term rise in a Sahelian water-table: The Continental Terminal in South-West Niger. *Journal of Hydrology*, *243*(1–2), 43–54. https://doi.org/10.1016/S0022-1694(00)00403-0

Lutz, A., Minyila, S., Saga, B., Diarra, S., Apambire, B., & Thomas, J. (2015). Fluctuation of Groundwater Levels and Recharge Patterns in Northern Ghana. *Climate*, *3*, 1–15. https://doi.org/10.3390/cli3010001

Lutz, A., Thomas, J. M., & Diarra, S. (2013). Chemistry of Hand-Pump Waters in Ghana, Mali, and Niger, West Africa: Potential Health Effects. *Procedia Earth and Planetary Science*, *7*, 541–545. https://doi.org/10.1016/j.proeps.2013.03.050

Machens, E. (1967). Notice explicative sur la carte geologique du Niger occidental, Carte geol. 1/200 000eme. Dir. Mines Geol. Niger, 36.

Mahler, B. J. (2008). Statistical analysis of major ion and trace element geochemistry of water, 1986–2006, at seven wells transecting the freshwater/saline-water interface of the Edwards aquifer, San Antonio, Texas: U.S. *Geological Survey Scientific Investigations.*, *Report 200*, 46p.

Marechal, J. C., Dewandel, B., & Subrahmanyam, K. (2004). Use of hydraulic tests at different scales to characterize fracture network properties in the weathered-fractured layer of a hard rock aquifer. *Water Resources Research*, *40*(11). https://doi.org/10.1029/2004WR003137

Nagi, R. (2011). Classifying Landsat image services to make a land cover map. Retrieved from https://blogs.esri.com/esri/arcgis/2011/05/28/classifying-landsat-image-services-to-make-a-land-cover-map/

Nesse, W. D. (2000). *Introduction to Mineralogy*. Oxford University Press.

Palarea-Albaladejo, J., & Martín-Fernández, J. A. (2015). ZCompositions - R package for multivariate imputation of left-censored data under a compositional approach. *Chemometrics and Intelligent Laboratory Systems*, *143*, 85–96.

https://doi.org/10.1016/j.chemolab.2015.02.019

Pons, J., Barbey, P., Dupuis, D., & Leger, J. M. (1995). Mechanisms of Pluton Emplacement and Structural Evolution of a 2.1-Ga Juvenile Continental-Crust - the Birimian of Southwestern Niger. *Precambrian Research*, *70*(3–4), 281–301.

Qadir, A., Malik, R. N., & Husain, S. Z. (2008). Spatio-temporal variations in water quality of Nullah Aik-tributary of the river Chenab, Pakistan. *Environmental Monitoring and Assessment*, *140*(1–3), 43–59. https://doi.org/10.1007/s10661-007-9846-4

Raju, N. J., Patel, P., Reddy, B. C. S. R., Suresh, U., & Reddy, T. V. K. (2016). Identifying source and evaluation of hydrogeochemical processes in the hard rock aquifer system: geostatistical analysis and geochemical modeling techniques. *Environmental Earth Sciences*, *75*(16), 1–23. https://doi.org/10.1007/s12665-016-5979-5

Reimann, C., Filzmoser, P., Garrett, R. G., & Dutter, R. (2008). Statistical Data Analysis Explained. *Statistics*, 359. https://doi.org/10.1002/9780470987605

Rodríguez-Fonseca, B., Janicot, S., Mohino, E., Losada, T., Bader, J., Caminade, C., … Voldoire, A. (2011). Interannual and decadal SST-forced responses of the West African monsoon. *Atmospheric Science Letters*, *12*(1), 67–74. https://doi.org/10.1002/asl.308

Rounds, S. A., Wilde, F. D., & Ritz, G. F. (2015). National Field Manual for the Collection of Water Quality Data. *Techniques for Water Resources Investigations: Book 9*, (Book 9), 1532.

Seyhan, E., Van De Griend, A. A., & Engelen, G. B. (1985). Multivariate Analysis and Interpretation of the Hydrochemistry of a Dolomitic Reef Aquifer, Northern Italy. *Water Resources Research*, *21*(7), 1010–1024. https://doi.org/10.1029/WR021i007p01010

Shimodaira, H. (2014). Higher-order accuracy of multiscale-double bootstrap for testing regions. *Journal of Multivariate Analysis*, *130*, 208–223. https://doi.org/10.1016/j.jmva.2014.05.007

Shrestha, S., & Kazama, F. (2007). Assessment of surface water quality using multivariate statistical techniques: A case study of the Fuji river basin, Japan. *Environmental Modelling and Software*, *22*(4), 464–475. https://doi.org/10.1016/j.envsoft.2006.02.001

Silliman, S. E., Boukari, M., Crane, P., Azonsi, F., & Neal, C. R. (2007). Observations on elemental concentrations of groundwater in central Benin. *Journal of Hydrology*, *335*(3–4), 374–388. https://doi.org/10.1016/j.jhydrol.2006.12.005

Singh, K. P., Malik, A., & Sinha, S. (2005). Water quality assessment and apportionment of pollution sources of Gomti river (India) using multivariate statistical techniques - A case study. *Analytica Chimica Acta*, *538*(1–2), 355–374. https://doi.org/10.1016/j.aca.2005.02.006

Smedley, P. L., Knudsen, J., & Maiga, D. (2007). Arsenic in groundwater from mineralised Proterozoic basement rocks of Burkina Faso. *Applied Geochemistry*, *22*(5), 1074–1092. https://doi.org/10.1016/j.apgeochem.2007.01.001

Sohn, R. A., & Menke, W. (2002). Application of maximum likelihood and bootstrap methods to nonlinear curve-fit problems in geochemistry. *Geochemistry, Geophysics, Geosystems*, *3*(7), 1–17. https://doi.org/10.1029/2001GC000253

Steinhorst_et_al-1985-Water_Resources_Research.pdf. (n.d.).

Stumm, W., & Morgan, J. J. (1993). *Aquatic Chemistry: Chemical Equilibria and Rates in Natural Waters*. *Environmental science and technology* (Vol. Third). https://doi.org/10.1016/S0016-7037(97)81133-7

Taylor, R. G., Scanlon, B., Doell, P., Rodell, M., van Beek, R., Wada, Y., … Treidel, H. (2013). Ground water and climate change. *Nature Climate Change*, *3*(4), 322–329. https://doi.org/10.1038/nclimate1744

The World Bank. (2017). Data Bank: Population estimates and projections. Retrieved from http://databank.worldbank.org/data/reports.aspx?source=Health-Nutrition-and-Population-Statistics:-Population-estimates-and-projections

United Nations. (2015). *The Millennium Development Goals Report*.

United Nations. (2016). Sustainable Development Goals: 17 Goals to Transform our World. Retrieved from http://www.un.org/sustainabledevelopment/water-and-sanitation/

United Nations Development Programme. (2016). Trends in the Human Development Index, 1990-2015.

Valentin, C., & D'Herbès, J. M. (1999). Niger tiger bush as a natural water harvesting system. *Catena*, *37*(1–2), 231–256. https://doi.org/10.1016/S0341-8162(98)00061-7

Varol, M., Gökot, B., Bekleyen, A., & Şen, B. (2012). Spatial and temporal variations in surface water quality of the dam reservoirs in the Tigris River basin, Turkey. *Catena*, *92*, 11–21. https://doi.org/10.1016/j.catena.2011.11.013

Wanda, E., Monjerezi, M., Mwatseteza, J. F., & Kazembe, L. N. (2011). Hydro-geochemical appraisal of groundwater quality from weathered basement aquifers in Northern Malawi. *Physics and Chemistry of the Earth*, *36*(14–15), 1197–1207. https://doi.org/10.1016/j.pce.2011.07.061

WHO/UNICEF. (2015). 2015 Update and MDG Assessment. *World Health Organization*, 90. https://doi.org/10.1007/s13398-014-0173-7.2

WHO/UNICEF. (2017). Progress on Drinking Water, Sanitation and Hygiene: 2017 Update and SDG baseline.

Wright, E. P. (1992). The hydrogeology of crystalline basement aquifers in Africa. *Geological Society, London, Special Publications*, *66*(1), 1–27. https://doi.org/10.1144/GSL.SP.1992.066.01.01

Wyns, R. (1999). Caracterisation multiparametres des horizons de subsurface (0-100 m) en contexte de socle altere. (pp. 105–110). Orleans, France.

Wyns, R., Baltassat, J.-M., Lachassagne, P., Legchenko, A., Vairon, J., & Mathieu, F. (2004). Application of proton magnetic resonance soundings to groundwater reserve mapping in weathered basement rocks (Brittany, France). *Bulletin de La Societe Geologique de France*, *175*(1), 21–34. https://doi.org/10.2113/175.1.21

Yidana, S. M. (2010). Groundwater classification using multivariate statistical methods: Southern Ghana. *Journal of African Earth Sciences*, *57*(5), 455–469. https://doi.org/10.1016/j.jafrearsci.2009.12.002

Yidana, S. M., Banoeng-Yakubo, B., Aliou, A.-S., & Akabzaa, T. M. (2012). Groundwater quality in some Voltaian and Birimian aquifers in northern Ghana—application of mulitvariate statistical methods and geographic information systems. *Hydrological Sciences Journal*, *57*(6), 1168–1183. https://doi.org/10.1080/02626667.2012.693612

Yidana, S. M., Banoeng-Yakubo, B., & Sakyi, P. A. (2012). Identifying key processes in the hydrochemistry of a basin through the combined use of factor and regression models. *Journal of Earth System Science*, *121*(2), 491–507. https://doi.org/10.1007/s12040-012-0163-0

Youngstedt, S. M., & Keough, S. B. (2016). Water Vendors in Niamey : Considering the Economic and Symbolic Nature of Water, *16*(2).

Zhang, Z., Ouyang, Z., Xiao, Y., Xiao, Y., & Xu, W. (2017). Using principal component analysis and annual seasonal trend analysis to assess karst rocky desertification in southwestern China. https://doi.org/10.1007/s10661-017-5976-5

Zones, F. E. (2005). Niger Livelihood Profiles January 2005 FEWS NET, (January).